Realistic Characterizations of Biodegradation

The research presented in this thesis was carried out at the Department of Theoretical Biology, Vrije Universiteit Amsterdam, The Netherlands, and was supported by the Technology Foundation STW, applied science division of NWO and the technology programme of the Ministry of Economic Affairs, STW-project 790.44.151.

VRIJE UNIVERSITEIT

REALISTIC CHARACTERIZATIONS OF BIODEGRADATION

ACADEMISCH PROEFSCHRIFT

ter verkrijging van de graad van doctor aan
de Vrije Universiteit Amsterdam,
op gezag van de rector magnificus
prof.dr. T. Sminia,
in het openbaar te verdedigen
ten overstaan van de promotiecommissie
van de faculteit der Aard- en Levenswetenschappen
op donderdag 12 september 2002 om 15.45 uur
in de aula van de universiteit,
De Boelelaan 1105

door

Bernd Willem Brandt

geboren te Leiden

promotor: prof.dr. S.A.L.M. Kooijman

Aan mijn ouders

Thesis 2002-02 of the Institute of Ecological Science, Vrije Universiteit,
Amsterdam, The Netherlands

Contents

Preface

Humankind has produced over 70.000 chemicals that are all sooner or later released into the environment. In the sixties resistant pesticides and persistent detergents caused environmental pollution. Later the first tests on biodegradability were conceived and the Environmental Protection Agency formed the Office of Pollution Prevention and Toxics (OPPT) in 1977. Nowadays, new chemicals are tested for toxicity and biodegradability before they are admitted to the consumer market. These tests are carried out world-wide according to the guidelines established by the Organization for Economic Co-operation and Development, the European Union, the International Organization for Standardization, and the Environmental Protection Agency.

Task forces on biodegradation tests of, for example, the Society of Toxicity and Environmental Chemistry (SETAC) and of the industry recognize shortcomings in the protocols and in the interpretation of standardized biodegradation tests, in particular with the analysis of the test results. This thesis finds its basis in such problems. Three areas have been selected to work on: (*i*) mass-transfer limitation and growth of microbial flocs, (*ii*) multiple-substrate utilization and co-metabolism, and (*iii*) slow microbial adaptation to changing substrate availability.

This thesis is organized as follows. The first chapter introduces biodegradation tests and models. The growth of microorganisms during biodegradation is described by the Dynamic Energy Budget (DEB) theory as well as by the well-known Monod model. After a brief overview of the DEB model, the chapters on mass-transfer limitation, co-metabolism, and adaptation follow.

1

Tests and models in biodegradation

1.1 Introduction

In the 1960s, several chemicals such as polychlorinated biphenyls (PCBs), halogenated solvents, and synthetic detergents have caused environmental problems. It became clear that chemicals should be tested for their degradation and their toxicity before governments approve their production. Since then a large number of chemicals is tested each year. For instance, the US Environmental Protection Agency alone has reviewed 30.000 substances since 1979.

Before going into the tests, the main concepts should be defined. Degradation of a compound refers to its breakdown into smaller molecules. It can be a physical, chemical, or biological process. Biodegradation is mainly due to microorganisms and has been defined as "the biologically catalyzed reduction in complexity of chemicals [2]." Biodegradation can be divided into three categories:

- mineralization: the organic chemical is broken down into inorganic compounds. It is also known as 'ultimate biodegradation.' Typical products of aerobic mineralization are carbon dioxide, water, and ammonia.
- biotransformation: the organic chemical only undergoes small structural changes.
- co-metabolism: "the transformation of a non-growth substrate in the obligate presence of a growth substrate or another transformable compound [7]."

Biodegradation, in addition to chemical and physical degradation, plays an important role in the removal of substances from the environment and influences the environmental concentration of released chemicals. Therefore, biodegradability of chemicals in sewer systems, wastewater treatment plants, and natural waters constitutes a crucial factor in deciding their production approval [12, 16, 27]. This chapter introduces tests and models used to evaluate biodegradability.

1.2 Biodegradability tests

The OECD and EEC[1] regulations require the biodegradability of new chemicals to be tested. The strategy for testing adopted by the OECD consists of three levels [23], which are summarized in the next subsections:

1. ready biodegradability tests or screening tests
2. inherent biodegradability tests
3. simulation tests

Depending on the test results, three levels of degradability are distinguished: readily biodegradable, inherently biodegradable, and persistent. Due to the variety of experimental methods available, the biodegradability quantification can significantly vary among tests.

The tests are batch or (semi-)continuous and they differ in the amount of biomass and substrate concentration used. Furthermore, the degradation may depend on the type of test used. Biodegradation is first assessed in screening tests, which are defined as "Biodegradation screening tests comprise all those tests that do not attempt to simulate an environmental compartment" [9]. These tests are carried out worldwide and their results should be reproducible. Furthermore, these tests should be easy to carry out and have been designed "without any intent for deriving kinetic constants" [9].

Biodegradability tests generally ignore kinetics, because biodegradation rates are currently not required for the admission of new chemicals [9]. However, the rate of biodegradation is crucial in estimating the environmental concentration of a chemical and, thus, in risk assessment [12]. As biodegradation rates in different environmental compartments can vary considerably, accurate estimation and calculation methods of such rates are needed to predict environmental concentrations. Models of, for example, waste water treatment plants

[1] See Abbreviation section on page 13.

are often very sensitive to variations in the assumed biodegradation rate [17]. If it is possible to determine and extrapolate a rate (and kinetics) obtained from a test to the environment, it might be possible to come to risk assessment schemes based on sound models.

The range of currently used biodegradability tests are briefly reviewed below. The differences among them that influence the degradation kinetics are discussed. Thereafter some models for biodegradation kinetics are introduced. For further details on biodegradability testing, the reader is referred to reviews by, for example, Blok and Balk [5], and Painter [23].

1.2.1 Ready biodegradability tests

All chemicals are at least be subjected to a ready biodegradability test. It is assumed that chemicals passing the ready test will "rapidly and completely biodegrade in aquatic environments under aerobic conditions" [9, 21, Annex I]. The degradation of such chemicals is assumed to exceed 90% in a wastewater treatment plant (WWTP) [27].

Although a chemical is degraded in a test, it may not be degraded in the environment. The reverse is also true: a chemical which does not meet the test criterium may be degraded in the environment. This is due to differences in substrate concentrations and in the composition of the inoculum. The percentage of chemicals not released into the environment yet, so-called 'new' chemicals, failing a ready tests is high [23]. Probably this is because inocula are used that are not yet exposed or adapted to the chemical.

A test for ready biodegradability is stringent. Incubation time is limited, seed density is low (compared with the density in inherent tests), and the seed is unadapted to the chemical being tested [5].

The source of the inoculum of the tests is the environment (activated sludge, sewage effluents, surface waters and soils or a mixture of these [21]) and the synthetic medium is inoculated to about 10^6 cells/ml. The inoculum for a MITI(I) test differs from that for other tests: it is collected from at least ten different locations and kept on a medium containing 0.1 g/l glucose, peptone, and potassium orthophosphate for one month before it is used in the MITI(I) test [21]. During this period the inoculum will change and loose diversity, since the medium does not mimic wastewater.

Tests for ready biodegradability are batch incubations with a maximum duration of 28 days. A chemical is called readily biodegradable if the extent of degradation exceeds the 'pass' level. This level must be reached within 10 days (10-day window) after the end of the lag phase, which is the time when degradation reaches 10%. The value for the pass level depends on the method

used for analyzing the amount of residual chemical: 80% for specific analysis, 70% DOC and 60% ThOD or $ThCO_2$ [23].

In a OECD ready test, pretreatment or preconditioning of the inoculum is allowed, but should not include exposure to the test chemical. It only involves exposing the inoculum to the test conditions [23]. To reduce blank respiration, the sludge may be starved by aerating in absence of a carbon source. Test guidelines do not specify the length of this aeration period. However, the biodegradation capacities of the sludge have not changed noticeably after one week starvation, according to J. Blok (pers. comm.).

The tests are initiated by adding the test chemical as the sole carbon source to a mineral medium. The percentage removal, the final removal, and the 10-day window have to be reported [21]. The different OECD tests for assessing ready biodegradability are summarized in Table 1.1.

If a chemical does not pass the ready test, either degradation starts too late or the substance is not degraded fast enough. Thus, both the duration of the lag phase and the biodegradation rate are crucial to pass a test. The lag time is highly variable [23, p179]. However, the results from screening tests have proven to be good predictors of the behavior of the chemical in a WWTP [23, p167, B.1].

The result of a ready test may vary according to the protocol used. For instance, a chemical may pass a certain test on the basis of DOC, but fail on the basis of $ThCO_2$ [23, p86]. The pass level on DOC base (70%) is higher than on $ThCO_2$ base (60%), because the carbon from the test substance will partly be incorporated into the biomass. It seems that the $ThCO_2$ pass level may have to be lowered to solve the problem [23, p86].

Table 1.1: The six different OECD ready biodegradability tests (from [21]). The table summarizes the corresponding amount of test substance and inoculum that should be used in each test.

Test	DOC die-away	CO_2 evolution	Manometric respirometry	Modified OECD Screening	Closed bottle	MITI(I)
Concentrations of test substance						
mg/l			100		2-10	100
mg DOC/l	10-40	10-20		10-40		
mg ThOD/l			50-100		5-10	
Concentration of inoculum						
mg SS/l	≤ 30					30
ml effluent/l	≤ 100			0.5	$\leq$5	
approx. cells/l	10^7-10^8			10^5	$10^4 - 10^6$	$10^7 - 10^8$

Table 1.2: OECD inherent biodegradability tests (from [19, 20, 23]).

Test	Zahn-Wellens/EMPA[a]	SCAS	MITI(II)
Concentrations of test substance			
mg DOC/l	50-400	20	
mg ThOD/l			30
Concentration of inoculum			
mg dry SS/l	200-1000 (washed)		100
ml effluent/l		[b]	

[a] The Zahn-Wellens test has an inoculum to substrate-concentration ratio of 2.5:1 to 4:1. [b] Mixed liquor from suitable WWTP.

1.2.2 Inherent biodegradability tests

To test inherent biodegradability, a higher concentration of inoculum and substrate is used than in the ready tests. This results in a more diverse microbial community, enhancing adaptation possibilities. The inherent tests are summarized in Table 1.2.

The Zahn-Wellens test lasts for up to 28 days. The semi-continuous activated sludge test (SCAS) has a maximal duration of 12 to 26 weeks. Once a day aeration is stopped for one hour and two thirds of the total volume[2] is discarded, giving a retention time of 36 hours, after which new sewage or synthetic waste is added. When the COD or DOC of the discarded waste reaches a steady state, the test chemical is added with the feed [23]. The modified MITI(II) uses an inoculum collected from at least ten different places as with the MITI(I) test. The test lasts 14 to 28 days and continuously measures the biochemical oxygen demand during the degradation of the test chemical.

1.2.3 Simulation tests

To assess biodegradability potentials that are relevant in the environment, it is important not to deviate too much from environmental conditions in lab tests. When a chemical has not passed a ready test, but passed a test for inherent biodegradability, a simulation test may be started. The OECD simulation test is based on the OECD confirmatory test for surfactant biodegradation and uses

[2] According to the OECD guidelines, 2/3 of the volume is discarded *after* settling of the sludge, giving a very large retention time of the deposited material [19].

the Husmann apparatus [22]. Basically, a WWTP is simulated with representative hydraulic and sludge retention times.

1.2.4 Biodegradability prediction

As stated above, a variety of test parameters may influence the test results, such as:

- Source and size of the inoculum and, thus, also the inoculum viability and species diversity.
- The adaptation period of the inoculum. Adaptation of bacteria to the chemical and the initial amount of specific degraders significantly influences the test result.
- Concentration of the test chemical.
- The analytic method to determine the extent of degradation (DOC, ThOD, $ThCO_2$, specific analysis).

The analytic method is only important because the pass levels depend on them. As such this is more a test protocol issue. The other items always are important in assessing biodegradability.

1.3 Kinetic Models

This section discusses models that have been widely used to describe or fit biodegradation data. For ease of reference, the symbols used in the model equations below are the same as those in the original articles. Often models are mainly chosen according to their goodness of fit. Simply to improve the fits, sometimes an alternative model is chosen or a model is extended to incorporate additional parameters.

1.3.1 Monod and Michaelis-Menten kinetics

Different kinetic models have been used to study biodegradation processes. However, all the models for growth and substrate consumption are mainly based on the Monod (1.1) or Michaelis-Menten (1.2) equations [1, 4, 5, 23, 26].

$$\mu = \mu_{max}\frac{S}{K_s + S} \quad \frac{dX}{dt} = \mu\, X \quad \text{and} \quad \frac{dS}{dt} = -\frac{1}{Y}\frac{dX}{dt} \tag{1.1}$$

$$v = v_{max}\frac{S}{K_s + S} \quad \text{with} \quad v_{max} = kE_t \tag{1.2}$$

Michaelis-Menten kinetics applies when a compound is transformed by non-growing biomass or by biomass growing on another substrate than the test compound [26]. In the latter situation, the maximum reaction rate v_{max} varies and is equal to $kE_t(t)$, where E_t is the total amount of enzyme/biomass and k the rate constant. Degradation by growing cells and by non-growing cells is obtained by the summation of the Monod and Michaelis-Menten equations [28]. Growing biomass degrade the compound according to the Monod equations, and non-growing cells according to the Michaelis-Menten equation. Michaelis-Menten and Monod kinetics result in the same kinetics when biomass growth is negligible.

Monod originally devised his equation to describe the growth of a single species with a constant yield on a single growth-limiting substrate [14]. The Monod model assumes negligible maintenance and a constant yield factor. Moreover, it also presupposes a constant biomass composition. The use of Monod kinetics may be criticized, because degradation is usually carried out by a consortium consuming a variety of substrates [18]. However, Simkins and Alexander [25] have shown by curve fitting that the model describes mixed culture growth in a number of cases.

Biodegradation rates are calculated from the test results by using Monod kinetics or simplifications of Monod kinetics, resulting in first or zero-order kinetics. First order kinetics ($\frac{dS}{dt} = -kS$) results if biomass formation is negligible and $S \ll K_s$; zero order kinetics ($\frac{dS}{dt} = -k$) results if biomass formation is negligible and $S \gg K_s$. Thus, first order kinetics should only be used if the growth is negligible and adaptation is absent, which implies low (test)substrate concentrations and a short incubation time.

Simkins and Alexander [25] formulate different kinetic expressions that can be applied in biodegradation (see also [1, 2]):

- logarithmic or exponential (small inoculum, $S \gg K_s$).
- zero-order (no significant growth, $S \gg K_s$).
- first order (constant biomass concentration, substrate limitation: thus, $S \ll K_s$).
- Monod kinetics (with or without growth).
- logistic growth (low biomass and substrate concentration: rate falls with diminishing and always limiting substrate).

Basically, Monod (or logistic degradation) is assumed, which changes to a first order process at low substrate concentration.

1.3.2 Other types of kinetics

Haldane kinetics

For Monod growth on inhibitory substrates, Haldane's equation [8] has been used [10]. The Haldane expression originally added an inhibition term to the Michaelis-Menten expression. Later, Andrews [3] used the expression to describe the consumption of inhibitory substrates as phenol by bacteria.

$$\mu = \mu_{max} \frac{S}{S + K_s + S^2/K_i}$$

The curve of the specific growth rate μ as a function of the substrate concentration S has a maximum, from which μ decreases with increasing substrate concentration. If the inhibition constant K_i is very large, the model reduces to the Monod model.

First order kinetics

First order kinetics is used when the test chemical concentration is low compared to initial biomass concentration. When $ThCO_2$ is measured, the first order equation can be used to describe the carbon dioxide production [11, 13]

$$\begin{aligned} P(t) &= P_\infty \left(1 - e^{-k_1 (t - t_{lag})}\right) \quad \text{for } t \geq t_{lag} \\ P &= CO_2 \text{ production} \\ P_\infty &= \text{asymptote of } CO_2 \text{ production} \\ t_{lag} &= \text{lag time} \\ k_1 &= \text{first order degradation constant} \end{aligned}$$

It has been argued that the use of first order kinetics may be validated by using a range of substrate concentrations [17]. If the rate constant does not vary over a 10-fold concentration range (e.g., 5–50 μg/l), the chemical is believed to be degraded according to a first order process [17]. Indeed, the rate of mineralization of a number of organic compounds in samples of fresh water is directly proportional to their concentration over a wide range of concentrations [1].

Logistic kinetics

Larson [11, 13] used a logistic function to fit CO_2 production data. The logistic function has been extended with an empirical constant n, converting the standard logistic function into a more flexible logist. This improves the fits, but the introduction of n is not based any biological mechanism. The inflection point of the curve is no longer located at $a/2$, but may be at a smaller or larger value depending on the value of n. The intrinsic growth rate has become a function of n (intrinsic growth rate $= k_1/n$).

$$\begin{aligned} y(t) &= a(1 - b\,\mathrm{e}^{-k_1 t})^{-1/n} \\ y &= \text{cumulative \% ThCO}_2 \\ a &= \text{asymptote of curve \% ThCO}_2 \\ k_1 &= \text{rate constant (day}^{-1}\text{)} \\ n &= \text{'empirical constant'} \\ b &= \text{'coordinate scaling factor'} \end{aligned}$$

This function is known as the generalized logist or the n-logist. It can also be written as:

$$\begin{aligned} \frac{d}{dt}y &= \frac{k_1}{n}\, y \left(1 - \left(\frac{y}{a}\right)^n\right) \quad \text{with } y(0) = y_0 \\ y(t) &= a\left(1 - \left\{1 - \left(\frac{a}{y_0}\right)^n\right\} \mathrm{e}^{-k_1 t}\right)^{-1/n} \end{aligned}$$

Thus, b equals $1 - (a/y_0)^n$. However, the meaning of b is unclear. Larson [13] states that this coordinate scaling factor equals unity in singe-dose batch experiments. However, in that case $y(t)$ becomes undefined at time zero (for $n > 0$).

3/2 order kinetics

The 3/2 order model is a combination of zero and first order elements to describe linear and exponential degradation (in time). It has been used by, for example, Shimp and Larson [24]:

$$\begin{aligned} P(t) &= P_0(1 - \mathrm{e}^{-k_1 t}) + k_0 t \\ P &= \%\ ^{14}\text{C-labeled material mineralized} \\ P_0 &= \%\ ^{14}\text{C-labeled material converted to } ^{14}\text{CO}_2 \text{ during first order degradation} \\ k_1 &= \text{first order degradation rate constant (day}^{-1}\text{)} \\ k_0 &= \text{zero order rate constant (\%}\ ^{14}\text{C day}^{-1}\text{)} \end{aligned}$$

These authors claimed that "this model consistently provided the best fits to the experimental data [24]." The zero order rate constant may represent either the liberation of incorporated label from biomass or "the rate at which sorbed chemicals are desorbed and become available for degradation [24]."

1.4 Relevant processes in biodegradation

Pollution problems have occurred with, for example, pesticides and detergents that are not biodegradable and consequently accumulated in the environment. Therefore, we currently test a number of properties of a chemical. However, biodegradability is not an intrinsic feature of the chemical, as it also depends on specific environmental conditions, such as the pH and the chemical composition of the soil. Availability of the chemical to microbes, biomass concentration, and microbial diversity are also key factors determining the extent of degradation.

As pointed out by Alexander [1], the occurrence, kinetics, and products of microbial transformation observed at the high substrate concentrations used in tests, cannot simply be extrapolated to the low substrate concentrations found in nature. At low substrate concentrations, non-growing eutrophic or growing oligotrophic species may be responsible for biodegradation of the chemical. Some chemicals may be mineralized at trace level concentration, but co-metabolized at higher concentrations. Furthermore, high substrate concentrations as used in the ready biodegradability test can be toxic to microorganisms. This is exemplified by triclosan, a bacteriostatic compound used in toothpaste. It does not pass a ready test and therefore does not classify as readily biodegradable, but it is degraded rapidly at environmentally relevant concentrations (μg/l, pers. comm. T. Federle, P&G). However, low concentrations do not guarantee biodegradation either. A threshold concentration may exist below which certain molecules are not converted to CO_2 [1]. The existence of such threshold concentrations may be the reason for the persistence of low levels of biodegradable organic substances in natural environments. To understand threshold concentrations, maintenance requirements for growth, enzyme induction and enzyme activity, and the use of substrate mixtures have to be understood [1].

The length of the lag period and the rate of degradation are influenced by various processes, such as mass-transfer, co-metabolism, and adaptation. The adaptation of activated sludge to the test chemical can often be explained by the growth of competent degrading microorganisms. It can also be explained by the induction of enzymes, transfer of genetic material or development of

tolerance to toxicity [18].

1.5 Modeling biodegradation

At the moment biodegradation modeling tends to be a bit *ad hoc*, as exemplified by the number of models in the section on kinetic models above. After the test results are known a model is chosen; alternatively a model is selected that provides the best fit. For a thorough analysis of biodegradation tests, a number of complete data sets are needed. However, due to the pass/fail nature of the ready tests, these data sets generally contain a small number of measurements. Two or three measurements may be enough to determine a pass or fail, but are not enough for kinetic modeling. In addition, most data sets on chemicals are publicly available.

The need for kinetic modeling has been acknowledged, however. The 1997 SETAC report on biodegradation kinetics [9] stated that more 'kinetic data' is needed to assess biodegradability. A problem with modeling biodegradation from a process point of view is the lack of biomass data. Generally, only the substrate concentration is measured as a function of time, whereas little is known about the microorganisms responsible for substrate consumption and about the mass balances, for instance. However, knowledge on biomass and mass balances is required to figure out what the bacteria do with the test chemicals. The size and viability of the inoculum, the percentage of specific degraders and their specific growth rate have a significant influence on the biodegradation rate. Nowadays, biomass itself is receiving more attention [6]. The concentration of specific degraders in activated sludge or in a biodegradation test can be measured with quantitative PCR (AstraZeneca, data classified), microautoradiography [15], or flow cytometry [29].

As stated before, various processes are believed to be important in biodegradation modeling: mass-transfer limitation, adaptation, co-metabolism, maintenance and decay, toxicity, and sorption-desorption kinetics. Within this project a number of these processes were chosen for further study because of their importance in biodegradation tests: mass-transfer limitation (Chapter 3), multiple substrate utilization and co-metabolism (Chapter 4), and adaptation (Chapter 5). In the context of the complex nature of biodegradation testing these models must be seen as a development towards understanding some of the processes that take place. Understanding these processes is a step towards understanding what is going on in a biodegradation test.

1.6 Abbreviations

COD	Chemical Oxygen Demand
DOC	Dissolved Organic Carbon
EEC	European Economic Community
EMPA	Eidgenössische Materialprüfungs- und Forschungsanstalt
EPA	Environmental Protection Agency, USA
MITI	Ministry of International Trade and Industry, Japan
OECD	Organization for Economic Co-operation and Development
P&G	Procter & Gamble
PCR	Polymerase Chain Reaction
SCAS	Semi-Continuous Activated Sludge Test
SRT	Sludge Retention Time
SS	Suspended Solids
$ThCO_2$	Theoretical CO_2 production
ThOD	Theoretical Oxygen Demand
WWTP	Waste Water Treatment Plant

References

[1] Alexander M. (1985). Biodegradation of organic chemicals. *Environmental Science & Technology* 18:106–111.

[2] Alexander MA. (1999). *Biodegradation and bioremediation*. Academic Press, San Diego, second edition.

[3] Andrews JF. (1968). A mathematical model for the continuous culture of microorganisms utilizing inhibitory substrates. *Biotechnology and Bioengineering* 10:707–723.

[4] Battersby NS. (1990). A review of biodegradation kinetics in the aquatic environment. *Chemosphere* 21:1243–1284.

[5] Blok J, Balk F. (1994). Commission of the European Communities: guidance document for the interpretation of biodegradability test data. Technical report, BKH Consulting Engineers, Delft, The Netherlands.

[6] Cronje GL, Beeharry AO, Wentzel MC, Ekama GA. (2002). Active biomass in activated sludge mixed liquor. *Water Research* 36:439–444.

[7] Dalton H, Stirling DI. (1982). Co-metabolism. *Philosophical Transactions of the Royal Society of London B (Biological Sciences)* 297:481–496.

[8] Haldane JBS. (1930). *Enzymes*. Longmans, Green, London.

[9] Hales SG, Feijtel T, King H, Fox K, Verstraete W, editors. (1997). *Biodegradation kinetics: generation and use of data for regulatory decision making*. SETAC-Europe.

[10] Kumaran P, Paruchuri YL. (1997). Kinetics of phenol biotransformation. *Water Research* 31:11–22.

[11] Larson RJ. (1984). Kinetic and ecological approaches for predicting biodegradation rates of xenobiotic organic chemicals in natural ecosystems. In: Klug MK, Reddy CA, editors. *Current perspectives in microbial ecology*, pp. 677–686. American Society for Microbiology, Washington, D.C.

[12] Larson RJ, Cowan CE. (1995). Quantitative application of biodegradation data to environmental risk and exposure assessments. *Environmental Toxicology and Chemistry* 14:1433–1442.

[13] Larson RJ, Hansmann MA, Bookland EA. (1996). Carbon dioxide recovery in ready biodegradation tests: mass transfer and kinetic considerations. *Chemosphere* 33:1195–1210.

[14] Monod J. (1958). *Recherches sur la croissance des cultures bactériennes*. Hermann, Paris, second edition. Thèse de 1942.

[15] Nielsen JL, Nielsen PH. (2002). Enumeration of acetate-consuming bacteria by microautoradiography under oxygen and nitrate respiring conditions in activated sludge. *Water Research* 36:421–428.

[16] Nyholm N. (1991). The European system of standardized legal tests for assessing the biodegradability of chemicals. *Environmental Toxicology and Chemistry* 10:1237–1246.

[17] Nyholm N, Ingerslev F, Berg UT, Pedersen JP, Frimer-Larsen H. (1996). Estimation of kinetic rate constants for biodegradation of chemicals in activated sludge wastewater treatment plants using short term batch experiments and μg/L range spiked concentrations. *Chemosphere* 33:851–864.

[18] Nyholm N, Madsen T. (1995). Comments on guidance document for the interpretation of biodegradability data by BKH consulting engineers.

[19] OECD. (1984). *OECD guideline for testing of chemicals. 302A: Inherent biodegradability: modified SCAS test*. OECD, Paris.

[20] OECD. (1984). *OECD guideline for testing of chemicals. 302C: Inherent biodegradability: modified MITI(II) test*. OECD, Paris.

[21] OECD. (1992). *OECD guideline for testing of chemicals. 301: Ready biodegradability*. OECD, Paris.

[22] OECD. (2001). *OECD guideline for testing of chemicals. 303: Simulation test – Aerobic sewage treatment. 303A: Activated sludge units*. OECD, Paris.

[23] Painter HA. (1995). *Detailed review paper on biodegradability testing. Environment monograph no. 98*. Environment Directorate, OECD, Paris.

[24] Shimp R, Larson R. (1996). Estimating the removal and biodegradation potential of radiolabeled organic chemicals in activated sludge. *Ecotoxicology and Environmental Safety* 34:85–93.

[25] Simkins S, Alexander M. (1984). Models for mineralization kinetics with the variables of substrate concentration and population density. *Applied and Environmental Microbiology* 47:1299–1306.

[26] Stringer DA. (1991). Biodegradation kinetics. Technical Report no. 44, ECETOC, Brussels, Belgium.

[27] Struijs J, Stoltenkamp J, van de Meent D. (1991). A spreadsheet-based box model to predict the fate of xenobiotics in a municipal wastewater treatment plant. *Water Research* 25:891–900.

[28] Winkler M. (1981). *Biological treatment of waste-water*. Ellis Horwood, Chichester, England.

[29] Ziglio G, Andreottola G, Barbesti S, Boschetti G, Bruni L, Foladori P, Villa R. (2002). Assessment of activated sludge viability with flow cytomety. *Water Research* 36:460–468.

2

The Dynamic Energy Budget theory

2.1 Introduction

The Dynamic Energy Budget (DEB) theory provides rules for uptake and use of energy by organisms. It exploits conservation laws and stoichiometric constraints. Energy and mass fluxes through the organisms and their surroundings are central in the DEB framework. As this theory focuses on the similarities between organisms rather than on the differences, it applies to a wide variety of organisms, including animals, plants, and microorganisms. In the following chapters, the DEB model is used to describe the growth of microorganisms. Below the DEB theory is briefly introduced.

2.2 The DEB theory

Individuals are the starting point in the DEB theory. They can consume nutrients, grow, and reproduce. To introduce the main issues of the DEB model, I explain the processes of substrate uptake and use. Substrate is conceived as material that bears energy. Generally substrate refers to one growth-limiting nutrient. Clearly, the substrate uptake rate is dependent on the size or volume of an individual. In relation to nutrient uptake, we can make the following observations:

- Nutrient uptake does not always result in growth, because of the existence of maintenance. Moreover, organisms can survive short periods without nutrients.
- Individuals react slowly to changes in their feeding conditions.

- Well-fed individuals show a different chemical composition than poor-fed individuals. Thus, the chemical composition is a function of nutrient consumption.

The DEB theory incorporates these observations by decomposing an individual into 'structural biomass' and 'reserve materials.' The structural materials are continuously degraded and reconstructed, whereas the reserves are used and replenished. Three processes are central: assimilation, growth, and maintenance. A microorganism takes up substrate at a rate proportional to its surface area and assimilates it into reserves.

From the reserves an individual pays maintenance costs and growth costs. The former are paid to maintain the integrity of a cell and to maintain gradients across the cell membrane. These costs are assumed to be proportional to the amount of structural biomass. The specific costs for growth are assumed to be constant during an organism's life. This implies that the structural biomass has a constant chemical composition ('strong homeostasis'). Strong homeostasis is also assumed for the reserves and, consequently, the specific weight of the reserves (amount of reserves per volume of reserve) is constant. The macro-chemical composition of the whole organism can vary, since the ratio of structure and reserves can change.

Substrate uptake is proportional to a surface area and maintenance costs are proportional to a volume. To facilitate surface-volume relationships, the DEB theory deals with isomorphic organisms, which retain their shape during growth. A population of isomorphic organisms can be modeled using structured population dynamics, where the state of each individual in the population is a function of its reserves and structure. Often a microorganism can be regarded as a filament: the surface area increases proportionally to the increase in volume. The main advantage of modeling microorganisms as filaments is that a population of filaments behaves in the same way as an individual. This is a useful approximation for dividing organisms, which reset their volume after a two-fold increase [6], even in the case where they change differently in shape during growth. Thus, the theory of structured population dynamics is not required to describe a population of microorganisms, which simplifies the mathematics considerably. Indeed, it results in a population dynamics that is unstructured (total structure and total reserves), rather than structured and clearly gives an attractive simplicity at the population level.

2.3 The DEB theory for microorganisms

Although the DEB theory applies to a wide range of organisms, the equations presented in this section are valid for microorganisms and filamentous organisms only, since the simplification for unstructured population dynamics explained above is used.

The symbols used in the DEB theory differ from those a microbiologist or process engineer is used to. This is because the DEB theory encompasses much more than growth of (micro)organisms. In addition to the growth process, also life cycles, body-size scaling relationships, ageing, and food webs are described within the DEB theory. This calls for a uniform and consistent notation. For example in the literature, D denotes a diffusion coefficient or a dilution rate and μ denotes a growth rate or a chemical potential. To prevent misunderstandings, Kooijman [7] has chosen an alternative notation. This notation is defined as follows: the symbol set contains a number of root symbols, where each root symbol corresponds to a specific dimension. Subscripts provide additional information about the processes and the compounds involved. The following examples illustrate the use of the symbols:

- J represents a flux (or rate) in mol/time. For organic compounds the dimension is C-mol/time. A subscript, generally consisting of two letters, specifies J: the first letter in the subscript refers to a compound; the second indicates the process associated with the flux. For example, S refers to a certain substrate and A refers to the assimilation process. Thus J_{SA} is the assimilation flux of substrate (or the substrate consumption rate). In engineering J_{SA} is often known as r_s.

- j represents a specific flux with dimension C-mol/(C-mol time). In engineering, the specific substrate consumption rate, j_{SA}, is generally denoted by q_s.
  The symbol j_{EM} is the specific flux (j) of reserves (E) involved in the maintenance (M) process.

- y denotes a stoichiometric constant or mass-mass coupler. The efficiency of a transformation of A into B is given by y_{BA} in C-mol B per C-mol A. The transformation of B into A then has an efficiency y_{AB}, where y_{AB} is equal to y_{BA}^{-1}. In contrast to the biomass yield factor, the parameters y_{ik} are real constants.

Below the DEB model equations are given. I start with the uptake of nutrients and, then, describe the assimilation process and reserve dynamics, leading to

the growth equation. The equation for the uptake of a growth limiting nutrient is equivalent to the equation for nutrient consumption in the Monod and Pirt models. The consumption rate is a hyperbolic function of the nutrient concentration (S), of the specific maximum consumption rate (j_{SAm}), and of the the amount of structural biomass (X):

$$J_{SA} = j_{SAm} f X \quad \text{with } f \stackrel{\text{def}}{=} \frac{S}{S+K} \tag{2.1}$$

where f is the scaled functional response. The substrate is converted into reserves during the assimilation process with a fixed conversion efficiency y_{ES}. Thus, the specific production flux of reserves j_{EA} equals $y_{ES} j_{SA}$. The change in the amount of reserves is a function of the input and of the energy requirements of the different cellular processes. The dynamics of the reserve density (C-mol reserves per C-mol structure, m_E) are first order for a number of reasons, which are explained in detail elsewhere [7]. This results in:

$$\frac{d}{dt} m_E = j_{EA} - k_E m_E \tag{2.2}$$

where k_E denotes the reserve turnover rate. The first term of the equation above corresponds to the assimilation of substrate into reserves. Remember that j_{EA} equals $y_{ES} j_{SA}$. The equation for reserve dynamics may be scaled with the maximum reserve density m_{Em}, which equals j_{EAm}/k_E. This scaling yields:

$$\frac{d}{dt} e = k_E (f - e)$$

where k_E equals $j_{SAm} y_{ES} / m_{Em}$ and $e = m_E / m_{Em}$.

The reserves are used to carry out cellular processes (Figure 2.1). The catabolic flux (or reserve utilization rate) is denoted by J_{EC}. The change in the amount of reserves is the difference between the assimilation flux and the catabolic flux. In mathematical terms this means:

$$\frac{d}{dt} M_E = J_{EA} - J_{EC}$$

or

$$J_{EC} = J_{EA} - \frac{d}{dt}(m_E X) = J_{EA} - X \frac{d}{dt} m_E - m_E \frac{d}{dt} X \tag{2.3}$$

The catabolic flux is allocated to growth and maintenance. The costs for growth are proportional to the change in structural biomass and, as explained

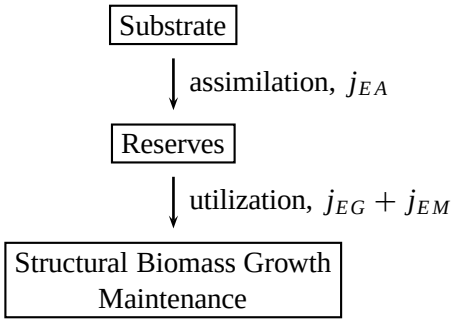

Figure 2.1: Overview of the fluxes in the DEB model for microorganisms. Substrates are converted into reserves and added to the reserve pool (assimilation, j_{EA}). The reserves are used for maintenance (j_{EM}) and growth (j_{EG}).

in the previous section, the costs for maintenance are proportional to structural biomass. Thus, the catabolic flux can be written as:

$$J_{EC} = y_{EV}\frac{d}{dt}X + j_{EM}X \tag{2.4}$$

where y_{EV} is the specific cost for growth and j_{EM} the specific maintenance flux (dimensions C-mol reserve/C-mol structure and C-mol reserve/(C-mol structure time), respectively). The specific catabolic flux is $j_{EC} = y_{EV}r + j_{EM}$, with r the specific growth rate. Using equations (2.2), (2.3), and (2.4), we deduce the expression for the specific growth rate:

$$r = \frac{1}{X}\frac{d}{dt}X = \frac{k_E m_E - j_{EM}}{m_E + y_{EV}} \tag{2.5}$$

The specific maintenance flux (or maintenance-associated specific reserve consumption j_{EM}) has dimension C-mol reserve per C-mol structural biomass per time. Within the DEB theory, maintenance requirements are often expressed as the maintenance rate coefficient k_M with dimension t^{-1}, while j_{EM} equals $k_M y_{EV}$.

The basic unstructured DEB model for microbial growth is now complete. Equations (2.1), (2.2), and (2.5) define substrate uptake, reserve dynamics, and change in structural biomass. However, in experiments only total-biomass weight, the sum of structure and reserves, is measured. The total weight equals:

$$W = w_V X + w_E m_E X$$

The conversion from C-moles to grams is made with molar weights w_V (g/C-mol structure) and w_E (g/C-mol reserve).

2.4 Comparison of the DEB model with the Monod and Pirt models

2.4.1 Comparison of the model frameworks

In microbiology and process engineering, biomass growth is often described with the Monod model. If a constant yield factor cannot be assumed and maintenance is important, the Pirt model is used instead. Sometimes reserves are important and are, therefore, included in a growth model. This may result in models where reserve dynamics is not fully integrated into the dynamics of the whole system. There may be several reasons to use the DEB model instead of the Monod or Pirt model. However, microorganisms are not the only organisms, and one may wonder if there is a fundamental difference in substrate uptake and use between microorganisms and other organisms that justifies the utilization of different models in different situations. A positive answer to this question implies that a boundary between microorganisms and other organisms must and can be defined. Within the DEB theory, there is no such fundamental difference among organisms, since all organisms share a lot of their metabolic features. All organisms take up a limiting nutrient and posses some sort of reserves. It is easily accepted that animals (or higher organisms) posses reserves, but why would microorganisms not posses reserves. The contribution of the DEB theory is that it is able to describe growth of a population of microorganisms, but also to describe the growth of an animal. In a way, this does not come as a surprise since microorganisms as a group are much more versatile than animals.

A microbiologist may wonder why to use the DEB model, since it looks somewhat more complex than, for instance, the Monod model. A few remarks can be made. First, organisms are not really different, focusing on energetics. However, for modeling batch growth of microorganisms the Monod model is used, for modeling chemostats with different dilution rates the Pirt model is used and for modeling growth of animals the Von Bertalanffy model is used. Clearly, also microorganisms have maintenance requirements. They consume substrate and maintain their cellular structure by rebuilding proteins. Thus any growth model should include maintenance. Reserves seem more complicated. However, when reserves are needed, for example in describing growth of algal or phosphate accumulating microorganisms, they are incorporated. Furthermore, a modeler should notice that cellular composition changes, for example, in function of the available nutrients or the growth rate. Although the Monod and Pirt models implicitly assume that the biomass composition is constant and do not allow (significant) changes in cellular composition they are often used in

situations where the composition changes (pers. comm. S.A.L.M. Kooijman).

As explained in the previous section, the DEB theory starts with a framework where reserves play a central role (Figure 2.1). This means that biomass composition is a function of the amount of reserves and that the change of composition can be described. Furthermore, maintenance has a more natural role than in other models. According to the Pirt model, lack of substrate directly results in death of biomass. In the DEB model the reserves are drawn on during a short interruption in assimilation, which has a more direct link with biochemical processes. The presence of reserves is indeed the main difference between DEB and other microbiological growth models, such as the Monod [9], Herbert [5], Marr [8], and Pirt [11] models.

Sometimes there may be a reason to use, for example, the Monod model to describe growth of bacteria instead of the DEB model. Lack of data generally is such a reason. However, it makes sense to keep using the DEB framework and make assumptions on parameter values to arrive at the Monod equations. Furthermore, within the DEB framework additional reserve pools can be added straightforwardly, preventing *ad hoc* modeling of reserve pools. For example, at low growth rates microorganisms can generate reserves from non-limiting nutrients. An increase in the limiting reserve density results in an increase in the growth rate. The non-limiting reserve density decreases with increasing growth rate, however.

The DEB framework account for both maintenance and reserves, and embraces the Monod and Pirt models. If reserve dynamics is excluded from equation (2.3), the Pirt model appears. Alternatively, if reserve turnover is very fast or if the maximum reserve density is very small, reserves are virtually absent and the change in reserve density remains zero. This can be seen from $\frac{d}{dt} m_E = j_{EA} - k_E m_E^*$, which gives a steady state for $m_E^* = j_{SAm} y_{ES} f / k_E$ and m_E^* approaches zero. Substituting this expression into equation (2.5) yields the Pirt growth equation:

$$\frac{d}{dt} X = (j_{SAm} y_{VS} f - k_M) X$$

where $y_{VS} = y_{ES}/y_{EV}$ is the so-called true or maximum yield and $j_{SAm} y_{VS}$ is the maximum specific growth rate, when maintenance is zero. As with the Pirt model, this growth rate can be rewritten to really represent the maximum observable specific growth rate. The specific maintenance is represented by the maintenance rate coefficient k_M, which equals j_{EM}/y_{EV}. If maintenance is negligible, the Monod growth equation results.

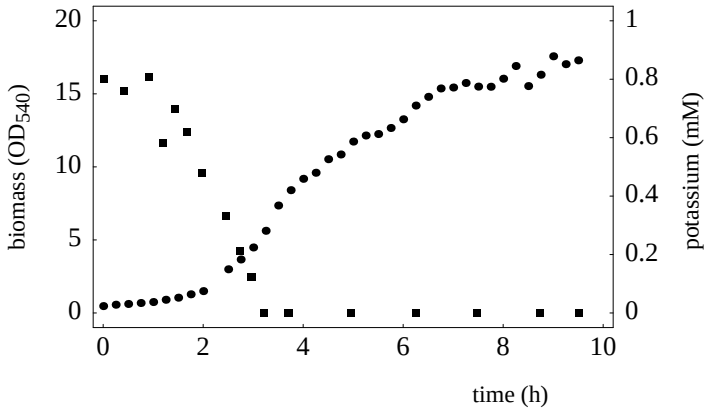

Figure 2.2: The importance of reserves in the potassium limited growth of *E. coli* (data from [10]). Growth (●) continues for about five hours after the depletion of potassium (■).

2.4.2 The influence of reserves

Within the DEB framework reserves are important and for higher organisms the importance of reserves is generally clear. However, reserves of limiting nutrients can also significantly affect growth dynamics of microorganisms. Potassium limited growth of *Escherichia coli* (Figure 2.2) exemplifies the influence of reserves well. Growth continues after the depletion of the growth-limiting substrate and most of the biomass is even produced from the reserves.

As explained above, the DEB model assumes first order dynamics on the basis of densities. Beun [1] obtained empirical support for this. The poly-β-hydroxybutyrate density in aerobic activated sludge decays exponentially, as shown in Figure 2.3.

Algae are known for their carbohydrate or phosphate reserves. Growth of algae can be modeled with the Droop model [3], in which the growth rate depends on the intracellular 'cell quota.' Button [2] found that "for phosphate-limited continuous culture of *Rhodotorula rubra* there was a monotonic increase in the concentration of cytoplasmic phosphate with both a net rate of phosphate uptake and a unidirectional inward flux of phosphate." He used this finding to construct whole cell uptake kinetics, combining kinetics of transport into cytoplasm and kinetics of use from the cytoplasmic pool [2], and applied it to oligotrophic bacteria. Since in this model both uptake and use obey Michaelis-Menten kinetics, the existence of a steady-state depends highly on the parameter values ($v_{\max}$ and K). The DEB reserve dynamics does not suffer

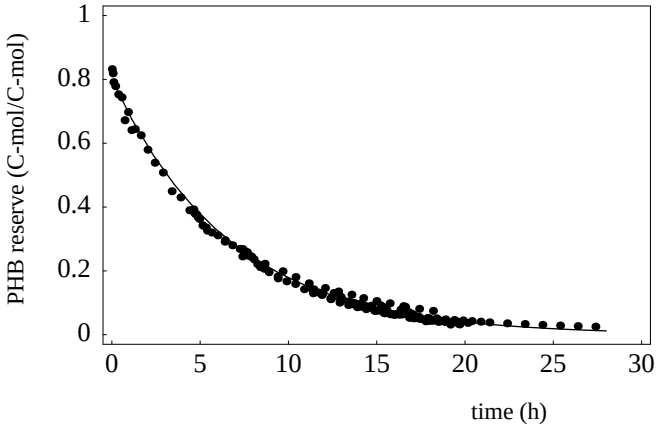

Figure 2.3: Exponential decay of poly-β-hydroxybutyrate density in aerobic activated sludge at 20°C as a function of time. The rate constant equals 0.15 h^{-1} (data and fit from [1]).

from this and predicts the behavior observed by Button. Figure 2.4 illustrates a monotonic relationship between the (total) uptake rate and the reserve density according to the DEB model. In steady state, the reserve density, m_E equals $j_{SAm} y_{ES} f / k_E$ (equation 2.2). The use of the reserves (inward flux) is proportional to the amount of reserves (see equation 2.2).

2.4.3 Comparison of the model parameters

Most people are familiar with the Monod and Pirt models and their parameters. The equations of these models can be written in the new symbol set as shown above. The maximum specific growth rate (r_{max}) is equal to the product of the biomass yield and the specific substrate consumption rate. The DEB model does not use the yield factor itself because it never is constant, but rather a ratio of two fluxes ($\frac{dX/dt}{dS/dt} = \frac{r}{j_{SAm} f}$). However, the Monod or Pirt yield expression can be given.

- The Monod yield factor (or true yield) Y equals $y_{VS} = \frac{y_{ES}}{y_{EV}}$.
- The yield expression for the Pirt model is $Y = \frac{j_{SAm} y_{VS} f - k_M}{j_{SAm} f}$, which can be rewritten to obtain $\frac{1}{Y} = \frac{k_M}{y_{VS} r} - \frac{1}{y_{VS}}$. The true yield is denoted by y_{VS}, the specific maintenance by $\frac{k_M}{y_{VS}}$ (C-mol substrate / (C-mol biomass time)), and the growth rate by r. The expression above is often written as $\frac{1}{Y} = \frac{m}{\mu} + \frac{1}{Y_{\max}}$, where m is equal to $\frac{k_M}{y_{VS}}$.

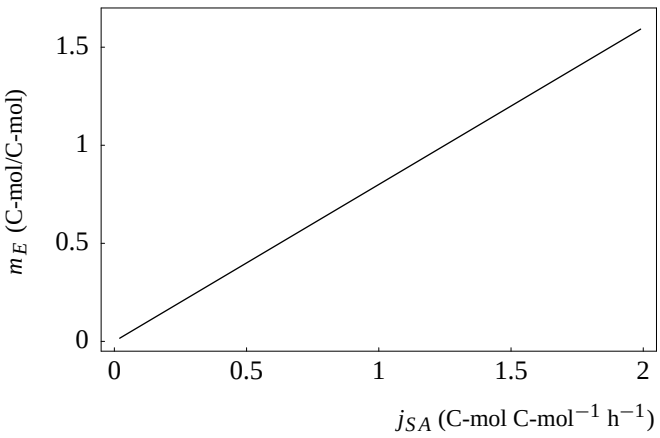

Figure 2.4: The reserve density is proportional to the uptake rate in a steady state chemostat. Parameter values: $K = 0.01$ C-mol/l, $k_E = 1$ h^{-1}, $k_M = 0.01$ h^{-1}, $y_{EV} = 0.8$ C-mol/C-mol, $y_{ES} = 0.8$ C-mol/C-mol, $S_{\text{feed}} = 2$ C-mol/h; $j_{SAm} = 2$ C-mol/(C-mol h).

- For the DEB model two yields can be defined: the yield of structural biomass and the yield of total biomass, which includes the reserves (yield in gram/C-mol substrate). The yield of total biomass is given by:

$$\frac{(m_E w_E + w_V)\,(k_E m_E - k_M y_{EV})}{j_{SAm} f\,(m_E + y_{EV})}$$

  If reserves and maintenance or reserves only are neglected, this expression reduces to the Monod or Pirt yields, respectively.

As illustrated above, the classic Monod and Pirt parameters can be expressed in terms of DEB parameters. The DEB model has more parameters than the Pirt model since it includes reserve dynamics. As stated in the previous subsections, this allows for several phenomena that the Monod and Pirt model do not account for.

2.5 Application to anaerobic ammonium oxidation

This section applies the DEB theory to anaerobic ammonium oxidation. First anaerobic ammonium oxidation is introduced. Then the overall stoichiometry of this process is taken apart into different DEB reactions. These reactions have a constant reaction stoichiometry, whereas the overall stoichiometry depends on the growth conditions. After the calculation of the stoichiometry of the DEB reactions, the overall stoichiometry at different growth rates is calculated.

2.5.1 Anaerobic ammonium oxidation

Anaerobic ammonium oxidation, or anammox, has been discovered in 1985 in a denitrifying pilot plant at Gist Brocades [12, p28] and involves the oxidation of ammonium with nitrite as electron acceptor. The reaction is carried out by a chemolitho-autotrophic planctomycete (*Brocadia anammoxidans*) [13]. This microorganism produces the reduction equivalents that it needs for the carbon dioxide fixation via the oxidation of nitrite to nitrate. In this reaction nitrite is used as electron donor. The reactions of ammonium oxidation, carbon fixation, and biomass growth are shown in Table 2.1. Although nitrite is needed as electron donor and acceptor, it is also a toxic substrate: concentrations higher than 10 mM are suboptimal and growth is inhibited at concentrations higher than 20 mM [12].

Below the macroscopic reaction of the anammox process is delineated into five DEB fluxes and consequences of growth and maintenance rates are analyzed. Although the degree of enrichment of the anammox population stabilized at 74% [12], the example below treats the anammox culture as pure, which is in growing in a steady state. It is unclear why the culture stabilized at 74% and what the function of the other 26% is [12]. The presence of other biomass is probably due to cryptic growth and the entrance of small quantities of organic carbon and sulfide into the reactor (pers. comm. M.C.M. van Loosdrecht).

2.5.2 Anammox reactions

The macroscopic reaction of overall biomass growth is not an ordinary chemical reaction, since its stoichiometry highly depends on the culture conditions and substrate availability, for example. The stoichiometric coefficients, or yields, are therefore not constant. This macroscopic reaction is delineated into five reactions with constant coefficients below.

The DEB model describes three main fluxes: assimilation, maintenance, and growth. Both the assimilation process and the growth process can be split into a catabolic and anabolic part, where the catabolic part can be regarded as overhead costs. These reactions have constant yield coefficients. It is possible to delineate the macroscopic stoichiometry with some additional knowledge: (*i*) dinitrogen gas is formed from ammonia nitrogen and nitrite nitrogen, and (*ii*) nitrogen in biomass comes from ammonium. The chemical coefficients are denoted as Y_{ij}, which are defined as ratios of fluxes. Thus Y_{ij} is negative if one of the compounds disappears and the other appears. Table 2.2 gives the five reactions and chemical indices of the nine involved compounds. The specific

Table 2.1: Reactions involved in the anaerobic ammonium oxidation.

Energy generation:
$NH_4^+ + NO_2^- \rightarrow N_2 + 2\ H_2O$
Carbon fixation:
$CO_2 + 2\ NO_2^- + H_2O \rightarrow CH_2O + 2\ NO_3^-$
Overall growth:
$1\ NH_4^+ + 1.32\ NO_2^- + 0.066\ HCO_3^- + 0.13\ H^+ \rightarrow$ $1.02\ N_2 + 0.26\ NO_3^- + 0.066\ CH_2O_{0.5}N_{0.15} + 2.03\ H_2O$

rates of each reaction are taken positive. The reactions for maintenance and for the catabolic part of growth are taken equal, since both processes burn reserves.

If **Y** denotes the matrix of yield coefficients and **n** denotes the matrix of chemical indices of the compounds, then the unknown yield coefficients can be calculated using the conservation law for the elements and charge: $\mathbf{nY} = \mathbf{0}$. This gives the yield coefficients as functions of the composition of structure and reserves. The specific rates of assimilation, maintenance, and growth are j_{EA}, j_{EM}, and j_{EG}, respectively. The specific substrate uptake rate j_{SA} equals $y_{SE}\ j_{EA}$. The flux of reserves associated with growth is $j_{EG} = y_{VE}r$. The catabolic and anabolic assimilation in Table 2.2 contain the composition parameter n_{NE}. This parameter appears in these fluxes because the stoichiometry of the corresponding reactions has been normalized with respect to the substrate NH_3 (i.e., the value of the stoichiometric coefficient of NH_3 has been set to 1).

While the yield matrix **Y** is now known, the specific rates are not, because they depend on the DEB parameter values. When **k** denotes the vector of specific rates given in Table 2.2, the specific fluxes of the nine compounds are given by **Yk**. With additional data about these fluxes, the DEB parameters can be estimated.

Strous [12] determined the macroscopic stoichiometry of the anammox process in a sequencing batch reactor under nitrite limitation in the presence of 5 mM ammonium and nitrate as well as the biomass composition. This information can be used to calculate some of the DEB fluxes. The vector of the compound-specific fluxes is denoted **j** (see Table 2.2):

$$\mathbf{j} = (j_C,\ j_{H1},\ j_H,\ j_S,\ j_N,\ j_{N3},\ j_{N5},\ j_E,\ j_V)^T$$

The production flux of reserves, j_E, equals $j_W j_{EA}/(j_{EA}+k_E)$ and the production flux of structural biomass, j_V, is $j_W k_E/(j_{EA}+k_E)$, where j_W represents the production flux of total biomass. For solving the system $\mathbf{Yk} = \mathbf{j}$, it is easier to change $\mathbf{k}$ and replace $(1-y_{VE})j_{EG}$ with $j_{EG}-r$ and $y_{VE}j_{EG}$ with r. Furthermore, the following relations are useful: $j_{EC} = j_{EG} + j_{EM}$, $r = y_{VE}j_{EG}$, $j_{EM} = y_{EV}k_M$. The system is solved using mass balances for the macroscopic reaction:

$$\begin{aligned}
0 &= j_C + j_W && \text{C balance}\\
0 &= j_C + j_{H1} + 2j_H + 3j_S + j_W n_{HW} && \text{H balance}\\
0 &= 3j_C + j_H + 2j_{N3} + 3j_{N5} + j_W n_{OW} && \text{O balance}\\
0 &= j_S + 2j_N + j_{N3} + j_{N5} + j_W n_{NW} && \text{N balance}\\
0 &= -j_C + j_{H1} - j_{N3} - j_{N5} && \text{charge balance}\\
n_{iW} &= \frac{n_{iV} + m_E\, n_{iE}}{1+m_E} && \text{for } i \in \{\text{C, H, O, N}\}
\end{aligned}$$

where m_E equals j_{EA}/k_E. The chemical composition of the biomass is a function of the constant composition of both reserves and structure and can be written as $n_{iW} = \frac{n_{iV}+m_E\, n_{iE}}{1+m_E}$ for chemical element i. The system above provides y_{SE}, n_{HV}, n_{OV}, n_{NV}, n_{OE}, j_{EA}, and j_{EG} as functions of k_E, j_W, and the composition of reserves, structure, and total biomass.

Measurements of the total-biomass composition and the macroscopic reaction give information on the amount of reserves and on the composition of reserves and structure. Here, measurements at one growth rate are used and, therefore, some parameter values cannot be obtained. The following exact stoichiometry was constructed from the overall growth stoichiometry above:

$$\begin{aligned}
&1\ NH_4^+ + 1.32\ NO_2^- + 0.0676\ HCO_3^- + 0.128\ H^+ \rightarrow\\
&1.02513\ N_2 + 0.2596\ NO_3^- + 0.0676\ CH_2O_{0.5}N_{0.15} + 2.0302\ H_2O
\end{aligned}$$

The substrate consumption rate is approximately 0.021 mol NH_3 per C-mol biomass per hour and the growth rate approximately $1.4\ 10^{-3}\ h^{-1}$. The following parameters have been assigned a value: $k_E = 0.0127\ h^{-1}$, $y_{VE} = 0.8$ C-mol/C-mol, $n_{HE} = 2$, $n_{NE} = 0.25$. Indeed, the limiting (DEB) reserves are proteinaceous and often the N content of the reserves is higher than that of the structural biomass (*cf.* [4]). The other parameters, including those relating to the composition of reserves and structure, are known from the overall stoichiometry and the five DEB reactions. With the fixed and estimated parameter values, the fluxes of the compounds, **j**, involved in the macroscopic growth

reaction are expressed as a function of the growth rate. Figure 2.5 shows all fluxes as functions of the growth rate.

The macroscopic reaction of the anammox process with non-constant coefficients was delineated into five DEB reactions with constant coefficients. The use of catabolic and anabolic reactions for the assimilation and growth is possible because the energy generating reaction is known and the catabolic growth reaction equals the maintenance reaction. The stoichiometry of the overall growth reaction consists of the five DEB reactions. As can be seen in Table 2.2, ammonium is used in energy generation but also produced from nitrite in the growth and maintenance processes. This means that in transient situations, where the rate of ammonium oxidation is reduced, a nett production of ammonium can take place.

The estimation of parameter values above assumes that steady-state growth is possible and that the assimilation, maintenance, and growth reactions do not change as a function of the nutrient concentrations or the growth rate. Given these assumptions, the stoichiometry of the reactions at different growth rates is known, as shown in Table 2.3. Furthermore, this table shows the differences in total-biomass composition for different growth rates.

Table 2.2: The yield coefficients (transposed matrix, $\mathbf{Y}^T$, upper panel) and the chemical indices (lower panel) for the nine compounds that are involved in the five transformations by anammox bacteria. Following microbiological tradition, substrate is chosen as reference in the yield coefficients: ammonium for assimilation, and reserves for maintenance and growth. The yield coefficients follow from the conservation law for elements. The DEB theory provides the specific rates j_{EA}, j_{EM}, and j_{EG} (see text). Note that the yield coefficients for the catabolic aspect of growth equal those for maintenance.

symbol	processes	C: HCO_3^-	H_1: H^+	H: H_2O	S: NH_3	N: N_2	N_3: NO_2^-	N_5: NO_3^-	E: reserve	V: structure	specific rates
A_C	assim. (cat.)	0	–1	2	–1	1	–1	0	0	0	$(y_{SE} - n_{NE})\, j_{EA}$
A_A	assim. (ana.)	Y^A_{CS}	$Y^A_{H_1S}$	Y^A_{HS}	–1	0	$Y^A_{N_3S}$	$-Y^A_{N_3S}$	$-Y^A_{CS}$	0	$n_{NE}\, j_{EA}$
M	maintenance	1	$Y^M_{H_1E}$	Y^M_{HE}	Y^M_{SE}	0	$Y^M_{N_3E}$	0	–1	0	j_{EM}
G_C	growth (cat.)	1	$Y^M_{H_1E}$	Y^M_{HE}	Y^M_{SE}	0	$Y^M_{N_3E}$	0	–1	0	$(1 - y_{VE})\, j_{EG}$
G_A	growth (ana.)	0	$Y^G_{H_1E}$	Y^G_{HE}	Y^G_{SE}	0	$Y^G_{N_3E}$	0	–1	1	$y_{VE}\, j_{EG}$
C	carbon	1	0	0	0	0	0	0	1	1	
H	hydrogen	1	1	2	3	0	0	0	n_{HE}	n_{HV}	
O	oxygen	3	0	1	0	0	2	3	n_{OE}	n_{OV}	
N	nitrogen	0	0	0	1	2	1	1	n_{NE}	n_{NV}	
$+$	charge	–1	1	0	0	0	–1	–1	0	0	

Table 2.3: The overall anammox stoichiometry at different growth rates. The coefficient of ammonia is taken unity. The specific rate of nett ammonia uptake provides information on the reaction rate. The reserve density required to calculate the total-biomass composition is $m_E = y_{EV}\frac{r+k_M}{k_E-r}$
Parameters values used (* indicates parameter values that were chosen):
n_{HE} = 2*, n_{OE} = 0.459, n_{NE} = 0.250*, n_{HV} = 2, n_{OV} = 0.510, n_{NV} = 0.125, y_{VE} = 0.80*, y_{SE} = 8.80, k_E = 0.0127* h^{-1}, k_M = 0.000811 h^{-1}, r_{max} = 0.003 h^{-1}.

	C: HCO_3^-	H_1: H^+	H: H_2O	S: NH_3	N: N_2	N_3: NO_2^-	N_5: NO_3^-	E: reserve	V: structure	j_{SA}: specific rate
$r = 0$	0	–1.18	2.09	–1	1.09	–1.46	0.277	0	0	0.00794
$r = 0.1\,r_{max}$	–0.0291	–1.16	2.07	–1	1.06	–1.40	0.269	0.00294	0.0262	0.0114
$r = r_{max}$	–0.0845	–1.11	2.01	–1	1.01	–1.28	0.255	0.0278	0.0567	0.0530

	total-biomass composition
$r = 0$	$CH_2O_{0.51}N_{0.13}$
$r = 0.1\,r_{max}$	$CH_2O_{0.50}N_{0.14}$
$r = r_{max}$	$CH_2O_{0.49}N_{0.17}$

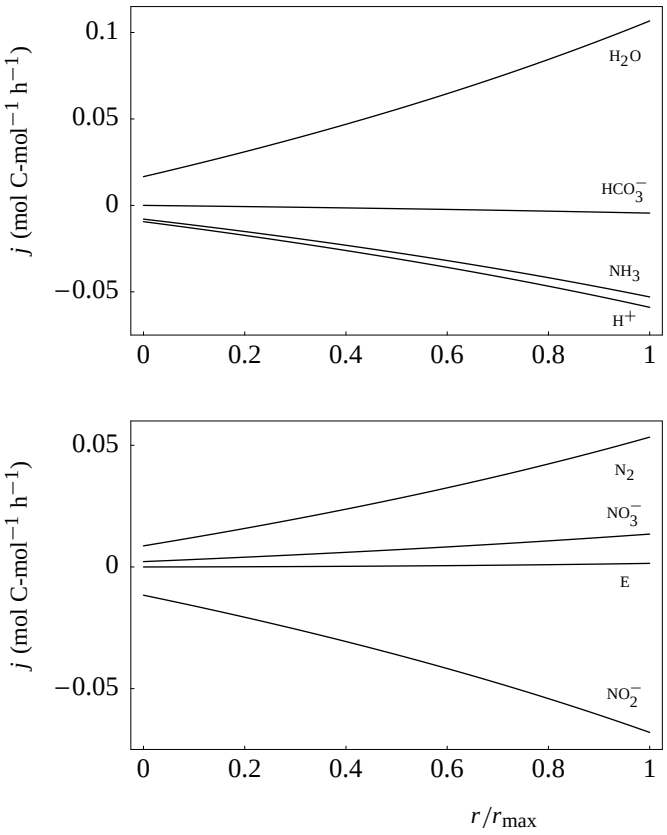

Figure 2.5: The specific fluxes of the compounds as a function of the scaled specific growth rate of the anammox bacteria. The maximum specific growth rate is 0.003 h^{-1}. Parameters: $k_E = 0.0127$ h^{-1}, $k_M = 0.000811$ h^{-1}, $y_{SE} = 8.80$, $y_{VE} = 0.8$ C-mol/C-mol reserve. Composition parameters: $n_{HE} = 2, n_{OE} = 0.46, n_{NE} = 0.25, n_{HV} = 2, n_{OV} = 0.51, n_{NV} = 0.125$.

2.5.3 Alternative anammox reactions

Nitrite is used as electron acceptor in all five reactions above. During the growth and maintenance processes described in Table 2.2 nitrite is reduced to ammonium. Bacteria transform or burn reserve material, which results in a nitrogen waste flux. Most bacteria and animals produce ammonium during this process and the oxidation of biomass itself also produces ammonium. Furthermore, anammox produces one molecule dinitrogen gas from one molecule ammonium and one molecule nitrite. The production of dinitrogen gas in other reactions would bias the stoichiometry of N_2 production, depending on the relative values of the the five fluxes. The reasoning above underlies the stoichiometry as presented in Table 2.2.

Discussions with Marc van Loosdrecht resulted in two different pathways for these reactions. In this section extra knowledge on denitrifying bacteria is used. Reduction of nitrite to ammonium seems unlikely, because the presence of ammonium in the medium probably inhibits it. This leaves two alternative reactions, which both (slightly) change the stoichiometry of dinitrogen formation. For the maintenance process all three possible reactions are:

$$CH_{n_{HE}}O_{n_{OE}}N_{n_{NE}} + a\ NO_2^- + b\ H_2O \rightarrow (a + n_{NE})\ NH_3 + HCO_3^- + c\ H^+$$

$$CH_{n_{HE}}O_{n_{OE}}N_{n_{NE}} + a\ NO_2^- + b\ H_2O \rightarrow (a + n_{NE})\ N_2 + HCO_3^- + c\ H^+$$

$$CH_{n_{HE}}O_{n_{OE}}N_{n_{NE}} + a\ NO_2^- + b\ H_2O \rightarrow \tfrac{a}{2}\ N_2 + n_{NE}\ NH_3 + HCO_3^- + c\ H^+$$

The first reaction was used in the subsection above. The second reaction involves the formation of dinitrogen gas from the reserve-nitrogen and nitrite. Only anammox bacteria can carry out this transformation. Other denitrifyers cannot produce dinitrogen from ammonium and nitrite, but reduce nitrite to dinitrogen and reserve-nitrogen to ammonium.

With the alternative transformation, illustrated by the second reaction above, a matrix similar to Table 2.2 was constructed (see Table 2.4). The influences on the DEB fluxes were evaluated as before. Again, the overall stoichiometry in combination with the five DEB fluxes provides information on the composition of reserves and structure. In this case n_{HE} and n_{OE} had to be fixed. These parameters have the same values as in the previous example. This implies that the overall stoichiometry and the biomass composition hardly change. Table 2.5 shows the results for the alternative reaction. The plots of the fluxes as functions of the growth rate are very similar to Figure 2.5.

Table 2.4: The yield coefficients (transposed matrix, $\mathbf{Y}^T$, upper panel) and the chemical indices (lower panel) for the nine compounds that are involved in the five transformations by anammox bacteria. In the reactions for maintenance and growth, nitrite is not reduced to ammonium but to dinitrogen gas. The DEB theory provides the specific rates j_{EA}, j_{EM}, and j_{EG} (see text). Note that the yield coefficients for the catabolic aspect of growth equal those for maintenance.

symbol	processes	C: HCO_3^-	H_1: H^+	H: H_2O	S: NH_3	N: N_2	N_3: NO_2^-	N_5: NO_3^-	E: reserve	V: structure	specific rates
A_C	assim. (cat.)	0	–1	2	–1	1	–1	0	0	0	$(y_{SE} - n_{NE})\, j_{EA}$
A_A	assim. (ana.)	Y^A_{CS}	$Y^A_{H_1S}$	Y^A_{HS}	–1	0	$Y^A_{N_3S}$	$-Y^A_{N_3S}$	$-Y^A_{CS}$	0	$n_{NE}\, j_{EA}$
M	maintenance	1	$Y^M_{H_1E}$	Y^M_{HE}	0	Y^M_{NE}	$Y^M_{N_3E}$	0	–1	0	j_{EM}
G_C	growth (cat.)	1	$Y^M_{H_1E}$	Y^M_{HE}	0	Y^M_{NE}	$Y^M_{N_3E}$	0	–1	0	$(1 - y_{VE})\, j_{EG}$
G_A	growth (ana.)	0	$Y^G_{H_1E}$	Y^G_{HE}	0	Y^G_{NE}	$Y^G_{N_3E}$	0	–1	1	$y_{VE}\, j_{EG}$

C	carbon	1	0	0	0	0	0	0	1	1	
H	hydrogen	1	1	2	3	0	0	0	n_{HE}	n_{HV}	
O	oxygen	3	0	1	0	0	2	3	n_{OE}	n_{OV}	
N	nitrogen	0	0	0	1	2	1	1	n_{NE}	n_{NV}	
$+$	charge	–1	1	0	0	0	–1	–1	0	0	

Table 2.5: The overall anammox stoichiometry at different growth rates. The coefficient of ammonia is taken unity. The specific rate of nett ammonia uptake provides information on the reaction rate.
Parameters values used (* indicates parameter values that were chosen):
n_{HE} = 2*, n_{OE}= 0.46*, n_{NE} = 0.249, n_{HV} = 2, n_{OV} = 0.510, n_{NV} = 0.125, y_{VE} = 0.80*, y_{SE} = 8.34, k_E= 0.0127* h^{-1}, k_M= 0.000811 h^{-1}, r_{max} = 0.003 h^{-1}.

	C: HCO_3^-	H_1: H^+	H: H_2O	S: NH_3	N: N_2	N_3: NO_2^-	N_5: NO_3^-	E: reserve	V: structure	j_{SA}: specific rate
$r = 0$	0	–1.17	2.09	–1	1.09	–1.43	0.260	0	0	0.00846
$r = 0.1\,r_{max}$	–0.0281	–1.15	2.06	–1	1.06	–1.39	0.260	0.00283	0.0253	0.0119
$r = r_{max}$	–0.0860	–1.12	2.01	–1	1.01	–1.29	0.260	0.0283	0.0576	0.0520

	total-biomass composition
$r = 0$	$CH_2O_{0.51}N_{0.13}$
$r = 0.1\,r_{max}$	$CH_2O_{0.50}N_{0.14}$
$r = r_{max}$	$CH_2O_{0.49}N_{0.17}$

Nomenclature

The following symbols are used for the dimensions: –, no dimension; t, time; l, length; #, amount (number or mol).

Symbol	Description	Dimension
e	scaled reserve density (m_E/m_{Em})	–
J_{ik}	flux of compound i in process k	$\#t^{-1}$
J_{SA}	flux of substrate associated with assimilation	$\#t^{-1}$
J_{EA}	flux of reserves associated with assimilation	$\#t^{-1}$
J_{EC}	flux of reserves associated with catabolism	$\#t^{-1}$
j_{ik}	specific flux of compound i associated with process k	$\#\#^{-1}t^{-1}$
j_E	structure-specific production flux of reserves	$\#\#^{-1}t^{-1}$
j_{EA}	specific flux of reserves associated with assimilation	$\#\#^{-1}t^{-1}$
j_{EG}	specific flux of reserves associated with growth	$\#\#^{-1}t^{-1}$
j_{EM}	specific flux of reserves associated with maintenance	$\#\#^{-1}t^{-1}$
j_{SA}	specific flux of substrate associated with assimilation	$\#\#^{-1}t^{-1}$
j_{SAm}	maximum specific substrate assimilation flux (max. specific substrate consumption rate)	$\#\#^{-1}t^{-1}$
j_V	structure-specific production flux of structure	$\#\#^{-1}t^{-1}$
j_W	structure-specific production flux of total biomass	$\#\#^{-1}t^{-1}$
k_E	reserve turnover rate	t^{-1}
k_M	maintenance rate coefficient	t^{-1}
m_E	molar reserve density	$\#\#^{-1}$
m_{Em}	maximum molar reserve density	$\#\#^{-1}$
M_E	amount of reserves	#
n_{ik}	number of atoms of element i present in compound k	$\#\#^{-1}$
r	specific growth rate	t^{-1}
S	substrate concentration	$\#l^{-3}$
w_V	molar weight of structure	$m\#^{-1}$
w_E	molar weight of reserves	$m\#^{-1}$
X	biomass concentration	$\#l^{-3}$
y_{ik}	stoichiometric coefficient (coupler): compound i needed per compound k formed	$\#\#^{-1}$
y_{SE}	substrate needed per reserves formed	$\#\#^{-1}$
y_{EV}	reserves needed per structure formed	$\#\#^{-1}$
y_{SV}	substrate needed per structure formed	$\#\#^{-1}$

Acknowledgements

I thank Mark van Loosdrecht and Marc Strous for information on the anammox process.

References

[1] Beun JJ. (2001). *PHB metabolism and N-removal in sequencing batch granular sludge reactors*. PhD thesis, Delft University of Technology.

[2] Button DK. (1991). Biochemical basis for whole-cell uptake kinetics: specific affinity, oligotrophic capacity, and the meaning of the Michaelis constant. *Applied and Environmental Microbiology* 57:2033–2038.

[3] Droop MR. (1975). The nutrient status of algal cells in batch culture. *Journal of the Marine Biological Association of the United Kingdom* 55:541–555.

[4] Hanegraaf PPF. (1997). *Mass and energy fluxes in microorganisms according to the Dynamic Energy Budget theory for filaments*. PhD thesis, Vrije Universiteit, Amsterdam, The Netherlands.

[5] Herbert D. (1958). Some principles of continuous culture. In: Tunevall G, editor. *Recent progress in microbiology*, pp. 381–396. Almquist & Wiksell, Stockholm.

[6] Kooi BW, Kooijman SALM. (1994). Existence and stability of microbial prey-predator systems. *Journal of Theoretical Biology* 170:75–85.

[7] Kooijman SALM. (2000). *Dynamic Energy and Mass Budgets in Biological Systems*. Cambridge University Press, Cambridge, second edition.

[8] Marr AG, Nilson EH, Clark DJ. (1963). The maintenance requirement of *Escherichia coli*. *Annals of the New York Academy of Sciences* 102:536–548.

[9] Monod J. (1958). *Recherches sur la croissance des cultures bactériennes*. Hermann, Paris, second edition. Thèse de 1942.

[10] Mulder MM. (1988). *Energetic aspects of bacterial growth: a mosaic non-equilibrium thermodynamic approach*. PhD thesis, Universiteit van Amsterdam, The Netherlands.

[11] Pirt SJ. (1965). The maintenance energy of bacteria in growing cultures. *Proceedings of the Royal Society of London B (Biological Sciences)* 163:224–231.

[12] Strous M. (2000). *Microbiology of anaerobic ammonium oxidation*. PhD thesis, Delft University of Technology.

[13] Strous M, Fuerst JA, Kramer EHM, Logemann S, Muyzer G, van de Pas-Schoonen KT, Webb R, Kuenen JG, Jetten MSM. (1999). Missing lithotroph identified as a new planctomycete. *Nature (London)* 400:446–449.

3

Two parameters account for the flocculated growth of microbes in biodegradation assays

Abstract

Microbes in activated sludge tanks mostly occur in flocs rather than in cell suspensions. Flocculation results in a limited supply of substrate to the bacteria inside the flocs, which reduces the biodegradation rate of organic compounds by several orders of magnitude. This chapter presents a simple two-parameter extension of growth models for cell suspensions to account for the ensuing reduction of the degradation rate. The additional parameters represent floc size at division and diffusion length. The biomass of small flocs initially increases exponentially at a rate equal to that of cell suspensions. After this first phase, the growth rate gradually decreases and finally the radius becomes a linear function of time. At this time flocs are large and have a kernel of dead biomass. This kernel arises when the substrate concentration decreases below the threshold level at which cells are just able to pay their maintenance costs. We deduce an explicit approximative expression for the interdivision time of flocs, and thereby for the growth of flocculated microbial biomass at constant substrate concentrations. The model reveals that the effect of stirring on degradation rates occurs through a reduction of the floc size at division. The results can be applied in realistic biodegradation quantifications in activated sludge tanks as long as substrate concentrations change slowly.

3.1 Introduction

Biodegradation of household chemicals primarily takes place by activated sludge in wastewater treatment plants (WWTPs). The quantification of this biodegradation process is important in judging and developing household chemicals.

A lot of data on biodegradation rates relate to free cell suspensions. However, it would not be realistic to use these rates for WWTPs, because most biomass present in these systems is coagulated and only a thin outer layer of the aggregates is metabolically active. This substantially reduces degradation rates.

Microorganisms in activated sludge mainly exist in floccules (flocs). Flocculation depends on the ability of cells themselves to form flocs, on cell density, and on favorable hydrodynamic shear forces. Mixing regime and cell density determine the collision frequency of cells and fragments, which, in combination with a sticking probability, determines the rate of floc formation.

Floc sizes have a wide range in continuous activated sludge processes. For instance, Knudson *et al.* (1982) observed flocs with sizes from 0.5 to 1000 μm, with most of the flocs being smaller than 100 μm. In contrast, Zhang *et al.* (1997) found that 77% of the flocs were larger than 100 μm. Sizes ranging from 400 μm to 4 mm were also reported [10]. Flocs of brewers' yeast during fermentation were found ranging in size from 60 μm to 400 μm [18].

The average mass-transfer rate from the bulk fluid to individual bacteria reduces with floc size. This results in a decrease in the biodegradation rate of organic compounds of several orders of magnitude compared with that by cell suspensions. Growth rates of cell suspensions cannot easily be used to predict growth rates of flocs. However, such a prediction may help to link degradation rates by flocs to those by cell suspensions.

In this chapter, we present a mathematical model for the growth of floc suspensions in terms of that of free cell suspensions. In order to describe mass-transfer and microbial activity, we assume a simple spherical floc geometry. We use this floc growth model to analyze the biodegradation of compounds in activated sludge, and show how the maximum floc size affects the degradation rates.

The combination of diffusion-limited degradation and microbial floc growth is new, to our knowledge, although rather complex models exist for some of the underlying processes. Winkler (1981) and Du *et al.* (1996), for instance, described the degradation by flocs, but did not account for growth. Logan and Wilkinson (1991) used fractal geometry to describe the floc structure accurately; the fractal dimension of flocs has been found to be around

2.5 [10, 16, 18, 21]. Zartarian *et al.* (1997) modeled the three-dimensional activated sludge floc structure using 'discrete smooth interpolation' of digitized microtome sections. Their method makes it possible to quantify size, surface area, and volume of the floc. These rather detailed models of floc geometry are too complex to be useful for implementation in a dynamic context, where substrate concentration and biomass densities change simultaneously. The few useful and scattered data on degradation do not contain information enough to extract the large amount of required parameter values.

The combination of diffusion-limited uptake and growth also occurs in tumor biology. Detailed quantitative and potentially useful descriptions have been formulated in this field of related interest [3, 13, 19]. These models, however, are too complex to be applied in degradation studies.

Substrate availability, advective, and diffusive transport are important factors influencing the induction of biodegradative pathways as well as the biodegradation of chemicals themselves [5]. An incorporation of these factors in degradation studies would improve their realism.

Our aim is to study the reduction of mass-transfer rates due to the coagulation of bacteria and its implications for both biodegradation rates and growth rates. We clearly distinguish the different levels of organization: the individual cells in a floc, the floc as a 'super individual,' and the population of flocs in a reactor. The population model includes 'birth and death' of flocs. After disintegration of a floc, the fragments will start to form new aggregates or serve as substrate for other microbes. Ciliates, for example, could attack individual bacteria.

In the following sections we present a simplified model for diffusion-limited growth of individual flocs. Thereafter, we evaluate the growth of flocculated microbial biomass in a reactor and the degradation of substrate according to this model.

3.2 Approximative growth of flocs

The irregular floc structure is approximated by a sphere. This geometry defines the relationship between the growth of active microbial biomass in the outer shell of the floc and the generation of dead mass in the kernel. Although the detailed growth of this idealized floc must be evaluated numerically (partial differential equations), approximations can be given when a steady-state substrate concentration profile builds up in the floc. Such a steady state can be expected if growth is slow enough with respect to diffusive transport. We take the volume-specific amount of biomass (mass/volume) within the floc to

be constant, which entails that the floc expands if biomass increases.

Cells are assumed to die when they cannot pay their maintenance costs. Hence, our approach to the growth of flocs involves a growth model for individual cells that accounts for maintenance costs. The well-known Marr-Pirt model [11, 14] provides the simplest way to take these costs into account. A more realistic but also a somewhat more complex one is given by the Dynamic Energy Budget theory, which is based on mechanistic rules for the uptake and use of substrates by organisms [4, 9].

A spherical floc of radius $L_T(t)$ has a volume of $V_T(t) = \frac{4}{3}\pi L_T(t)^3$. Let L_M denote the maximum thickness of the living layer (Figure 3.1). Index M relates to the fact that living mass requires maintenance. For a floc without a dead kernel $L_T \leq L_M$ holds. In this case we assume that a floc grows exponentially at rate r, thus:

$$\frac{dV_T}{dt} = r\,V_T \tag{3.1}$$

However, when the floc consists of a dead core and an outer living layer, the following equation gives the change in total volume:

$$\frac{d}{dt}V_T(t) = \frac{d}{dt}[V_M(t) + V_\dagger(t)] = r\,V_M(t) \tag{3.2}$$

where V_M and $V_\dagger$ denote the volume of living and dead biomass, respectively. Living volume relates to total floc radius as:

$$V_M(t) = \frac{4}{3}\pi\left[L_T(t)^3 - (L_T(t) - L_M)^3\right] = 4\pi\left[L_T(t)^2 L_M - L_T(t)L_M^2 + \frac{L_M^3}{3}\right]$$

Furthermore, from the fact that the dead kernel has a radius $L_T - L_M$, it is easy to deduce:

$$\frac{dV_\dagger}{dt} = 4\pi(L_T - L_M)^2\frac{dL_T}{dt}$$

Substitution of the expressions for $V_T(t)$ and $V_M(t)$ in the differential equations (3.1) and (3.2) leads to the equation describing the change in floc radius:

$$\frac{d}{dt}L_T = \begin{cases} \frac{r}{3}L_T & \text{for } L_T \leq L_M \\ r\,L_M\left(1 - \frac{L_M}{L_T} + \frac{L_M^2}{3L_T^2}\right) & \text{for } L_T > L_M \end{cases} \tag{3.3}$$

For a floc without a dead kernel, we have $L_T \leq L_M$. The thickness of the living layer increases up to its maximum value, L_M, which is associated

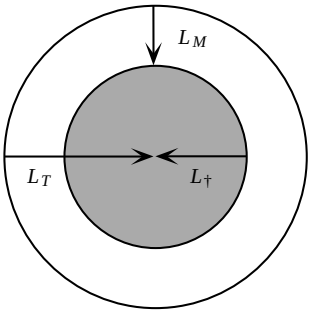

Figure 3.1: Length indications of a floc. L_T: total radius. L_M: maximum thickness of the living layer. $L_\dagger$: radius of the dead kernel.

with a given substrate concentration in the environment. The floc continues to grow; thus, L_T still increases and a dead kernel appears. For $L_T \gg L_M$, the growth rate of floc radius becomes constant, that is, the cube root of floc volume increases linearly with time. This has been known for a long time [2], and also applies to tumors [12, 17], and mammalian fetuses [7, 9], for the same reason: mass exchange between a (living) structure and its environment occurs across its surface area.

When a floc develops an increasing dead kernel, it eventually becomes mechanically unstable and falls apart. This event depends on turbulent shear forces and on the size and porosity of the floc [15, 18]. The porosity generally changes with size and thus with age of the floc. However, we refrain from modeling these details and assume that the floc falls apart at a given volume V_d, which depends on environmental conditions. We denote the radius at division as L_d.

At fragmentation of the floc, the dead material becomes suspended and the living shell falls apart into n small flocs without a dead kernel (Figure 3.2). We suppose that the living shell partitions into daughter flocs without changing thickness, which implies that these newly formed flocs have a radius of $L_b = \frac{1}{2}L_M$ for $L_d \geq L_M$ (if $L_d < L_M$, $L_b = \frac{1}{2}L_d$). The number of daughter flocs per mother floc is thus:

$$n = \begin{cases} \frac{L_d^3}{L_b^3} & \text{for } L_\dagger = 0 \\ 8\frac{L_d^3 - L_\dagger^3}{L_M^3} = 8\frac{3L_d^2 - 3L_d L_M + L_M^2}{L_M^2} & \text{for } L_\dagger > 0. \end{cases}$$

The growth equation (3.3) can be solved explicitly for the interdivision

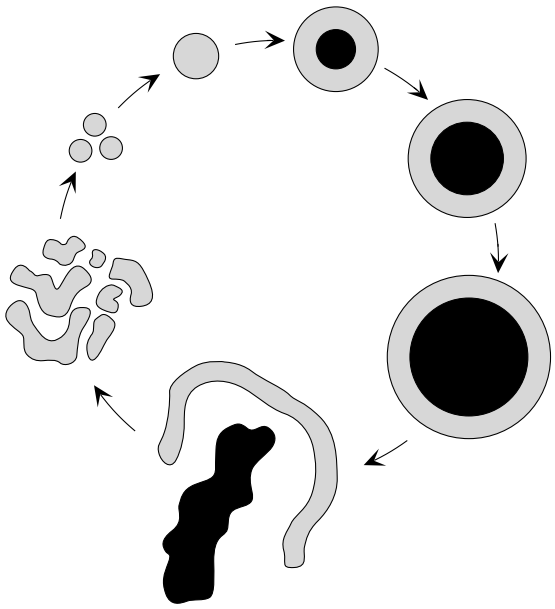

Figure 3.2: Life cycle of a floc. The floc starts to grow with a diameter equal to the maximum thickness of the living layer ($L_b = \frac{1}{2}L_M$), develops a dead kernel (indicated in black) and disintegrates. The biomass in the living layer is redistributed to new flocs.

time t_d of flocs. For $l_d^* = \frac{L_d}{L_M}$ we obtain:

$$rt_d = \begin{cases} 3\ln 2 & \text{for } l_d^* \leq 1 \\ 3\ln 2 - 1 + l_d^* - \frac{\pi}{3\sqrt{3}} + \frac{1}{\sqrt{3}} \arctan\left(\sqrt{3}(2l_d^* - 1)\right) & \\ \quad + \frac{1}{2}\ln\left(1 - 3l_d^* + 3{l_d^*}^2\right) & \text{for } l_d^* > 1 \end{cases} \tag{3.4}$$

The values of r, L_M (thus also of n, l_d^* and t_d) depend on the substrate concentration S. The specific growth rate of the floc population, r_F, is given by:

$$r_F(S) = \frac{\ln n(S)}{t_d(S)} \tag{3.5}$$

The equations above quantify the relationship between the specific growth rate of flocs and that of free cells via the interdivision time:

$$\frac{r_F(S)}{r} = \frac{\ln n(S)}{rt_d(S)} \tag{3.6}$$

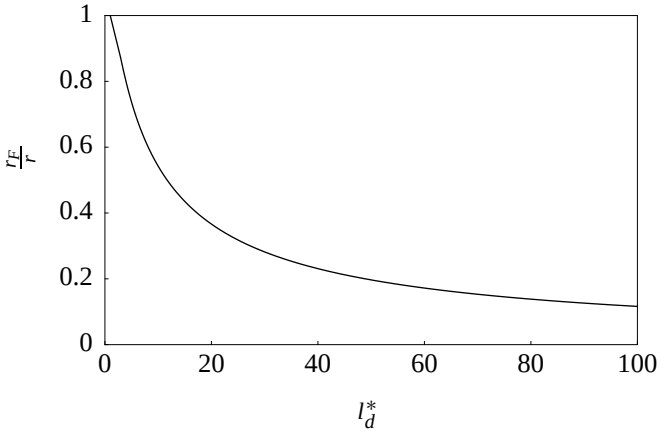

Figure 3.3: The scaled specific growth rate of flocs ($\frac{r_F}{r}$) as a function of its scaled radius at division ($l_d^* = \frac{L_d}{L_M}$). The specific growth rate of small flocs equals the specific growth rate of suspended cells.

Figure 3.3 shows the ratio of r_F to r as a function of the size at division l_d^*. Figure 3.4 shows the specific population growth rate r_F as a function of the scaled substrate concentration. The specific growth rate of suspended cells, r, required to calculate r_F, is given by the assumed cell growth model. In the Appendix an expression for the growth rate of a floc is derived, using the Dynamic Energy Budget theory to describe cell dynamics.

The maximum thickness of the living layer, which is needed to calculate n, follows from a closer analysis of the substrate concentration profile in the floc. This subject is addressed in the next section.

3.3 Steady-state substrate profiles

In this section we analyze the steady-state substrate profiles in a floc. We start with introducing a number of parameters and equations. The analysis results in an equation to calculate the maximum thickness of the living layer, L_M.

A large floc of radius L_T consists of a living layer of thickness L_M around a dead kernel of radius $L_\dagger$, that is, $L_T = L_M + L_\dagger$. Let $S(L)$ denote the substrate concentration along the radius of a sphere, where $L = 0$ corresponds with the surface and $L = L_T(t)$ corresponds with the center of the sphere. Let $f(L) = \frac{S(L)}{K+S(L)}$ be the scaled functional response, with saturation coefficient K. The term functional response was originally conceived in ecology and relates consumption rate to food density (e.g., Holling, 1959). We obtain a

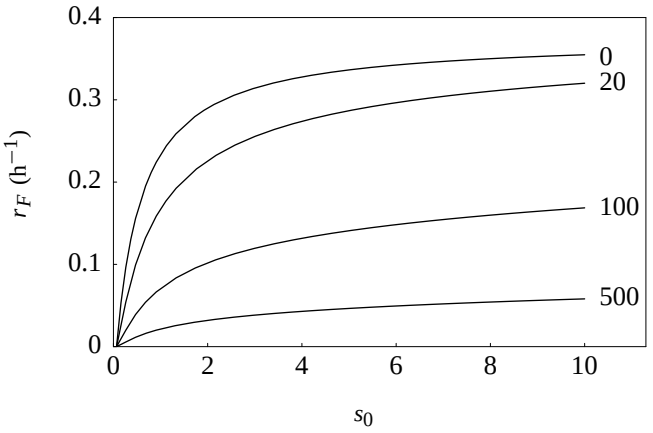

Figure 3.4: The specific growth rate of flocs as a function of the scaled bulk substrate concentration. The numbers next to the curves indicate the length at division as fraction of diffusion length. The specific growth rate of cells according to the DEB theory is $r = \frac{k_E f - k_M g}{f+g}$ (Appendix). The minimum scaled substrate concentration $s_\dagger$, found by solving $r = 0$, equals $\frac{k_M}{k_E/g - k_M}$ (with $k_E = 0.8\,\mathrm{h}^{-1}$, $k_M = 0.05\,\mathrm{h}^{-1}$, $g = 1$).

scaled functional response by dividing a functional response by its maximum value. The function f defined above also appears in the Monod equations. Within the floc, $f(L)$ decreases from a relative high value at $L = 0$ to some threshold value at the edge of the dead kernel. Inside the (increasing) dead kernel the substrate concentration, and consequently the functional response, is uniform.

The scaled functional response at the edge of the dead kernel is $f_\dagger = f(L_M)$. At this position, the biomass can just pay its maintenance costs and therefore the growth rate is zero. This means that the substrate assimilation rate equals the maintenance rate. The scaled functional response multiplied by the maximum assimilation rate yields the amount of energy which is taken up. Thus, $f_\dagger [p_{Am}] - [p_M] = 0$, where $[p_{Am}]$ is the volume-specific maximum assimilation rate and $[p_M]$ the volume-specific maintenance rate [9]. Hence, the value of $f_\dagger$ follows from solving $r = 0$, where r is the specific growth rate of cells. The substrate concentration at the edge of the dead kernel is $S_\dagger = S(L_M) = s_\dagger K$, where $s_\dagger = \frac{f_\dagger}{1-f_\dagger}$.

Now we are able to calculate the minimum substrate concentration that is needed to support life. The position L_M, where this concentration $S_\dagger$ is reached, is calculated from the substrate concentration profile. This is the solution of equation (3.7), which describes the diffusion in a sphere. Since

biomass takes up substrate, a consumption term ($f(L,t)\,j_{SAm}X_F$) is present in this equation. The factor $(L_T - L)^2$ appears because the coordinate origin is located on the surface of the sphere.

$$\frac{\partial}{\partial t}S(L,t) = \frac{D}{(L_T - L)^2}\,\frac{\partial}{\partial L}\left\{(L_T - L)^2\frac{\partial}{\partial L}S(L,t)\right\} - f(L,t)\,j_{SAm}X_F \tag{3.7}$$

X_F denotes the biomass density in the floc (C-mol/volume), j_{SAm} the maximum mass-specific substrate uptake rate for biomass, and D the substrate diffusion coefficient. The initial condition $S(L,0)$ and the boundary condition $S(0,t)$ are assumed to be given. The derivative of the substrate concentration with respect to L in the center of the floc or at the edge of the dead kernel is zero; that is, $\frac{\partial}{\partial L}S(L_T,t) = 0$ or $\frac{\partial}{\partial L}S(L_M,t) = 0$.

Let the substrate concentration in the environment be constant and let growth be slow with respect to the change in the substrate profile. Let L_D denote the 'diffusion length,'

$$L_D = \sqrt{\frac{DK}{j_{SAm}X_F}}.$$

At steady state $\frac{\partial}{\partial t}S = 0$ and $S(L,t)$ is constant in time. In this case, substitution of the dimensionless scaled length $l = \frac{L}{L_D}$ and the scaled functional response $f(l) = \frac{s(l)}{s(l)+1}$ in equation (3.7) yields:

$$0 = \frac{1}{(l_T - l)^2}\,\frac{d}{dl}\left\{(l_T - l)^2\frac{ds}{dl}\right\} - f(l) \tag{3.8}$$

with boundary conditions $s(0) = s_0$ and $\frac{d}{dl}s(l_M) = 0$. The latter condition results in $s(l_M) = s_\dagger$ if $l_T > l_M$.

The steady-state substrate profile can be further simplified if $(l_T - l) \gg 2\frac{d}{dl}s$. This occurs, for instance, if the curvature of the floc surface is negligibly small. Equation (3.8) then reduces to:

$$0 = \frac{d^2s}{dl^2} - f(l)$$

The implicit solutions for the profiles of the scaled substrate concentration (s)

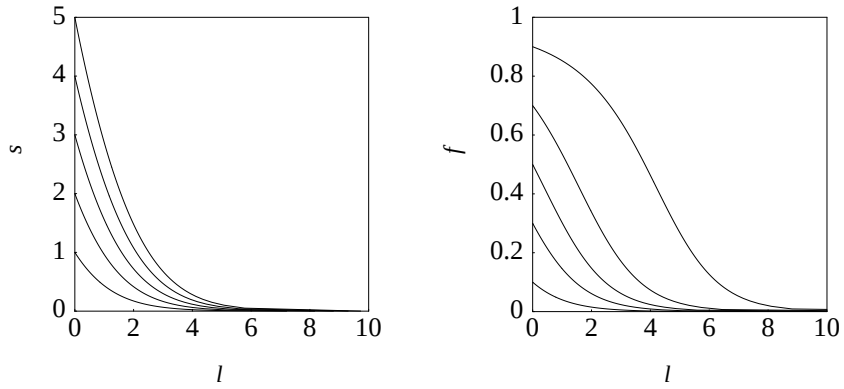

Figure 3.5: The profiles of scaled substrate concentration ($s = \frac{S}{K}$) and scaled functional response ($f = \frac{s}{1+s}$) in the floc for various choices of substrate concentrations in the environment (with $s_\dagger = 0$).

and the scaled functional response (f) are:

$$l(s) = \frac{1}{\sqrt{2}} \int_s^{s_0} \frac{dy}{\sqrt{y - s_\dagger + \ln \frac{1+s_\dagger}{1+y}}}$$

$$l(f) = \frac{1}{\sqrt{2}} \int_f^{f_0} \frac{dz}{(1-z)^2 \sqrt{\frac{z}{1-z} - \frac{f_\dagger}{1-f_\dagger} + \ln \frac{1-z}{1-f_\dagger}}}$$

This directly leads to the scaled maximum thickness of the living layer:

$$l_M(s_\dagger) = 2^{-1/2} \int_{s_\dagger}^{s_0} \left\{ y - s_\dagger + \ln \frac{1+s_\dagger}{1+y} \right\}^{-1/2} dy \tag{3.9}$$

Figure 3.5 illustrates the s- and f-profiles. Figure 3.6 shows the scaled thickness of the living layer l_M as a function of the scaled substrate concentration.

In the present section we carried out a study of the concentration profile inside the floc and obtained an expression for the maximum thickness of the living layer, equation (3.9). The value of L_M ($= l_M L_D$) is required in the previous section to calculate the interdivision time of flocs, equation (3.4), given that r is the specific growth rate of cells. Nevertheless, a direct substitution of L_M into equation (3.4) gives an overestimation of the floc population growth rate. This overestimation is due to the gradual decrease in the specific growth rate of individual cells from the surface of the floc to the edge of the dead kernel. The derivation of l_M does not account for the decreasing curvature of the growing floc, which gives rise to an error in the opposite direction.

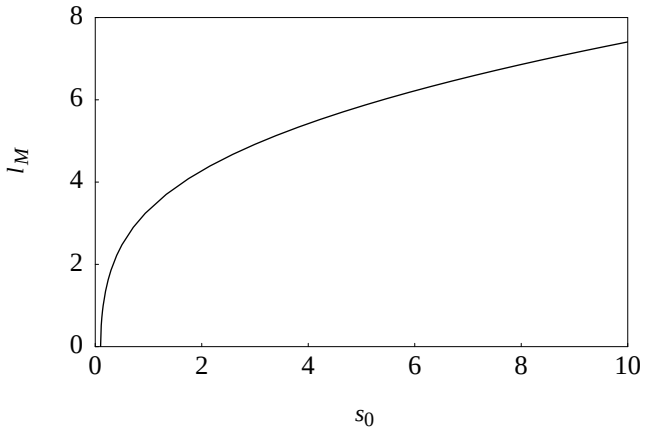

Figure 3.6: The relation between the scaled thickness of the living layer and the scaled bulk substrate concentration. The minimum scaled substrate concentration for support ($s_\dagger$) equals 0.1.

3.4 Reactor dynamics

The specific growth rate of flocculated microbial mass at substrate concentration S, as given by equation (3.5), depends on the following parameters: length at division L_d, diffusion length L_D, and the parameters included in the specific growth rate of cell suspensions (for the Marr-Pirt model: the substrate to biomass conversion factor, y_{SV}, the maintenance rate coefficient, k_M, the maximum mass-specific uptake rate, j_{SAm}, and the saturation coefficient, K). This means that steady-state growth of flocs has two extra parameters compared to that of cell suspensions. If we use the Marr-Pirt model for cellular growth, the floc dynamics of a batch reactor amounts to:

$$\begin{aligned}
&\frac{d}{dt}S = -y_{SV}\left(\frac{d}{dt}X_V + \frac{d}{dt}X_{V\dagger}\right) - j_{SM}X_V \\
&\frac{d}{dt}X_V = X_V\, r_F(S) \\
&\frac{d}{dt}X_{V\dagger} = \frac{V_\dagger(t_d) - V_\dagger(t_b)}{V_M(t_d) - V_M(t_b)}\,\frac{d}{dt}X_V = \left(\frac{\left(\frac{L_d}{L_M}\right)^3 - 2^{-3}}{(\frac{L_d}{L_M} - 1)^3} - 1\right)^{-1} X_V\, r_F(S)
\end{aligned} \tag{3.10}$$

with X_V and $X_{V\dagger}$ the density of living and dead biomass, y_{SV} the ratio of substrate uptake to biomass production, and j_{SM} the mass-specific maintenance rate of biomass. The first equation in (3.10) represents the use of substrate.

Substrate is going to the growth of biomass (first term) and to the maintenance of living biomass (second term). The second equation represents the growth of living biomass. The third equation describes the increase in dead biomass. The production rate of dead biomass is proportional to the growth rate of living biomass. The proportionality constant is the change in dead volume $\Delta V_\dagger$ relative to the change in living volume ΔV_M during the floc life cycle. Remember that the value of $V_\dagger(t_b)$ is zero in the present model.

The derivation of the relationship between the specific growth rate r_F and the substrate concentration only applies at steady state. We expect, however, that the approximations are satisfactory as long as the medium-concentration changes slowly. If the substrate concentration rises fast, and the thickness of the living layer increases faster than the growth of the radius, a formal problem of resurrection occurs. We expect this to be of minor quantitative significance and the problem disappears if the kernel is dormant, rather than dead. The situation of a rapidly rising substrate concentration can only occur at the start of the experiment.

The present formulation includes neither the further degradation of dead biomass nor the process of co-metabolism. The extension to a CSTR is straightforward.

3.5 Discussion

Mass transfer into an organism takes place across its surface area. Organisms can be classified on the basis of how surface areas that are involved in the uptake of substrate change relative to volumes during growth. Surface area grows proportional to volume^0 in V0-morphs (such as biofilms), and proportional to volume^1 in V1-morphs (such as filaments). For V0-morphs this means that surface area remains constant. Spherical flocs with a dead kernel represent a dynamic mixture between a V1-morph and a V0-morph, with an increasing weight on the latter during the division interval [9].

We illustrated floc dynamics with the simplest possible model for cellular growth that takes maintenance into account. The Appendix shows how this dynamics combines with more realistic models based on cellular physiology.

The gist of our contribution is that we use simple diffusion arguments to reveal the relationship between substrate concentration and the thickness of the living layer, and a simple geometry of flocs to quantify the deactivation of microbial metabolism. Only two parameters appear to dominate the growth process: the floc volume at fragmentation and the diffusion length. The first parameter is affected by turbulence, thus by stirring. The latter parameter com-

bines a number of properties of the microbes and the compound: the maximum specific uptake rate, the saturation coefficient, the density of biomass in the floc, and the diffusion rate of the compound through the floc, which depends on the porosity of the living biomass. The set of equations (3.10) show how one can account for growth of microbes in flocs and the occurrence of inactive biomass in a very simple and yet mechanistically inspired way.

Although we are fully aware of the limitations of our idealizations, we believe that this relatively simple model does capture the main features of the effect of flocculation on microbial degradation of compounds. Our formulation can be used to link degradation rates by cell suspensions to that by flocs, and to quantify the effects of increased stirring (via a reduction of the floc size at division).

Nomenclature

Quantities which are expressed per unit of biovolume have square brackets, [ ]. The following symbols are used for the dimensions: –, no dimension; e, energy; l, length; t, time; #, amount.

Symbol	Description	Dimension
D	diffusion coefficient	l^2t^{-1}
$[E]$	energy density	el^{-3}
$[E_G]$	volume-specific costs of growth	el^{-3}
$[E_m]$	maximum energy density	el^{-3}
$f(L)$	scaled functional response: $\frac{S(L)}{K+S(L)}$	–
$f_\dagger$	scaled functional response at $L = L_M$	–
$\overline{f}$	average scaled functional response	–
g	energy investment ratio: $\frac{[E_G]}{[E_m]}$	–
k_E	specific energy conductance: $\frac{[p_{Am}]}{[E_m]}$	t^{-1}
k_M	maintenance rate coefficient: $\frac{[p_M]}{[E_G]}$	t^{-1}
j_{SAm}	maximum mass-specific substrate uptake rate	$\#\#^{-1}t^{-1}$
j_{SM}	mass-specific maintenance rate	$\#\#^{-1}t^{-1}$
K	saturation coefficient of scaled functional response	$\#l^{-3}$
l_d^*	scaled radius at division: $\frac{L_d}{L_M}$	–
l_M	scaled maximum thickness of living layer: $\frac{L_M}{L_D}$	–
l_T	scaled total radius of floc: $\frac{L_T}{L_D}$	–

Table continues on the next page.

L_D	diffusion length: $\sqrt{\frac{DK}{j_{SAm} X_F}}$	l
L_b	radius at birth	l
L_d	radius at division	l
L_M	maximum thickness of living layer of floc	l
L_T	total radius of floc	l
$L_\dagger$	radius of dead kernel of floc	l
M_E	amount of reserves in living biomass	#
$M_{E\dagger}$	amount of reserves in dead biomass	#
M_V	amount of living biomass in floc	#
$M_{V\dagger}$	amount of dead biomass in floc	#
n	number of daughters from a floc	#
$[p_{Am}]$	volume-specific maximum assimilation rate	$el^{-3}t^{-1}$
$[p_M]$	volume-specific maintenance rate	$el^{-3}t^{-1}$
r	specific (population) growth rate of cells	t^{-1}
r_F	specific (population) growth rate of flocs	t^{-1}
s	scaled substrate concentration: S/K	–
$s_\dagger$	minimum substrate concentration for support	–
$S(L)$	substrate concentration at L	$\#l^{-3}$
t	time	t
t_b	time at birth	t
t_d	interdivision time	t
V_d	volume at division	l^3
V_M	volume of living biomass	l^3
V_T	total volume of biomass	l^3
$V_\dagger$	volume of dead biomass	l^3
X_F	amount of biomass / volume floc	$\#l^{-3}$
X_V	structural biomass / volume	$\#l^{-3}$
$X_{V\dagger}$	dead biomass / volume	$\#l^{-3}$
y_{SV}	substrate (S) needed per biomass (V) formed	$\#\#^{-1}$
y_{SE}	substrate (S) needed per reserve (E) formed	$\#\#^{-1}$

Appendix: Floc growth on the basis of Dynamic Energy Budgets

The Marr-Pirt model for growth is attractively simple, but not very realistic. A substantial increase in realism can be obtain on the basis of the Dynamic Energy Budget (DEB) theory [9]. Here we derive the steady-state growth of the floc radius, given that the growth of bacterial cells follows the DEB theory.

This theory delineates structural mass and reserves (mixtures of carbohydrates, lipids, and proteins) as state variables; maintenance and growth of structural mass are at the expense of reserves. The volume-specific maintenance rate $[p_M]$ and volume-specific energy costs of growth $[E_G]$ are assumed to be constant. The reserve energy density (i.e., the ratio of reserve energy to structural volume) follows first order dynamics, thus $\frac{d}{dt}[E] = [p_{Am}]\left(f - \frac{[E]}{[E_m]}\right)$, where f is the scaled functional response and $[p_{Am}]$ is the volume-specific maximum assimilation rate of substrate into reserves.

The reserve dynamics implies that the reserve density of cells at steady state is proportional to the functional response. The local substrate concentration and, therefore, the functional response decreases with increasing distance from the edge of the floc. The distance between a non-moving cell and the edge of the floc increases in a growing floc, thus the local substrate concentration around a typical cell decreases with time, and so do the functional response and reserve density. Maintenance has priority over growth, thus the growth rate of cells decreases to zero at the edge of the dead kernel.

If the conversion from living to dead biovolume (biovolume: volume of biomass) does not affect the total volume, the growth of the floc is determined by the living outer shell, and is given by:

$$\frac{d}{dt}L_T = \int_0^{L_M} \frac{[p_{Am}]f(L) - [E_m](\frac{d}{dL}f)(\frac{d}{dt}L_T) - [p_M]}{[E_m]f(L) + [E_G]} \left(1 - \frac{L}{L_T}\right)^2 dL \tag{3.11}$$

$$= \left\{\int_0^{L_M} \frac{k_E f(L) - k_M g}{f(L) + g}\left(1 - \frac{L}{L_T}\right)^2 dL\right\} \left(1 - \int_{f_\dagger}^{f_0} \frac{(1 - \frac{L(f)}{L_T})^2}{f + g}\, df\right)^{-1}$$

$$\simeq \frac{L_T}{3} r \left\{1 - \left(1 - \frac{L_M}{L_T}\right)^3\right\} = r L_M \left\{1 - \frac{L_M}{L_T} + \frac{L_M^2}{3L_T^2}\right\} \tag{3.12}$$

$$\text{with } r = \frac{k_E \overline{f} - k_M g}{\overline{f} + g}\left(1 - \ln\frac{f_0 + g}{f_\dagger + g}\right)^{-1}$$

with $g = \frac{[E_G]}{[E_m]}$, $k_M = \frac{[p_M]}{[E_G]}$, $k_E = \frac{[p_{Am}]}{[E_m]}$, and $\overline{f} = L_M^{-1} \int_0^{L_M} f(L)\, dL$, and f_0 is the functional response at the surface of the floc. The energy investment ratio, g, is defined as the quotient of the volume-specific costs of growth, $[E_G]$, and the maximum energy density $[E_m]$. The maintenance rate coefficient, k_M, stands for the costs of maintenance with volume-specific maintenance rate, $[p_M]$, and cost of biovolume synthesis, $[E_G]$; the specific-energy conductance k_E is the quotient of the volume-specific maximum assimilation rate, $[p_{Am}]$, and $[E_m]$. The specific growth rate of suspended cells at steady state, according to the DEB theory, is $r = \frac{k_E f - k_M g}{f+g}$ [9, p108; p315].

The denominator of the integrand in equation (3.11) stands for the local costs of growth, which consist of a contribution to the reserves, $[E_m] f(L)$, and to the structural biomass, $[E_G]$. The first term of the numerator represents the assimilative input. The last term is the maintenance flux. The middle term stands for extra energy available from the reserves. As explained above, the functional response and reserve density of a typical cell decreases with time. The change in f is caused by the outward movement of the profile relative to the cell and equals $\frac{d}{dL} f \frac{d}{dt} L_T$; multiplied by $[E_m]$ this gives the small amount of extra energy available for growth. The second factor, $(1 - \frac{L}{L_T})^2$, weighs the contribution of the different shells in the floc as a function of the radius. This is necessary because more biomass is present in the outer shells, if the shells have a constant thickness dL. The reserve density of the dead biomass equals $f_\dagger = \frac{[E_\dagger]}{[E_m]}$. The approximation (equation 3.12) is obtained by replacing the profile of the functional response $f(L)$ by its mean value $\overline{f}$.

The floc sizes for which this derivation holds are $V_T \geq V_M$. If the floc is small enough, the inner cells can pay their maintenance costs and keep living, and $V_T = V_M$, while $V_\dagger = 0$. We simply replace L_M, the upper boundary of the integral, by L_T and $f_\dagger$ by $f_T = f(L_T)$ in equation (3.11) to obtain the description of the growth of flocs without a dead kernel.

The expression for the interdivision time (equation 3.4) still applies, but the specific growth rate of the cells differs from the Marr-Pirt model. For the Marr-Pirt model, the specific growth rate of cells is $k_E f/g - k_M$. When the maintenance rate coefficient (k_M) is zero, k_E/g represents the maximum specific growth rate.

Equations for batch reactor dynamics should account for reserves in living and dead biomass (M_E and $M_{E\dagger}$, respectively). The terms $\frac{d}{dt} X_{V\dagger}$ and $\frac{d}{dt} X_{E\dagger}$ appear because living biomass is transformed into dead biomass.

$$\frac{d}{dt}S = -y_{SV}\left(\frac{d}{dt}X_V + \frac{d}{dt}X_{V\dagger}\right) - y_{SE}\left(\frac{d}{dt}X_E + \frac{d}{dt}X_{E\dagger}\right) - j_{SM}X_V$$
$$\frac{d}{dt}X_V = X_V\, r_F(S)$$
$$\frac{d}{dt}X_E = X_V\, r_F(S)\frac{M_E(t_d) - M_E(t_b)}{M_V(t_d) - M_V(t_b)}$$
$$\frac{d}{dt}X_{V\dagger} = X_V\, r_F(S)\frac{M_{V\dagger}(t_d) - M_{V\dagger}(t_b)}{M_V(t_d) - M_V(t_b)}$$
$$\frac{d}{dt}X_{E\dagger} = \frac{d}{dt}X_{V\dagger}\frac{M_{E\dagger}}{M_{V\dagger}}$$

Acknowledgements

The authors thank J. Blok, P.P.F. Hanegraaf and B.W. Kooi for advice.

References

[1] Du YG, Tyagi RD, Bhamidimarri R. (1996). Neural network analysis of the diffusional limitations in activated sludge flocs. *Process Biochemistry* 31:753–763.

[2] Emerson S. (1950). The growth phase in *Neurospora* corresponding to the logarithmic phase in unicellular organisms. *Journal of Bacteriology* 60:221–223.

[3] Groebe K, Mueller-Klieser W. (1991). Distributions of oxygen, nutrient, and metabolic waste concentrations in multicellular spheroids and their dependence on spheroid parameters. *European Biophysics Journal* 19:169–181.

[4] Hanegraaf PPF. (1997). *Mass and energy fluxes in microorganisms according to the energy budget theory for filaments.*. PhD thesis, Vrije Universiteit, Amsterdam, The Netherlands.

[5] Harms H, Bosma TNP. (1997). Mass tranfer limitation of microbial growth and pollutant degradation. *Journal of Industrial Microbiology & Biotechnology* 18:97–105.

[6] Holling CS. (1959). The components of predation as revealed by a study of small-mammal predation of the European pine sawfly. *Canadian Entomologist* 91:293–320.

[7] Huggett ASG, Widdas WF. (1951). The relationship between mammalian foetal weight and conception age. *Journal of Physiology (London)* 114:306–317.

[8] Knudson MK, Williamson KJ, Nelson PO. (1982). Influence of dissolved oxygen on substrate utilization kinetics of activated sludge. *Journal Water Polution Control Federation* 54:52–60.

[9] Kooijman SALM. (2000). *Dynamic Energy and Mass Budgets in Biological Systems.*. Cambridge University Press.

[10] Logan BE, Wilkinson DB. (1991). Fractal dimensions and porosities of *Zoogloea ramigera* and *Saccharomyces cerevisae* aggregates. *Biotechnology and Bioengineering* 38:389–396.

[11] Marr AG, Nilson EH, Clark DJ. (1962). The maintenance requirement of *Escherichia coli*. *Annals of the New York Academy of Sciences* 102:536–548.

[12] Mayneord WV. (1932). On a law of growth of Jensen's rat sarcoma. *American Journal of Cancer* 16:841–846.

[13] McElwain DLS, Ponzo PJ. (1977). A model for the growth of a solid tumor with non-uniform oxygen consumption. *Mathematical Biosciences* 35:267–279.

[14] Pirt SJ. (1965). The maintenance energy of bacteria in growing cultures. *Proceedings of the Royal Society of London B (Biological Sciences)* 163:224–231.

[15] Ruiz J, Izquierdo A. (1997). A simple model for the break-up of marine aggregates by turbulent shear. *Oceanologica Acta* 20:597–605.

[16] Snidaro D, Zartarian F, Jorand F, Bottero JY, Block JC, Manem J. (1997). Characterization of activated sludge flocs structure. *Water Science and Technology* 36(4):313–320.

[17] Steel GG. (1977). *Growth kinetics of tumors*. Clarendon Press, Oxford.

[18] van Hamersveld EH, van der Lans RGJM, Luyben KCAM. (1997). Quantification of brewers' yeast flocculation in a stirred tank: effect of physical parameters on flocculation. *Biotechnology and Bioengineering* 56:190–200.

[19] Ward JP, King JR. (1997). Mathematical modelling of avascular-tumour growth. *IMA Journal of Mathematics Applied in Medicine and Biology* 14:39–69.

[20] Winkler M. (1981). *Biological treatment of waste-water*. Ellis Horwood series in biological chemistry. Ellis Horwood, Chichester, England.

[21] Zartarian F, Mustin C, Villemin G, Ait-Ettager T, Thill A, Bottero JY, Mallet JL, Snidaro D. (1997). Three-dimensional modeling of an activated sludge floc. *Langmuir* 13:35–40.

[22] Zhang B, Yamamoto K, Ohgaki S, Kamiko N. (1997). Floc size distribution and bacterial activities in membrane separation activated sludge processes for small-scale wastewater treatment/reclamation. *Water Science and Technology* 35(6):37–44.

4

Microbial multiple substrate utilization and co-metabolism

Abstract

The availability of multiple carbon/energy sources, as is common in wastewater treatment plants, often enhances the biodegradation of recalcitrant compounds. In this paper, we classify and model different modes of multiple substrate utilization in a systematic way, using the concept of Synthesizing Unit. According to this concept, substrates can be substitutable or complementary; their uptake (or processing) can be sequential or parallel. We show how the different modes of multiple substrate interaction can be described by a single general model. From the general model, we derive simple expressions for co-metabolism of substrates that are not structurally analogous. Both the general and the co-metabolism model have the advantage that they can be used in combination with any microbial growth model. To test the co-metabolism model's realism, we confront it with experimental data. The results attained with the co-metabolism model support that the general model constitutes a useful framework for modeling aspects of multiple substrate utilization.

4.1 Introduction

For microbial growth, the relevant features of an ecosystem include its physico-chemical conditions and the type and concentration of the available resources. Although the availability of one primary resource often suffices to ensure growth of a microbial population, many species are able to use more than one carbon source simultaneously. This phenomenon is known as co-utilization. Microorganisms can attain a considerable growth rate by using multiple carbon sources simultaneously, even when each of them is present in a very low concentration [10]. As it is the amount of biomass that determines nutrient requirements, co-utilization influences the biodegradation rates of the involved substrates. Co-utilization can thus enhance biodegradation simply by increasing the biomass of the degraders.

Simultaneous biodegradation of substrates is not only important for microorganisms, but also for bioremediation of polluted ecosystems. Our environment is polluted with many 'man-made' chemicals, but fortunately microorganisms are able to transform or even degrade many of them. Sometimes a contaminant is degraded because it serves as an (additional) energy source. We then deal with proper co-utilization of the contaminant. Yet, a contaminant can also be fortuitously degraded.

The presence of easily degradable carbon sources can enhance the biodegradation of more persistent chemicals. This is best illustrated by the process of co-metabolism. Such a variation on biodegradation has been defined as fortuitous transformation of a contaminant that cannot serve as primary energy source for the microorganisms [6, 7]. Although co-metabolized compounds can be a burden to the cell, the process is important as it determines the fate of chemicals in the environment [28, 33]. For instance, co-metabolic transformations can produce compounds which are readily degraded by other environmental microorganisms. Such a commensal relationship between microorganisms has been observed in the degradation of cyclohexane. *Mycobacterium vaccae*, growing on propane, transforms cyclohexane to cyclohexanone, which serves as a growth substrate for another species [3]. Quantitative knowledge of co-metabolism plays an important role in, for instance, bioremediation of chemically polluted soils by addition of readily metabolizable substrates.

The aim of this paper is to develop a general framework for modeling simultaneous substrate degradation. In the next section, we formulate the general model that accounts for the various modes of interaction between simultaneously degraded substrates. Thereafter, we use the general model to obtain a model for the co-metabolism of substrates that differ in structure. We show model fits against experimental data [25, 31] and compare the model with other

approaches. In the final section, we remark some features that distinguish our co-metabolism model from others and discuss its advantages and realism.

4.2 Model framework

As already emphasized above, the relationship between biodegradation and biomass growth is important. To account for this relationship, we devised a model for multiple substrate assimilation that is suited to be combined with any microbial growth model. The simplest microbial growth model takes the growth rate proportional to the substrate consumption rate: the well-known Monod model. It is at the basis of a series of models of increasing complexity and realism. This series includes models that account for maintenance only (Herbert [16], Marr [26], Pirt [27]), for reserves only (Droop [9]), and for both maintenance and reserves (DEB [21]). The latter has been recently extended to include growth of microbial flocculles [4]. The chemical composition of the biomass is constant in the Monod and Marr-Pirt models, whereas it depends on growth conditions in the Droop and DEB models. In the section 'Experimental data analysis' we exemplify how the Monod model can be used in combination with our biodegradation model.

We seek to quantitatively characterize the degradation of compounds in situations in which multiple substrate biodegradation takes place. In this paper, we focus on microorganisms degrading two substrates, A and B. The resulting mathematical model can be analogously formulated for an arbitrary number of substrates, however. We view a microorganism as a 'generalized enzyme' that transforms substrates A and B into a product C. The kinetics of the generalized enzyme then determines the expressions for the sought (biomass) specific biodegradation rates of substrates A and B, denoted by j_A^+ and j_B^+. The interpretation of the product C as well as the relation between the biodegradation rates and the microbial growth rate depend on what the microorganisms actually do with the degraded compounds. Firstly, they do not necessarily transform both compounds into new biomass. For instance, substrate B could be a fortuitously degraded no energy supplying contaminant. As long as B has no effect on growth, the microbial growth rate only depends on the A consumption rate. Secondly, as said above, the fate of assimilated substrates varies from one microbial growth model to another. According to the Monod model, any assimilated substrate molecule results in new biomass. The production rate (j_C) is then equal to the growth rate. Alternatively, according to the DEB model [21], assimilated substrates are first transformed into reserves.

To characterize the transformation of multiple substrates into a product C, the concept of Synthesizing Unit (SU) is particularly suited. Indeed, the SU-kinetics can be analytically generalized for an arbitrary number of substrates [20]. An SU can be defined as a generalized enzyme that follows classic association-dissociation kinetics with two modifications [20, 21]: (*i*) production rates relate to arrival rates of substrates at the SU, and (*ii*) the dissociation rate between substrate and SU is negligibly small. The translation of SU-kinetics into equations leads to an attractively simple mathematical model that can be applied in rather complex situations, such as multiple nutrient limitation of algal growth [21], photo-synthesis and photo-respiration [21], mixotrophy [23], and co-metabolism (this chapter). The versatility of the concept of SU becomes evident in spatially structured environments, like the interior of a cell, where the concept of concentration is difficult to apply [22]. In well-mixed environments, where the concept of concentration does apply, the arrival rates are proportional to concentrations on the basis of the law of mass action. The SU-based expression for single substrate uptake then simplifies to the well-known Michaelis-Menten kinetics.

During the transformation of one substrate molecule A into product C by an SU it is possible to define the following stages:

1. a substrate molecule arrives at the SU;
2. if the SU has already a bound substrate, the arriving molecule is rejected, whereas if the SU is not occupied, the arriving molecule has a certain probability $0 \leq \rho \leq 1$ to bind the SU;
3. the SU transforms the substrate molecule into product;
4. the product is released and the SU can bind substrate again.

When an SU transforms two substrates into product, this scheme complicates somewhat because interaction between the substrates can occur. For instance, substrate A could inhibit the biodegradation of substrate B. This means that B has a larger binding probability when it arrives at a free SU than when it arrives at an SU-A complex. Substrate interaction in multiple substrate uptake is the subject of the next section. Thereafter, we will show how the different modes of interaction can be systematically modeled using SU-kinetics.

4.2.1 Four types of dual substrate degradation

Degradation processes can be classified according to the relative role of substrates in product formation and to their interaction during processing. With

regard to their relative role in product formation, simultaneously degraded substrates can be substitutable or complementary. Substrates are called substitutable when they can be separately transformed into product C, that is $y_{AC}A \rightarrow C$ and $y_{BC}B \rightarrow C$. The symbol y denotes a coupler or stoichiometric coefficient. So, y_{CA} represents the amount of C formed per amount of A and y_{AC} the amount of A degraded per amount of C formed ($y_{AC} = y_{CA}^{-1}$). Simultaneously degraded substrates are called complementary when both are required to produce C, that is $y_{AC}A + y_{BC}B \rightarrow C$. The absence of one complementary substrate prevents the degradation of the other, since both substrates must bind to the SU before any product is released. Complementary degradation occurs, for example, if both oxygen and a carbon/energy source are growth limiting.

Both substitutable and complementary substrates can be classified according to the presence or absence of interaction at the substrate binding/processing level. For two substrates, this results in four possible modes of interaction, which we refer to as substitutable-sequential, substitutable-parallel, complementary-sequential, and complementary-parallel. The reaction diagrams for these possible modes of degradation are shown in Figure 4.1.

For complementary substrates, interaction in the binding process means that one of the substrates can only bind to an SU if it is already bound to the other substrate. In diagram II (Figure 4.1), for example, substrate B only binds to the SU-A complex. This is called complementary-sequential degradation. If no interaction between the complementary substrates occurs in the binding process, we deal with complementary-parallel degradation. Occurrence or absence of interaction between complementary substrates can be characterized in terms of binding orders. If the binding order of the substrates is relevant, complementary-sequential degradation results. In diagram II (Figure 4.1), for example, we assumed that substrate A must first bind to the SU. The mathematical expression for this mechanism is simple and has interesting mathematical properties [21, p45]. Its practical interest is limited as the binding order is usually not important and, thus, complementary-parallel degradation takes place. The corresponding model has been satisfactorily used to describe dual substrate limited growth of the haptophyte *Pavlova lutheri* [21, p170], where phosphorus and vitamin B12 were the limiting nutrients.

For substitutable substrates, interaction in the binding process means that a substrate of one type cannot bind to the SU while it is processing a substrate of the other type. An increase in the abundance of only one substrate decreases the biodegradation rate of the other. We refer to this situation as substitutable-sequential degradation. Indeed, it is equivalent to competitive interaction, which is often due to competition of structurally analogous sub-

strates for the same binding site [32].

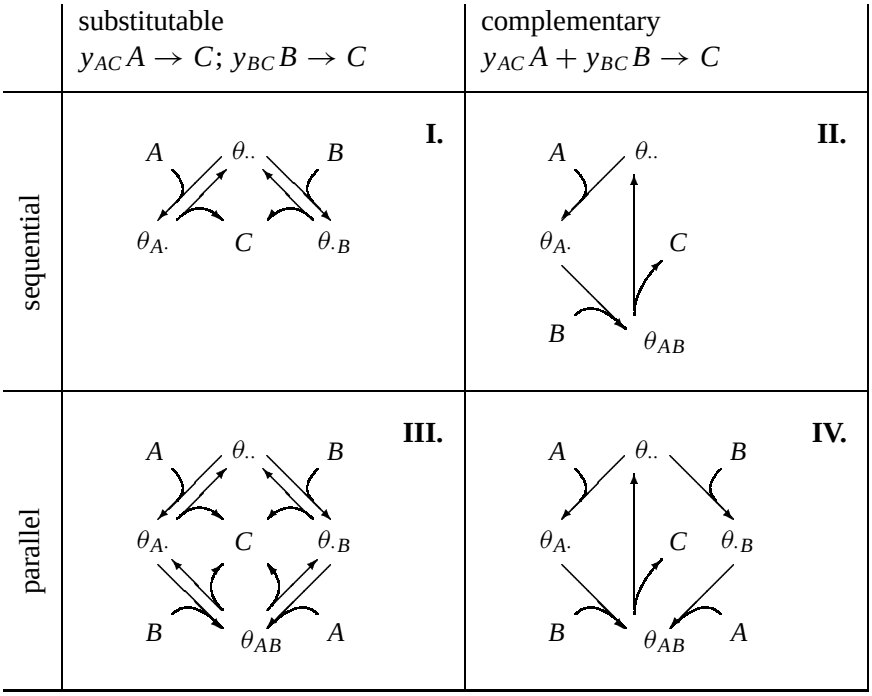

Figure 4.1: Modes of transformation of two substrates A and B into product C. The coefficient y_{CA} represents the amount of C formed per amount A consumed and, likewise, y_{BC} represents the amount of C produced per amount B consumed. The symbol θ_{**} represent the fraction of SUs in a particular binding-state. So, for instance, θ_{AB} represents the fraction of SUs with both substrates bound. A dot means absence of substrate, so $\theta_{..}$ represents the fraction of free SUs. According to the concept of SU, substrates are either substitutable or complementary; binding can be either sequential or parallel.

If two substitutable substrates do not interfere with each other in the binding process, we deal with substitutable-parallel degradation. Substitutable-parallel degradation occurs, for instance, when two substrates that support growth have a negligible interaction in the cell's metabolism. This results in additive uptake/growth models. Hanegraaf [15] modeled the simultaneous maltose and glucose utilization by *Saccharomyces cerevisiae* in this parallel way. The uptake of one substrate does not affect the uptake of the other substitutable substrate as long as their binding probabilities are independent. Al-

though the uptake processes hardly interact directly due to the use of different carriers, the subsequent processing shares common machinery. This can introduce some properties of sequential processing. We will deal with this kind of 'mixed degradation' in the next section.

4.2.2 Modeling mixed degradation

In this section, we deduce a general model that accounts for the four types of dual substrate degradation explained above. The reaction diagram described by this model is depicted in Figure 4.2. It is this general type of degradation that we above referred to as mixed degradation. To introduce this concept, let us consider a microorganism that assimilates both a carbon source (A) and a nitrogen source, for example an amino acid (B). If the microorganism is able to synthesize the amino acid *de novo*, a mixed type of assimilation results. When the amino acid is available from the medium, the microorganism uses this source, which results in an enhanced yield. The yield on A and B together exceeds the yield on A or B.

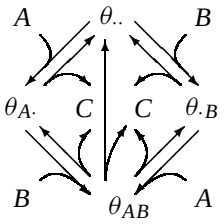

Figure 4.2: Mixed degradation. Notation as in Figure 4.1. This mixed diagram can be reduced to any of the diagrams shown in Figure 4.1 by deleting one or more arrows. In mathematical terms, this implies that once expressions describing mixed degradation are known, expressions for any of the four types of degradation can be obtained by choosing appropriate conditions on the model parameters.

Kooijman [20] has obtained a formulation for SU-kinetics that involves explicit stoichiometry (where the stoichiometric coefficients y are rational numbers of reacting molecules) in a stochastic setting. Because the formation of biomass cannot be specified at the molecular level, we use a simple deterministic approximation with implicit stoichiometry. Like in classic enzyme kinetics, this leads to expressions for the change in the fraction of free SUs and in the fractions of SUs that are bound to substrate A only, to substrate B only, or to both substrates. As can be seen from Figure 4.2, in mixed assimilation we deal with an SU that carries out three transformations $y_{AC}A \to C$, $y_{BC}B \to C$, and $y'_{AC}A + y'_{BC}B \to y_{C+}C$. When a substrate molecule arrives at the SU, it has a probability ρ to bind to the SU. As explained in the previous section,

this probability depends on the state of the SU. For substrate A, we have

$$\begin{cases} \rho_A & \text{if } A \text{ and } B \text{ are not bound} \\ \rho_{AB} & \text{if } B \text{ is bound, but } A \text{ is not} \\ 0 & \text{if } A \text{ is bound} \end{cases}$$

and for substrate B

$$\begin{cases} \rho_B & \text{if } A \text{ and } B \text{ are not bound} \\ \rho_{BA} & \text{if } A \text{ is bound, but } B \text{ is not} \\ 0 & \text{if } B \text{ is bound} \end{cases}$$

After binding the substrates, the SU enters the production stage. The handling rates (k_*), and the stoichiometric coefficients (y_{**}) can differ for both substrates. If only A or only B is used to produce C, we have handling rates k_A and k_B, respectively. If both A and B are required, the handling rate of the SU is denoted by k. Moreover, the handling rate of A can be different when B is also bound to an SU and *vice versa*: k_{AB} is the handling rate of A when B is bound to the SU; similarly k_{BA} is the handling rate of B when A is bound. When the product has been released, the SU is ready to bind other substrate molecules and the cycle starts again.

The different SU-fractions change according to the following dynamics:

$$\begin{aligned} \frac{d}{dt}\theta_{..} &= -(\rho_A j_A + \rho_B j_B)\theta_{..} + k_A\theta_{A\cdot} + k_B\theta_{\cdot B} + k\theta_{AB} \\ \frac{d}{dt}\theta_{A\cdot} &= \rho_A j_A\theta_{..} - (k_A + \rho_{BA} j_B)\theta_{A\cdot} + k_{BA}\theta_{AB} \\ \frac{d}{dt}\theta_{\cdot B} &= \rho_B j_B\theta_{..} - (k_B + \rho_{AB} j_A)\theta_{\cdot B} + k_{AB}\theta_{AB} \\ \frac{d}{dt}\theta_{AB} &= \rho_{BA} j_B\theta_{A\cdot} + \rho_{AB} j_A\theta_{\cdot B} - (k_{AB} + k_{BA} + k)\theta_{AB} \\ 1 &= \theta_{..} + \theta_{A\cdot} + \theta_{\cdot B} + \theta_{AB} \end{aligned} \tag{4.1}$$

where j_A and j_B represent the arrival rates of substrates A and B, respectively. Each θ_{**} denotes the fraction of SUs present in a particular binding-state. For further details on the interpretation of the θ's, see Figure 4.1.

In quasi steady-state, we can solve the system above analytically. The explicit expressions for the quasi steady-state SU-fractions (θ^*) are shown in the Appendix. The specific biodegradation rates (j_A^+ and j_B^+) and the corresponding specific production rate (j_C) are then given by:

$$j_A^+ = k_A\theta_{A\cdot}^* + (k_{AB} + y'_{AC}k)\,\theta_{AB}^* \tag{4.2}$$

$$j_B^+ = k_B\theta_{\cdot B}^* + (k_{BA} + y'_{BC}k)\,\theta_{AB}^* \tag{4.3}$$

$$j_C = y_{CA}k_A\theta_{A\cdot}^* + y_{CB}k_B\theta_{\cdot B}^* + (y_{CA}k_{AB} + y_{CB}k_{BA} + y_{C+}k)\theta_{AB}^*$$

These general equations for mixed kinetics embrace the four modes of degradation shown in (Figure 4.1), since these are characterized by specific sets of conditions on the SU parameters. Substitution of any set of conditions into the general equations suffices to obtain an expression for the corresponding SU-kinetics. The four sets are discussed below.

- In substitutable-sequential degradation (Figure 4.1, diagram I) each substitutable substrate can only bind to a free SU. As explained above, this interaction between substrates is equivalent to competitive inhibition. In terms of SU-kinetics it means $\rho_{AB} = \rho_{BA} = 0$ and, thus $\theta_{AB} = 0$. Consequently, the handling rates k, k_{AB}, and k_{BA} are not longer relevant.

- In complementary-sequential degradation (Figure 4.1, diagram II) both substrates are required to produce C and substrate B can only bind to the SU-A complex. The corresponding kinetics result from the general mixed kinetics by substituting $\rho_B = \rho_{AB} = 0$ and $k_A = k_{AB} = k_B = k_{BA} = 0$. The condition $\rho_B = 0$ implies $\theta_{.B} = 0$.

- Substitutable-parallel degradation (Figure 4.1, diagram III) takes place when two substitutable substrates do not interfere during the binding process. The solution results from the general solution by substituting $\rho_A \neq 0$, $\rho_B \neq 0$, $\rho_{AB} \neq 0$, $\rho_{BA} \neq 0$ and $k = 0$. In addition, for simplicity, we can assume $\rho_{AB} = \rho_A$, $\rho_{BA} = \rho_B$ and $k_{AB} = k_A$, $k_{BA} = k_B$.

- In complementary-parallel degradation (Figure 4.1, diagram IV) the binding order of the complementary substrates is not relevant. Since both A and B are needed to produce C, $k_A = k_{AB} = k_B = k_{BA} = 0$. In addition, for simplicity, we can assume $\rho_{AB} = \rho_A$, $\rho_{BA} = \rho_B$.

Thus it is possible to distinguish substitutable-sequential from complementary-sequential degradation on basis of binding probability alone. For the former, which is also known as cross-competitive inhibition, $\rho_{AB} = \rho_{BA} = 0$ holds whereas for the latter, the condition $\rho_B = \rho_{AB} = 0$ holds.

4.3 Application: Modeling co-metabolism

As early as 1959, Leadbetter and Foster [24] described the partial oxidation of certain hydrocarbons by *Pseudomonas methanica* growing on methane. These hydrocarbons did not support growth of the bacterium, but were ‘co-oxidized.’

In 1963 Jensen [19] reported oxalate-utilizing strains of *Pseudomonas dehalogens* that liberated chloride from trichloroacetate, while they were unable to grow on this compound. Since 1959 many examples of similar phenomena have been reported. For instance, the transformation by methane monooxygenase of chlorinated compounds, like trichloroethane, has received considerable attention. In the literature different names have been used to refer to the findings described above. Among them are co-oxidation [24], gratuitous or fortuitous metabolism [34], and co-metabolism [18]. In this paper, we use the term co-metabolism as it has become widely accepted.

The term co-metabolism has been defined to refer to transformations from which microorganisms do obtain neither energy nor 'nutritional benefit,' *cf.* [1, 13]. The current interpretation is less strict, as defined by Stirling and Dalton [34]: "*transformation of a compound, which is unable to support cell replication, in the requisite presence of another transformable compound.*" The former compound is referred to as co-metabolized or secondary substrate, whereas the latter is referred to as primary substrate. Further details about the term co-metabolism can be found in another article by Dalton and Stirling [8].

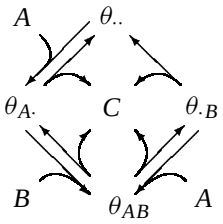

Figure 4.3: Co-metabolism of a co-metabolite B and a primary substrate A. Notation as in Figures 4.1 and 4.2. Substrate B can only bind to the SU-A complex and, consequently, the microorganisms can only degrade substrate B if substrate A is also available.

According to the current definition of co-metabolism, degradation of a secondary substrate may provide nutritional benefit, but the cell is unable to utilize it in absence of a primary substrate. The transformation of chlorinated aliphatics by methanotrophs, for example, fits well in this interpretation. For *Methylomicrobium album*, chloromethane cannot serve as sole growth substrate. But when co-fed with methanol, it enhances growth and its carbon is incorporated into the biomass for up to 38% [14]. Obviously, this example does not fit in the original 'non nutritional benefit' definition. Thus, the current view includes more substrates in the realm of co-metabolism. Furthermore, it seems to be more practical, since absence of benefits to the cell is not easy to confirm experimentally.

For different reasons, a primary substrate can be required to degrade a co-metabolite. First, co-metabolism can occur if the catabolic enzymes are not induced by the secondary substrate. This is exemplified by chloromethane that

does not induce methane mono-oxygenase, and by 4-chlorophenol that does not induce phenol oxidizing enzymes. Second, some co-metabolic transformations, as oxidations or reductive dehalogenations, require energy or reduction equivalents (e.g., NAD(P)H). Such transformations drain the cell's pool of reduction equivalents. However, the degradation of a primary substrate can make extensive catabolism of the secondary substrate possible by providing the necessary reduction equivalents. In this case, co-metabolism can reduce the biomass yield [17] and/or the maximum growth rate [17, 30] on the primary substrate. However, the loss of reducing equivalents during co-metabolism does not always result in a (detectable) decrease in yield [29, 30].

4.3.1 Model development

We can use the general framework above to model co-metabolism. Models described in literature [2, 5, 11, 12, 14, 17, 29, 30] focus on the co-metabolism of structurally similar compounds. Here we show how our general framework can be used to model the co-metabolism of structurally dissimilar substrates. As can be seen from Figure 4.3, we deal with a microorganism that carries out two transformations, $y_{AC}A \rightarrow C$ and $y_{BC}B \rightarrow C$. In terms of the conditions on the SU-parameters, substitutable-parallel implies $k_{BA} = k_B$, $k_{AB} = k_A$, and $k = 0$. Consequently, the expressions for the biodegradation rates (equations 4.2 and 4.3) reduce to:

$$\begin{aligned} j_A^+ &= k_A(\theta_{A\cdot}^* + \theta_{AB}^*) \\ j_B^+ &= k_B(\theta_{\cdot B}^* + \theta_{AB}^*) \end{aligned} \tag{4.4}$$

In terms of the specific biodegradation rates, the production rate is given by $j_C = y_{CA}\, j_A^+ + y_{CB}\, j_B^+$. Substitutable-parallel degradation also implies $\rho_A \neq 0$, $\rho_{AB} \neq 0$, which means that substrate B does not inhibit the binding probability of substrate A. If in addition $\rho_B \neq 0$, $\rho_{BA} \neq 0$ holds, we deal with proper substitutable-parallel degradation (Figure 4.1, diagram III). In contrast, if alternatively the conditions $\rho_{BA} \neq 0$ and $\rho_B = 0$ hold, microorganisms can only degrade B when A is also available. Substrate B is a then (xenobiotic) substrate that is co-metabolized with a (natural) substrate A as primary substrate. Under the conditions $\rho_A = \rho_{AB} \neq 0$, $\rho_{BA} \neq 0$, and $\rho_B = 0$, the expressions for the quasi steady-state SU-fractions (θ^*) become much more

simple. Hence, the specific degradation rates (equation 4.4) can be written as:

$$\begin{aligned} j_A^+ &= k_A \frac{\rho_A j_A}{\rho_A j_A + k_A} \\ j_B^+ &= k_B \frac{\rho_A j_A}{\rho_A j_A + k_A} \; \frac{\rho_{BA} j_B (\rho_A j_A + k_A + k_B)}{\rho_{BA} j_B (\rho_A j_A + k_B) + k_B (\rho_A j_A + k_A + k_B)} \end{aligned} \tag{4.5}$$

where j_B^+ is the specific biodegradation rate of the co-metabolized substrate. The production rate is given by $j_C = y_{CA}\, j_A^+ + y_{CB}\, j_B^+$. According to the definition of co-metabolism above, biodegradation of the co-metabolite may result in the formation of new biomass. That is, the coefficient y_{CB} is not necessarily zero. Alternatively, the co-metabolite can exert a toxic effect on the microorganisms. This typically results in degradation rates that are low as long as the concentration of the toxic compound is high. The relation between co-metabolism and toxicity has been modeled in, for instance, [2, 11, 12]. For the moment, we do not take such toxic effects into account.

4.3.2 Experimental data analysis

In this section, we present two examples that illustrate how the model for co-metabolism can be applied in combination with the Monod model. The first example concerns the anaerobic growth of *E. coli* on citrate, whereas the second concerns the co-metabolic degradation of 3-chloroaniline. Before going into the examples we rewrite equation (4.5) in terms of concentrations. In a well-mixed environment, the arrival rates of the compounds can be taken proportional to their concentrations. In mathematical terms this means $j_A = \alpha_A S_A$ and $j_B = \alpha_B S_B$. Substitution of these expressions into equation (4.5) yields:

$$\begin{aligned} j_C = {} & y_{CA} k_A \frac{S_A}{S_A + K_A} + \\ & y_{CB} k_B \frac{S_A}{S_A + K_A} \; \frac{S_B \left(S_A + K_A + \frac{k_B}{k_A} K_A\right)}{S_B \left(S_A + \frac{k_B}{k_A} K_A\right) + K_B \left(S_A + K_A + \frac{k_B}{k_A} K_A\right)} \end{aligned} \tag{4.6}$$

where the saturation constants are defined as $K_A = \frac{k_A}{\alpha_A \rho_A}$, $K_B = \frac{k_B}{\alpha_B \rho_{BA}}$. The compound parameters $y_{CA} k_A$ and $y_{CB} k_B$ are the maximum production rates from substrates A and B, respectively. Finally, to reduce the number of parameters, we scale the substrate concentrations with respect to their saturation constants ($a = S_A/K_A$, $b = S_B/K_B$) and we write:

$$j_C = y_{CA} k_A \frac{a}{a+1} + y_{CB} k_B \frac{a}{a+1} \; \frac{b}{b + 1 - b/\left(a + 1 + k_B/k_A\right)} \tag{4.7}$$

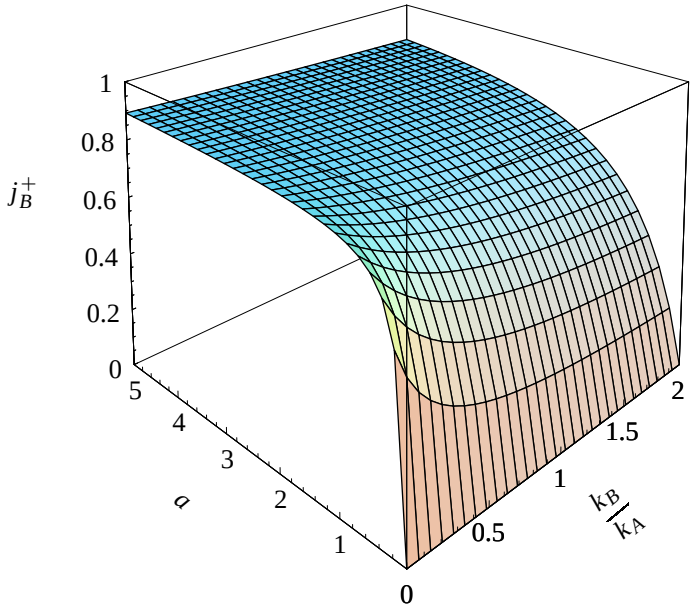

Figure 4.4: The scaled degradation rate of substrate B (j_B^+) as a function of the ratio k_B/k_A and scaled concentration of substrate A. The scaled rate has a maximum of 1. The value of b is 10. Especially at low values of a, the ratio of handling rates k_B/k_A influences the degradation rate of B.

From this expression it can be seen how the handling rates influence the degradation process. Clearly, the values of a and b are important in determining the amount of substrate B that is transformed. For high values of b, the amount of transformed B is proportional to the amount of transformed of A. The ratio of the handling rates (k_B/k_A) is also important. This ratio has more influence on the degradation rate of substrate B at low than at high scaled concentrations of substrate A (Figure 4.4).

The model implements strict coupling between the co-metabolic degradation of substrate B and the uptake of the primary substrate A. This strict coupling between the consumption of growth substrate and co-metabolite has been reported for anaerobic growth of *E. coli* on citrate [25]. Citrate is almost completely degraded with glucose, lactose, or L-lactate as primary substrate. However, citrate breakdown stops when glucose is exhausted, whereas glucose breakdown continues after depletion of citrate [25]. To test if the new model is able to describe the co-metabolic consumption of citrate, we confronted it

with an experiment by Lütgens and Gottschalk [25]. The following equations were used:

$$\frac{d}{dt}S_A = -k_A \frac{S_A}{S_A + K_A} S_C$$

$$\frac{d}{dt}S_B = -k_B \frac{S_A}{S_A + K_A} \frac{S_B \left(S_A + K_A + \frac{k_B}{k_A}K_A\right)}{S_B \left(S_A + \frac{k_B}{k_A}K_A\right) + K_B \left(S_A + K_A + \frac{k_B}{k_A}K_A\right)} S_C$$

$$\frac{d}{dt}S_C = y_{CA}\frac{d}{dt}S_A + y_{CB}\frac{d}{dt}S_B$$

where A refers to glucose, B to citrate, and C to biomass. The results are shown in Figure 4.5. In the experiment, citrate was exhausted first. With the estimated parameter values, we carried out a model simulation in which glucose is exhausted first. The model indeed predicts that citrate consumption stops after the depletion of glucose (Figure 4.5). Unfortunately, [25] did not include the experimental data.

The degradation of 3-chloroaniline (3CA) provides another example of co-metabolism [31]. In this case, the extent and rate of 3CA degradation depend on glucose concentration (Figure 4.6), but 3CA also disappears from the medium when glucose is absent. This means that a 'background' degradation process is taking place, which is not related to the oxidation of primary substrate. However, as illustrated in the previous example, our model predicts co-metabolic degradation to stop once the primary substrate is exhausted. To describe the background degradation of 3CA, we extended the model to account for background degradation. We did so by adding to equation 4.6 the term $k_d \frac{S_B}{S_B+K_B}$, where k_d represents the maximum decay rate of 3CA in the absence of glucose. Figure 4.6 shows the results of fitting this extended model against data from [31]. We conclude that the fit is quite acceptable.

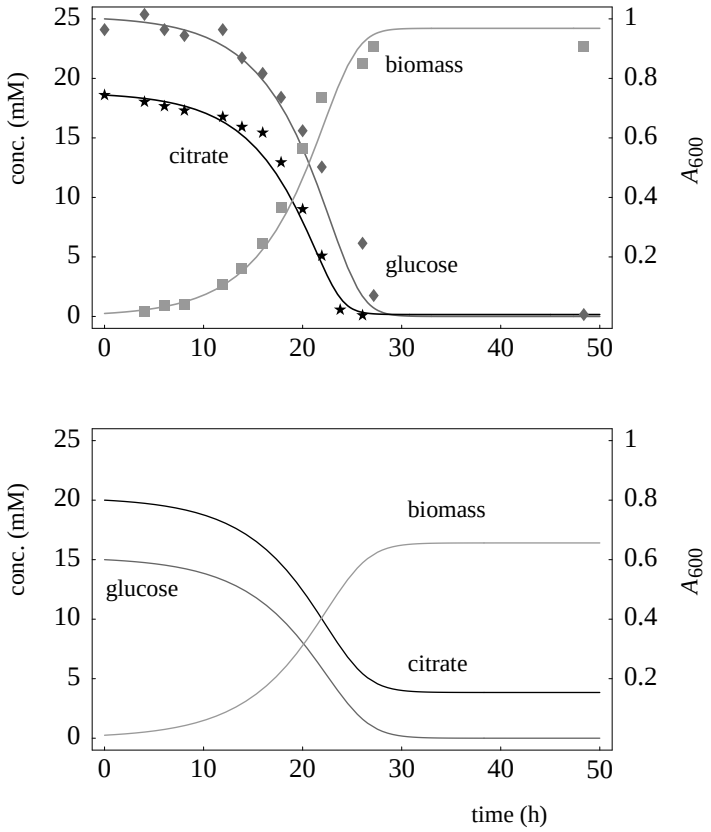

Figure 4.5: TOP: Result of fitting our co-metabolism model to data from Lütgens and Gottschalk [25]. *E. coli* consumes citrate anaerobically in the presence of glucose. Parameter values were obtained by fitting all data sets simultaneously. The Monod model was used to describe biomass growth. For the model equations, see text.

Parameter values (A represents glucose, B citrate, and C biomass): $y_{CA} = 0.028^* A_{600}$/mM; $y_{CB} = 0.014\, A_{600}$/mM; $k_A = 140$ mM/(A_{600} day); $k_B = 132$ mM/(A_{600} day); $K_A^* = 6$ mM; $K_B^* = 2$ mM; $S_A(0) = 25$ mM; $S_B(0)^* = 18.6$ mM (measured value); $S_C(0)^* = 0.01\, A_{600}$ (initial value); *: parameter has been fixed during minimization.

BOTTOM: Model simulation with the obtained parameter values (except for the initial conditions). The initial concentration of glucose (S_A) is 15 mM and that of citrate (S_B) 20 mM. Here, glucose is consumed completely and citrate partly remains in the culture. Indeed citrate consumption stops when the primary substrate (glucose) has been depleted as reported [25].

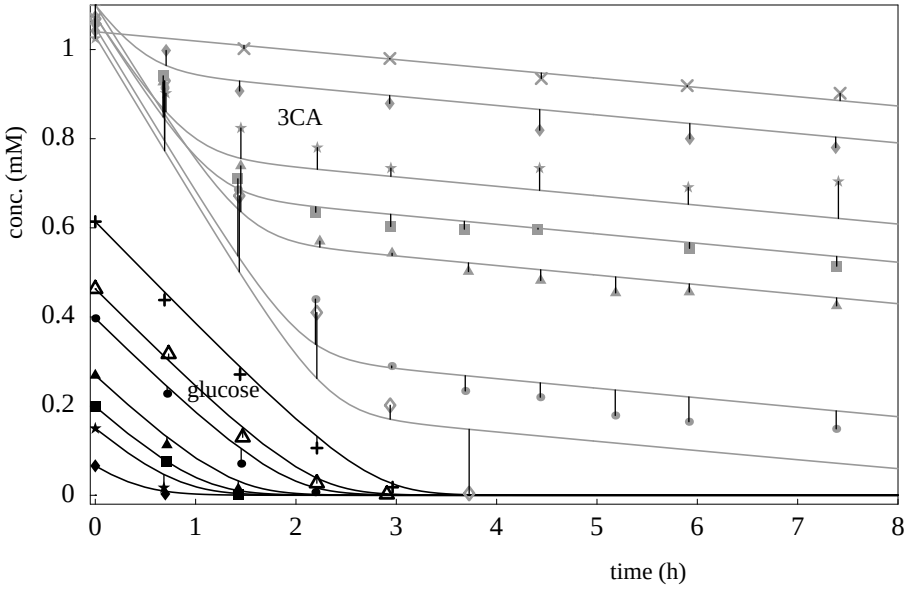

Figure 4.6: Result of fitting our co-metabolism model to data from Schukat *et al.* [31]. Co-metabolic degradation of 3-chloroaniline (3CA) by *Rhodococcus* with glucose as the primary substrate. The culture starting with 0.60 mM glucose serves as a control: 3CA is absent. The upper curves for 3CA ($\times$) and for glucose ($+$) relate to the single substrate case. We fitted all 14 datasets simultaneously.

Parameter values: (A represents glucose, B 3CA, and C biomass): $y^*_{CA} = 0.08$ mg dry weight/μmol glucose; $y^*_{CB} = 0$ mg dry weight/μmol 3CA; $k_A = 0.42$ mM h^{-1} (mg dry weight)$^{-1}$; $k_B = 0.60$ mM h^{-1} (mg dry weight)$^{-1}$; $K_A = 0.06$ mM; $K_B = 0.008$ mM; $k_d = 0.035$ mM h^{-1} (mg dry weight)$^{-1}$. The initial biomass concentration is 0.60 mg dry weight/ml. The initial glucose concentration are 0, 0.07, 0.15, 0.20, 0.27, 0.40, 0.46, and 0.61 mM. The initial 3CA concentrations from top to bottom are: 1.04, 1.1, 1.075, 1.075, 1.1, 1.05, 1.03, and 0.0 mM. *: parameter has been fixed during minimization.

4.4 Discussion

Let us remark four features that illustrate how our co-metabolism model relates to previous approaches. They are important to keep in mind when applying the model.

First, most modeling approaches have focused on co-metabolism of structurally analogous compounds. As competitive inhibition is often due to competition of structurally analogous substrates for the same binding site, these approaches often assume that competitive inhibition takes place. In contrast, the general framework allows us to describe co-metabolism also in situations in which no competitive inhibition occurs. We view co-metabolism as a 'degenerate' *parallel*-substitutable interaction, whereas competitive inhibition is equivalent to *sequential*-substitutable interaction. With the examples (previous section) we showed that our model succeeds in describing the co-metabolic biodegradation of non structurally analogous substrates well.

Second, co-metabolism concerns the simultaneous metabolism of two compounds, where the degradation of a secondary substrate depends on the presence of a primary substrate. We incorporated this dependency into our model such that it involves the obligate presence of a primary substrate. Consequently, co-metabolic degradation only occurs if the primary substrate is present. However, degradation of the secondary substrate can continue after depletion of the primary substrate. In some situations oxidation of dead biomass provides the necessary energy for background degradation, in other situations intracellular reserves provide it. The model can be extended to account for any of these situations, as shown in the previous section. If the rate of secondary substrate transformation is related to the rate of biomass decay or oxidation, biomass must be regarded as a substrate that provides energy.

Third, in our model the rate of secondary substrate transformation is a function of the concentration of both primary substrate and secondary substrate. Thus, as long as the concentration of secondary substrate is not toxic, its transformation rate increases with increasing concentration. This is in agreement with models that use cross-competitive inhibition to describe co-metabolism.

Fourth, we developed a general model for multiple nutrient utilization without using assumptions on intracellular pools of energy or reduction equivalents. Indeed, the general model connect biodegradation to substrate assimilation. This has the advantage that any microbial growth model can be used in conjunction with our model. This advantage also holds for our co-metabolism model being a special case of the general model. If intracellular reserves and changes in the chemical composition of biomass cannot be ignored, applica-

tion of the DEB theory [21] might be considered.

In sum, the general model presented in this paper constitutes a useful framework for modeling aspects of multiple nutrient utilization by microorganisms. The framework has wide applications such as the prediction of biodegradation rates and the study of multiple nutrient limitation. As an example, we showed how it can be applied to obtain a model that describes cometabolism of non structurally analogous substrates. This model inherits the general model's flexibility and can, therefore, be combined with any microbial growth model, and can also be easily extended to account for background degradation or substrate loss due to physical processes.

Nomenclature

The following symbols are used for the dimensions:
–, no dimension; l, length; t, time; #, amount (C-mol or mass).

Symbol	Description	Dimension
S_*	concentration of compound $*$	$\#l^{-3}$
j_*	specific arrival rate of compound $*$	$\#\#^{-1}t^{-1}$
j_*^+	specific biodegradation rate of compound $*$	$\#\#^{-1}t^{-1}$
j'_*	scaled arrival rate of compound $*$: $j'_* = \rho_* j_*$	$\#\#^{-1}t^{-1}$
j''_{*_1}	scaled arrival rate of compound $*$: $j''_* = \rho_{*_1*_2} j_{*_1}$	$\#\#^{-1}t^{-1}$
k_*	handling rate for compound $*$	t^{-1}
K_*	saturation coefficient of compound *	$\#l^{-3}$
$y_{*_1*_2}$	stoichiometric coefficient (coupler): compound 1 needed per compound 2 formed	$\#\#^{-1}$
ρ_*	binding probability of compound $*$ to SU	–
$\rho_{*_1*_2}$	binding probability of compound $*_1$ to SU–$*_2$ complex	–
$\theta_{*_1*_2}$	fraction of SUs occupied by substrates $*_1$ and $*_2$	–

Appendix

Quasi steady-state mixed kinetics

If we assume quasi steady-state, we are able to solve system (4.1). The solution is most easily expressed in terms of the net arrival rates, which are defined as $j'_A = j_A\rho_A$, $j''_A = j_A\rho_{AB}$, $j'_B = j_B\rho_B$, and $j''_B = j_B\rho_{BA}$. The quasi steady-state solution is then given by $\theta^*_{\cdot\cdot} = \Theta_{\cdot\cdot}/\Theta_+$, $\theta^*_{A\cdot} = \Theta_{A\cdot}/\Theta_+$, $\theta^*_{\cdot B} = \Theta_{\cdot B}/\Theta_+$ and

$\theta^*_{AB} = \Theta_{AB}/\Theta_+$, where $\Theta_+ = \Theta_{..} + \Theta_{A\cdot} + \Theta_{\cdot B} + \Theta_{AB}$ and

$$\begin{aligned}
\Theta_{..} &= j''_A j''_B k + j''_A k_A (k + k_{BA}) + j''_B k_B (k + k_{AB}) + k_A k_B k_+ \\
\Theta_{A\cdot} &= j''_A (j'_+ k_{BA} + j'_A k) + j'_A k_B k_+ \\
\Theta_{\cdot B} &= j''_B (j'_+ k_{AB} + j'_B k) + j'_B k_A k_+ \\
\Theta_{AB} &= j''_A j''_B j'_+ + j''_A j'_B k_A + j''_B j'_A k_B
\end{aligned}$$

with $k_+ = k + k_{AB} + k_{BA}$ and $j'_+ = j'_A + j'_B$. The specific biodegradation rates and the corresponding specific production rate are then given by:

$$\begin{aligned}
j^+_A &= k_A \theta^*_{A\cdot} + (k_{AB} + y'_{AC} k)\, \theta^*_{AB} \\
j^+_B &= k_B \theta^*_{\cdot B} + (k_{BA} + y'_{BC} k)\, \theta^*_{AB} \\
j_C &= y_{CA} k_A \theta^*_{A\cdot} + y_{CB} k_B \theta^*_{\cdot B} + (y_{CA} k_{AB} + y_{CB} k_{BA} + y_{C+} k) \theta^*_{AB}
\end{aligned}$$

Acknowledgements

The authors thank Paul Hanegraaf, Fleur Kelpin, Bob Kooi, and Gosse Schraa for valuable discussions and advice.

References

[1] Alexander MA. (1999). *Biodegradation and bioremediation*. Academic Press, San Diego, second edition.

[2] Alvarez-Cohen L, McCarty PL. (1991). A cometabolic biotransformation model for halogenated aliphatic compounds exhibiting product toxicity. *Environmental Science & Technology* 25:1381–1387.

[3] Beam HW, Perry JJ. (1974). Microbial degradation of cycloparaffinic hydrocarbons via co-metabolism and commensalism. *Journal of General Microbiology* 82:163–169.

[4] Brandt BW, Kooijman SALM. (2000). Two parameters account for the flocculated growth of microbes in biodegradation assays. *Biotechnology and Bioengineering* 70:677–684.

[5] Chang HL, Alvarez-Cohen L. (1995). Model for the cometabolic biodegradation of chlorinated organics. *Environmental Science & Technology* 29:2357–2367.

[6] Committee on In Situ Bioremediation, Water Science and Technology Board, Commission on Engineering and Technical Systems, National Reseach Council. (1993). *In Situ Bioremediation: When Does it Work?*. National Academy Press, Washington DC.

[7] Committee on Intrinsic Remediation, Water Science and Technology Board, Board on Radioactive Waste Management, Commission on Geosciences, Environment, and Resources, National Research Council. (2000). *Natural Attenuation for Groundwater Remediation*. National Academy Press, Washington DC.

[8] Dalton H, Stirling DI. (1982). Co-metabolism. *Philosophical Transactions of the Royal Society of London B (Biological Sciences)* 297:481–496.

[9] Droop MR. (1975). The nutrient status of algal cells in batch culture. *Journal of the Marine Biological Association of the United Kingdom* 55:541–555.

[10] Egli T. (1995). The ecological and physiological significance of the growth of heterotrophic microorganisms with mixtures of substrates. *Advances in Microbial Ecology* 14:305–386.

[11] Ely RL, Hyman MR, Arp DJ, Guenther RB, Williamson KJ. (1995). A cometabolic kinetics model incorporating enzyme-inhibition, inactivation, and recovery: II. Trichloroethylene degradation experiments. *Biotechnology and Bioengineering* 46:232–245.

[12] Ely RL, Williamson KJ, Guenther RB, Hyman MR, Arp DJ. (1995). A cometabolic kinetics model incorporating enzyme-inhibition, inactivation, and recovery: I. Model development, analysis, and testing. *Biotechnology and Bioengineering* 46:218–231.

[13] Fiedler H, Lau C. (1998). Transformation of chlorinated xenobiotics in the environment. In: Schüürmann G, Markert B, editors. *Ecotoxicology. Ecological Fundamentals, chemical exposure, and biological effects*, chapter 10, pp. 283–316. Wiley, New York.

[14] Han JI, Semrau JD. (2000). Chloromethane stimulates growth of *Methylomicrobium album* BG8 on methanol. *FEMS Microbiology Letters* 187:77–81.

[15] Hanegraaf PPF. (1997). *Mass and energy fluxes in microorganisms according to the Dynamic Energy Budget theory for filaments*. PhD thesis, Vrije Universiteit, Amsterdam, The Netherlands.

[16] Herbert D. (1958). Some principles of continuous culture. In: Tunevall G, editor. *Recent progress in microbiology*, pp. 381–396. Almquist & Wiksell, Stockholm.

[17] Hill GA, Milne BJ, Nawrocki PA. (1996). Cometabolic degradation of 4-chlorophenol by *Alcaligenes eutrophus*. *Applied Microbiology and Biotechnology* 46:163–168.

[18] Horvath RS. (1972). Microbial co-metabolism and the degradation of organic compounds in nature. *Bacteriological reviews* 36:146–155.

[19] Jensen HL. (1963). Carbon nutrition of some microorganisms decomposing halogen-substituted aliphatic acids. *Acta Agriculturae Scandinavica* 13:404–412.

[20] Kooijman SALM. (1998). The synthesizing unit as model for the stoichiometric fusion and branching of metabolic fluxes. *Biophysical Chemistry* 73:179–188.

[21] Kooijman SALM. (2000). *Dynamic Energy and Mass Budgets in Biological Systems*. Cambridge University Press, Cambridge, second edition.

[22] Kooijman SALM. (2001). Quantitative aspects of metabolic organization; a discussion of concepts. *Philosophical Transactions of the Royal Society of London B (Biological Sciences)* 356:331–349.

[23] Kooijman SALM, Dijkstra HA, Kooi BW. (2002). Light-induced mass turnover in a mono-species community of mixotrophs. *Journal of Theoretical Biology* 214:233–254.

[24] Leadbetter ER, Foster JW. (1959). Oxidation products formed from gaseous alkanes by the bacterium *Pseudomonas methanica*. *Archives of Biochemistry and Biophysics* 82:491–492.

[25] Lütgens M, Gottschalk G. (1980). Why a co-substrate is required for anaerobic growth of *Escherichia coli* on citrate. *Journal of General Microbiology* 119:63–70.

[26] Marr AG, Nilson EH, Clark DJ. (1963). The maintenance requirement of *Escherichia coli*. *Annals of the New York Academy of Sciences* 102:536–548.

[27] Pirt SJ. (1965). The maintenance energy of bacteria in growing cultures. *Proceedings of the Royal Society of London B (Biological Sciences)* 163:224–231.

[28] Rabbi MF, Clark B, Gale RJ, Ozsu-Acar E, Pardue J, Jackson A. (2000). In situ TCE bioremediation study using electrokinetic cometabolite injection. *Waste Management* 20:279–286.

[29] Reij M, Kieboom J, de Bont JAM, Hartmans S. (1995). Continuous degradation of trichloroethylene by *Xanthobacter* sp. strain Py2 during growth on propene. *Applied and Environmental Microbiology* 61:2936–2942.

[30] Saéz PB, Rittmann BE. (1993). Biodegradation kinetics of a mixture containing a primary substrate (phenol) and an inhibitory co-metabolite (4-chlorophenol). *Biodegradation* 4:3–21.

[31] Schukat B, Krebs D, Fritsche W. (1983). Cometabolic degradation of 2- and 3-chloroaniline because of glucose metabolism by *Rhodococcus* sp. An 117. *Current Microbiology* 9:81–86.

[32] Segel IH. (1993). *Enzyme Kinetics: Behavior and Analysis of Rapid Equilibrium and Steady-State Enzyme Systems*. Wiley, New York.

[33] Semprini L. (1997). Strategies for the aerobic co-metabolism of chlorinated solvents. *Current Opinion in Biotechnology* 8:296–308.

[34] Stirling DI, Dalton H. (1979). The fortuitous oxidation and cometabolism of various carbon compounds by whole-cell suspensions of *Methylococcus capsulatus* (Bath). *FEMS Microbiology Letters* 5:315–318.

5

Modeling microbial adaptation to changing availability of substrates

Abstract

In their natural environment microorganisms encounter changes in substrate availability, involving either nutrient concentrations or nutrient types. They have to adapt to the new conditions in order to survive. We present a model for slow microbial adaptation in response to changes in the availability of substrates. The model is based on reciprocal (or mutual) inhibition of expression of both the substrate-specific carriers and the associated assimilatory machinery. The inhibition kinetics is derived from the kinetics of Synthesizing Units. An interesting property of the adaptation model is that the presence of a single limiting resource results in a *constant* maximum specific substrate consumption rate for fully adapted microorganisms. Because the maximum specific consumption rate is not a function of substrate concentration, for growth on one substrate, the Monod and Pirt models for instance are still valid. Other adaptation models known to us do not fulfill this property. The simplest version of our model describes adaptation during diauxic growth, using only one preference parameter and one initial condition. The applicability of the model is exemplified by fitting it to published data from diauxic growth experiments.

5.1 Introduction

Most microorganisms are able to grow on a wide variety of substrates, the consumption of the substrates being either sequential or simultaneous. Indeed, sequential utilization resulting in diauxic growth [13] has often been observed. During diauxic growth, depletion of the first substrate is followed by a lag period in which the microorganisms adapt to the second substrate. After this lag phase, exponential growth on the second substrate starts. The length of the intermediate lag period depends on pre-culturing conditions and the relative concentrations of the substrates, as well as on the type of substrates [3].

In growth models, based on the Monod model, microorganisms consume substrate at a rate that depends hyperbolically on substrate concentration. The maximum specific consumption rate, however, does not depend on the substrate concentration. The parameters that control the uptake process are constant during fast changes of substrate types and availability, but can be subjected to slow adaptation processes that take several generations.

We modeled the slow microbial adaptation of consumption of various substitutable substrates (i.e., substrates that can fulfill the same role in metabolism). We assumed that the pathway for each substrate is inducible and that the presence of one substrate is able to influence the expression of the pathway of other substrates. The chapter is organized as follows. To start, we introduce binding inhibition kinetics in a Synthesizing Unit (SU) framework. Then we use the obtained binding-inhibition equations to describe the expression of a pathway in response to changes in substrate availability. Finally, we develop the adaptation model and confront it with experimental data on diauxic growth.

5.2 Substrate availability and signal fluxes

Regulatory mechanisms are responsible for adaptation. It is well known that the presence of a substrate induces a signal in the microorganisms that can alter their catabolic properties [16]. Mechanisms involved in the glucose-lactose diauxie in *Escherichia coli* have been known for a long time [16] and we may be tempted to model them in detail. However, it has recently been found that the main reason for the diauxie is inducer exclusion: while glucose is present, lactose is not taken up [5, 17]. Furthermore, the mechanisms of carbon catabolite repression differ substantially among bacteria [17]. These differences and changing insights into details of reported mechanisms convinced us to develop an adaptation model that focuses on the general processes rather than on the biochemical details. The model is species independent and, in addition, has

the advantage that it requires less parameters and equations than a model that describes the biochemical processes in detail. This is important for practical applications.

We assume that each substrate has a specific regulatory protein that handles the signal fluxes and decides whether to increase or decrease the catabolic capacity for the substrate. The regulatory protein functions as a Synthesizing Unit (SU) that controls the synthesis of assimilatory machinery for that substrate. A SU is a generalized enzyme that follows classic association-dissociation kinetics with two modifications [8, 9]: (*i*) production fluxes relate to arrival fluxes of substrates at the SU, and (*ii*) the dissociation rate between substrate and SU is negligibly small. We deal with a metabolic pathway as if we deal with a single rate-limiting enzyme. In sum, the availability of a certain substrate produces a signal flux, handled by a SU. For organisms that are able adapt, this results in adaptation to a substrate in response to the concentrations of all available substrates.

In this chapter we derive the adaptation model for two substrates, but the model can easily be extended to account for any number of substrates. When two substrates are present in the medium, two situations are possible. First, the presence of one substrate does not affect the consumption of the other. This situation results from "unilateral binding inhibition." Second, the presence of one substrate can influence the consumption of the other. This situation results from "bilateral binding inhibition." Both cases of inhibition are treated in detail below using the Synthesizing Unit concept. The production flux of a certain SU determines the change in the amount of the corresponding rate-limiting enzyme. In this section, we explain how unilateral and bilateral binding inhibition give rise to changing maximum specific substrate consumption rates in response to changing substrate availability. In the next section, we deduce simple equations describing the adaptation process.

5.2.1 Unilateral binding inhibition

In unilateral binding inhibition, one substrate can repress the utilization of another but not *vice versa*. We obtain an equation for the synthesis of enzyme that controls the maximum specific uptake rate of a particular substrate. As explained above, we assume that the presence of two substrates (A and B) induces two fluxes of signal molecules ($\tilde{A}$ and $\tilde{B}$). A signal molecule $\tilde{A}$, induced by the presence of substrate A, results in the synthesis of a certain number of enzymes. We deal with the reaction $y_{AC}\tilde{A} \rightarrow C$ that is inhibited by compound B. The presence of y_{AC} signal molecules $\tilde{A}$ gives rise to the production of one molecule of enzyme C; thus y_{AC} is a stoichiometric constant. The Synthesiz-

ing Unit can bind both $\tilde{A}$ and $\tilde{B}$, but it can bind $\tilde{A}$ only if $\tilde{B}$ is not bound. $\tilde{B}$ does not affect the production of C if $\tilde{A}$ is already bound; $\tilde{A}$ does not affect the binding or release of $\tilde{B}$. The SU can be in four different states: unoccupied ($\theta_{..}$), occupied by $\tilde{A}$ only ($\theta_{A.}$), occupied by $\tilde{B}$ only ($\theta_{.B}$), or occupied by both $\tilde{A}$ and $\tilde{B}$ (θ_{AB}). The equations for the change in the bound fractions of the SU become:

$$\begin{aligned}
\frac{d}{dt}\theta_{..} &= k_A\theta_{A.} + k_B\theta_{.B} - (j'_A + j'_B)\theta_{..} \\
\frac{d}{dt}\theta_{A.} &= j'_A\theta_{..} + k_B\theta_{AB} - k_A\theta_{A.} - j'_B\theta_{A.} \\
\frac{d}{dt}\theta_{.B} &= j'_B\theta_{..} + k_A\theta_{AB} - k_B\theta_{.B} \\
1 &= \theta_{..} + \theta_{A.} + \theta_{.B} + \theta_{AB}
\end{aligned}$$

with $j'_i = j_i\rho_i$, where ρ_i is the binding probability and j_i the arrival rate of signal molecules induced by substrate i. The steady state fractions of bound SUs are $\theta^*_{ij} = \Theta_{ij}/\Theta_+$, with $\Theta_+ = \Theta_{..} + \Theta_{A.} + \Theta_{.B} + \Theta_{AB}$ and

$$\begin{aligned}
\Theta_{..} &= k_Ak_B(j'_B + k_A + k_B) \\
\Theta_{A.} &= j'_Ak_B(k_A + k_B) \\
\Theta_{.B} &= k_Aj'_B(j'_A + j'_B + k_A + k_B) \\
\Theta_{AB} &= j'_Aj'_Bk_B
\end{aligned}$$

The C production flux is given by:

$$j_C = y_{CA}k_A(\theta^*_{A.} + \theta^*_{AB}) = \frac{y_{CA}j'_Ak_Ak_B}{(j'_B + k_B)(k_A + j'_A/(1 + j'_B/k_+))}$$

where $k_+ = k_A + k_B$. The maximum C production flux for $j'_A \to \infty$ is $j_{Cm} = \frac{y_{CA}k_Ak_B(1+j'_B/k_+)}{j'_B+k_B}$. If $j'_B = 0$, the production reduces to $j_C = \frac{y_{CA}j'_Ak_A}{k_A+j'_A}$ as expected from the Michaelis-Menten kinetics. If signal molecule $\tilde{B}$ results in the synthesis of an enzyme D, the D production flux is given by:

$$j_D = y_{DB}k_B(\theta^*_{.B} + \theta^*_{AB}) = \frac{y_{DB}j'_Bk_B}{j'_B + k_B}$$

This formulation of binding inhibition is the simplest. Additional biological details can be introduced, such as binding probabilities or dissociation rates that depend on whether or not the other compound is bound. Although the introduction of such dependencies can allow the description of more complex inhibition patterns, it also implies an increase in the number of parameters.

5.2.2 Bilateral binding inhibition

In bilateral binding inhibition, one substrate can repress the use of another and *vice versa*. As above, we deal with the reaction $y_{AC}\tilde{A} \rightarrow C$ that is inhibited by compound B. In addition, we now have the reaction $y_{BD}\tilde{B} \rightarrow D$ that is inhibited by compound A. Again, y_{AC} and y_{BD} are stoichiometric constants, and C and D are the key enzymes involved in processing substrates A and B. In this case, the inhibition is reciprocal. The SU can bind both $\tilde{A}$ and $\tilde{B}$, but it can bind $\tilde{A}$ only if $\tilde{B}$ is not bound, and *vice versa*. The equations for the change in the bound fractions of the SU now read:

$$\begin{aligned}
\frac{d}{dt}\theta_{..} &= k_A\theta_{A.} + k_B\theta_{.B} - (j'_A + j'_B)\theta_{..} \\
\frac{d}{dt}\theta_{A.} &= j'_A\theta_{..} + k_B\theta_{AB} - k_A\theta_{A.} \\
\frac{d}{dt}\theta_{.B} &= j'_B\theta_{..} + k_A\theta_{AB} - k_B\theta_{.B} \\
1 &= \theta_{..} + \theta_{A.} + \theta_{.B} + \theta_{AB}
\end{aligned}$$

with $j'_i = j_i\rho_i$, where ρ_i is the binding probability and j_i the arrival rate of signal molecules induced by substrate i. The steady state fractions of bound SUs are $\theta^*_{ij} = \Theta_{ij}/\Theta_+$, with $\Theta_+ = \Theta_{..} + \Theta_{A.} + \Theta_{.B} + \Theta_{AB}$ and

$$\Theta_{..} = k_Ak_B; \quad \Theta_{A.} = j'_Ak_B; \quad \Theta_{.B} = j'_Bk_A; \quad \Theta_{AB} = 0$$

The resulting C production flux is given by:

$$j_C = y_{CA}k_A\theta^*_{A.} = \frac{y_{CA}j'_Ak_Ak_B}{j'_Ak_B + j'_Bk_A + k_Ak_B} \tag{5.1}$$

The maximum flux of C for $j'_A \rightarrow \infty$ is $j_{Cm} = y_{CA}k_A$. If $j'_B = 0$, the production reduces to $j_C = \frac{y_{CA}j'_Ak_A}{k_A+j'_A}$ as expected. The situation for substrates A and B and their induced production fluxes are now symmetric.

5.3 Adaptation

5.3.1 Model development

The production of the key enzymes for the processing of substrates is controlled by signals to the synthesis machinery, while the signals are produced by substrates that are taken up. If enzyme production depends on the magnitude of these signals, the production at varying substrate concentrations varies

even when only one substrate is present. In this single substrate situation, the maximum specific consumption rate will become a function of substrate concentration. However, a constant maximum specific consumption rate is usually assumed in popular and successful microbial growth models (Monod [13], Pirt [15], Droop [2], DEB [9]). The empirical success of these models leads to the conclusion that the production of assimilation machinery does not respond to the absolute signal size, but to the *relative* signal size (i.e., the signal value divided by the maximum signal value).

If substrates A and B are processed in parallel and we have n_A assimilatory units for substrate A per unit of structural mass, the substrate processing rate for substrate A is proportional to $n_A f_A$, where $f_A = S_A/(S_A + K_A)$ with saturation constant K_A and substrate concentration S_A. The signal size is proportional to this flux (with proportionality constant p_i^*), so the relative signal size is $s_A = p_A^* n_A f_A / \sum_i p_i^* n_i f_i$. This formulation allows for a substrate-specific signal amplification via weight coefficients p_i^*, which also accounts for the binding probability of the signal to the signal processing unit (regulatory protein). The signal is actually a flux, so the relative signal flux can be written as $s_A k$, where k represents the flux proportionality constant as well as the total signal strength, since $s_A + s_B = 1$. In mathematical terms this means $j'_A = k s_A$ and $j'_B = k s_B$.

The signals are processed in a reciprocal inhibitory way to allow some metabolic memory and preferences for particular substrates. The production rate of assimilatory machinery is proportional to that of the biomass, which has specific growth rate r (see Biomass growth section below). Thus, we multiply the production rate by a factor r/r_0, with r_0 some reference rate. The dilution of assimilatory machinery by growth then amounts to $-r n_A$ for substrate A. In sum: $\frac{d}{dt} n_A = j_C \frac{r}{r_0} - r n_A$.

Using bilateral binding inhibition (equation 5.1), the change in the amount of rate-limiting machinery for substrate A is now given by:

$$\frac{d}{dt} n_A = r \left(\frac{n_A^* s_A (1 + k/k_A)}{s_A (1 + k/k_A) + s_B (1 + k/k_B)} - n_A \right)$$

where $n_A^* = \frac{y_{CA} k / r_0}{1 + k/k_A}$ is the steady-state rate-limiting enzyme concentration for substrate A for exposure to that substrate only.

The expression fraction is defined as $\kappa_i = n_i / n_i^*$. As it represents the ratio of the expression and the maximum attainable expression (n_i^*), it has a value between zero and one. From the equation above the change in these fractions

is given by:

$$\begin{aligned} \frac{d}{dt}\kappa_A &= r\left(\frac{p_A\kappa_A f_A}{p_A\kappa_A f_A + p_B\kappa_B f_B} - \kappa_A\right) \\ \frac{d}{dt}\kappa_B &= r\left(\frac{p_B\kappa_B f_B}{p_A\kappa_A f_A + p_B\kappa_B f_B} - \kappa_B\right) \end{aligned} \tag{5.2}$$

where $p_i = p_i^* n_i^*(1 + k/k_i)$ are substrate preference coefficients. Without loss of generality, we can take $p_A + p_B = p_+ = 1$. Please note that for $\kappa_+ = \kappa_A + \kappa_B$, we have $\frac{d}{dt}\kappa_+ = r(1 - \kappa_+)$, which gives the natural constraint $\kappa_A(0) + \kappa_B(0) = 1$ on the initial conditions. Once $\kappa_A(t) + \kappa_B(t) = 1$ for some value of time t, it remains one at all time points. These constraints reduce the system above to a single equation with effectively two parameters, p_A and $\kappa_A(0)$.

5.3.2 Model analysis

Prolonged exposure to substrate A only ($f_B = 0$) results in maximum expression ($\kappa_A \to 1$) of the corresponding rate-limiting enzyme, whereas prolonged absence of substrate A ($f_A = 0$) results in no expression at all ($\kappa_A \to 0$). For constant substrate concentrations, the expression is either maximum or zero at steady state, depending on which value for $p_i f_i$ is the largest. In a steady-state chemostat, dual substrate consumption can take place, since the microorganism adapts until $p_A f_A = p_B f_B$.

If the organisms have depleted their own substrates, the final values of the expression fractions depend on how the substrates were depleted. This is because the adaptation rate is linked to the growth rate. After complete depletion of the resources the adaptation equations above become mathematically undetermined. In the unlikely situation that this behavior poses a problem in a practical application, it can be avoided by adding a background signal for each substrate and replacing f_i by $f_i + \epsilon_i$ for $i = A, B$.

When a particular substrate has been absent for a very long period its expression fraction becomes zero. The microorganism then is not able to initiate the uptake of that substrate. Since this behavior is asymptotic only, it will probably not constitute a problem in practice. Moreover, it can be avoided by adding a small background signal as above or by introducing a background production flux as $r\kappa_i^\circ$ for $i = A, B$. As a consequence of the addition of the background production flux, the maximum value of κ_i will no longer be one. Substrate uptake now becomes $\frac{d}{dt}S_i = -\frac{\kappa_i}{\kappa_i^{\max}} f_i X$, where $\kappa_i^{\max} = 1 + \kappa_i^\circ$ represents the maximum value of the expression fraction κ_i.

The assimilation machinery, including the carriers, are part of cells' structure. Cells maintain their structure by degrading and reconstructing their functional proteins. Such enzyme-specific maintenance becomes visible in the adaptation process as a protein decay and an enhanced synthesis via term h. Incorporation of this enzyme turnover into the adaptation model, for an arbitrary number of substrates, leads to:

$$\frac{d}{dt}\kappa_i = (r+h)\left(\frac{p_i\kappa_i f_A}{\sum_j p_j\kappa_j f_j} + \kappa_i^\circ - \kappa_i\right) \tag{5.3}$$

with $\sum_i p_i = 1$. Notice that for $\kappa_+ = \sum_i \kappa_i$ and $\kappa_+^\circ = \sum_i \kappa_i^\circ$ we have

$$\frac{d}{dt}\kappa_+ = (r+h)\left(1 + \kappa_+^\circ - \kappa_+\right)$$

which implies that as soon as $\kappa_+(t) = 1 + \kappa_+^\circ$, it will never leave this value. This can be used as a constraint on the initial conditions for κ_i to remove one degree of freedom from the system.

Our adaptation model spans the full range of nutrient utilization, from simultaneous substrate consumption to sequential consumption. For two nutrients, the mode of consumption depends on the value of a single preference parameter (p_A); if it is very small, substrate B will be taken up first. Notice that we also have initial conditions for the expression fractions, which count as parameters in fits to experimental data, although their significance vanishes in time. The model can be extended in several ways, for example by accounting for sequential processing of the substrates, or for unilateral binding inhibition.

A very important feature of this model for adaptation is that once the cells are adapted, cell growth and substrate uptake are "normal" again. This means that the adaptation module can easily be combined with other modules, such as the Monod model [13], the Herbert-Marr-Pirt models [4, 12, 15], the Droop model [2] or the DEB model [9]. The crucial property is that the substrate availability and the growth rate do not influence the number of carriers of fully adapted organisms. Alternative models that are known to us [6, 7, 11] do not satisfy this property. This implies that the adaptation process as described by these models affects the dynamics of fully adapted cells, which seems unrealistic to us.

5.3.3 Biomass growth

Although the equations in the previous section fully specify substrate uptake, they do not yet specify the biomass growth process itself. However, as we

stated before, the adaptation model has the advantage that it can be combined with any microbial growth model. Hence, the Monod model [13] can be used. If, in addition, we know the maintenance requirements of the microorganism, Pirt's model [15] can be used. Alternatively, the DEB model [9] can be used. This is a more elaborate and realistic growth model that accounts for the presence of reserves. For more information about the DEB model we refer the reader to the Appendix.

For any of the growth models cited in this chapter, the consumption rate of substrate i and the biomass growth rate are given by:

$$\frac{d}{dt}S_i = -j_{im}\,\frac{\kappa_i}{\kappa_i^{\max}}\,\frac{S_i}{S_i + K_i}\,X \tag{5.4}$$

$$\frac{d}{dt}X = r\,X \tag{5.5}$$

with maximum specific uptake rate j_{im} and biomass concentration X. The change in the expression fractions are given by equation 5.3. In case of zero background expression, $\kappa_i^{\max}$ is equal to one. The expression for the specific growth rate r varies from one model to another. In the Monod model, for example, the yield factor Y_i relates substrate consumption to biomass growth: $r = \frac{1}{X}\sum_i Y_i \frac{dS_i}{dt}$.

5.3.4 Model equations

In the following sections we use the adaptation model, in combination with the Monod model, in simulations and in data fitting. We assume that background expression is absent (thus $\kappa_i^{\max} = 1$). For two substrates, the set of differential equations describing adaptation is:

$$\begin{aligned}
\frac{d}{dt}X &= r\,X\\
\frac{d}{dt}S_A &= -\frac{r_{A\max}}{Y_A}\,\kappa_A\,f_A\,X\\
\frac{d}{dt}S_B &= -\frac{r_{B\max}}{Y_B}\,\kappa_B\,f_B\,X\\
\frac{d}{dt}\kappa_A &= (r+h)\left(\frac{\kappa_A f_A}{\kappa_A f_A + w\kappa_B f_B} - \kappa_A\right)\\
\frac{d}{dt}\kappa_B &= (r+h)\left(\frac{\kappa_B f_B}{\kappa_A f_A/w + \kappa_B f_B} - \kappa_B\right)
\end{aligned}$$

where

$$f_A = \frac{S_A}{S_A + K_A}\,, \quad f_B = \frac{S_B}{S_B + K_B}$$
$$w = p_B/p_A$$
$$r = \kappa_A r_{A\max} f_A + \kappa_B r_{B\max} f_B$$

The adaptation module has only three parameters: $\kappa_A(0)$, h, and p_A/p_B. Remember that $\kappa_B(0) = 1 - \kappa_A(0)$. The Monod model for two substrates has nine parameters: $r_{i\max}$, Y_i, K_i, $S_i(0)$, for $i = A$, B, and $X(0)$.

Below we show model simulations in which we assigned values to the parameters. Thereafter, we apply the model to data. For the parameter estimation procedure, we assumed constant variance with no covariance for the observations.

5.4 Model simulation

A model simulation reveals the influence of the preference parameters p_i, and adaptation, on the diauxic lag and on the substrate consumption. We carried out the simulations below by numerically solving the set of differential equations above. We assigned the values obtained in [6] (Table 5.1) to the Monod parameters, whereas we gave representative values to the remaining parameters.

Figure 5.1 illustrates the influence of substrate preference on the lag phase. In this simulation, the microorganisms have the same preference for both substrates or a ten times higher preference for the first, respectively. A higher preference for the first substrate results in a longer lag phase before growth on the second starts. The initial value of the expression fraction $\kappa_A(0)$ was set to 0.90, which means that the biomass is 90% adapted to substrate A.

Figure 5.2 shows the result of adaptation for a steady-state continuous cul-

Table 5.1: Monod parameter values of *Klebsiella oxytoca* obtained in [6] from single substrate growth data. The maximum growth rate $r_{\max}$, the saturation constant K, and the yield factor Y are given.

Carbon source	$r_{\max}$ (h^{-1})	K (g/L)	Y (g dry wt/g)
Glucose (A)	1.08	0.01	0.52
Xylose (B)	0.82	0.2	0.50

ture. The expression fractions as well as the resulting steady-state biomass and substrate concentrations are shown as a function of the dilution rate. Experimental results often show that at low dilution rates both substrates are consumed, whereas at high dilution rate only one substrate is consumed. As can be seen from Figure 5.2, this is also predicted by the adaptation model.

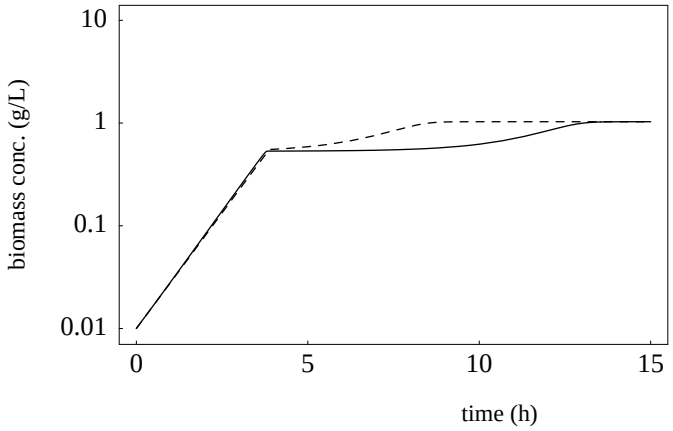

Figure 5.1: Influence of the preference parameter p_A on the length of the lag phase. The figure shows growth on two carbon sources with different preference parameter values ($p_B/p_A = 0.1$, solid line; $p_B/p_A = 1.0$, dashed line). When the microorganisms prefer the first substrate to the second substrate ($p_B/p_A = 0.1$), the length of the diauxic lag phase increases (parameter values from Table 5.1).
Adaptation-model parameters: $h = 0.0\ \mathrm{h}^{-1}$, $p_B/p_A = 0.1$ or $p_B/p_A = 1.0$.
Initial conditions: $S_A(0) = S_B(0) = 1.0$ g/L, $X(0) = 0.01$ g dry wt/L, $\kappa_A(0) = 0.90$.

5.5 Applications

In this section we use the model to describe data from the literature, starting with the growth of *Klebsiella oxytoca* on glucose and xylose [6]. A second example is the diauxic growth of *Pseudomonas oxalaticus* on acetate and oxalate [1]. A third example is the diauxic growth on fructose and succinate [14].

5.5.1 Diauxic growth on glucose and xylose

Kompala et al. [6] have reported the diauxic growth of *Klebsiella oxytoca* on, for example, glucose and xylose. We applied our model to their data, using

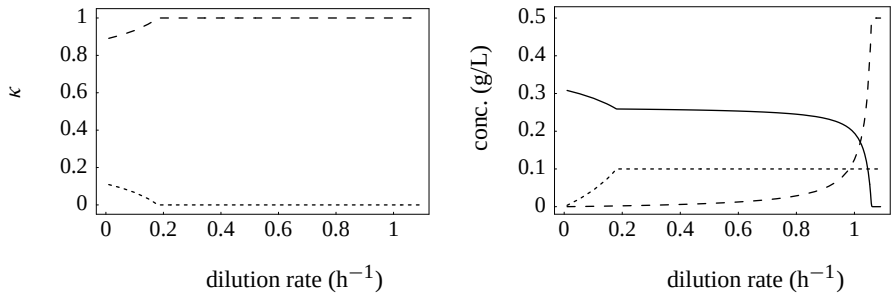

Figure 5.2: Influence of the dilution rate on the expression fractions and substrate concentrations in a steady-state chemostat with input concentrations of 0.5 g/L substrate *A* (dashed line) and 0.1 g/L substrate *B* (dotted line). LEFT: The expression fractions as a function of the dilution rate. RIGHT: The substrate concentrations and biomass (solid line) concentration as a function of the dilution rate (parameter values from Table 5.1). Adaptation-model parameters: $h = 0.0\ \mathrm{h}^{-1}$, $p_B/p_A = 0.5$.

the Monod model for growth. During the estimation process the Monod parameters remain fixed on the values given in Table 5.1. We fitted the data on the diauxic growth on glucose and xylose simultaneously. We show a series of model validations followed by a model prediction. In the following figures the dots represent the experimental data and the lines the model calculations.

Figures 5.3 and 5.4 show fits to data on the growth on glucose or xylose only of an inoculum pre-cultured on glucose. Figure 5.5 and 5.6 show fits to the data on glucose-xylose diauxie. These data come from an inoculum pre-cultured on glucose and an inoculum pre-cultured on xylose, respectively. Figure 5.7 shows a model prediction using the parameter values obtained in the simultaneous fits (Figures 5.3 to 5.6). Although none of the model parameters were fitted to the data, the predicted behavior corresponds with the experimental results.

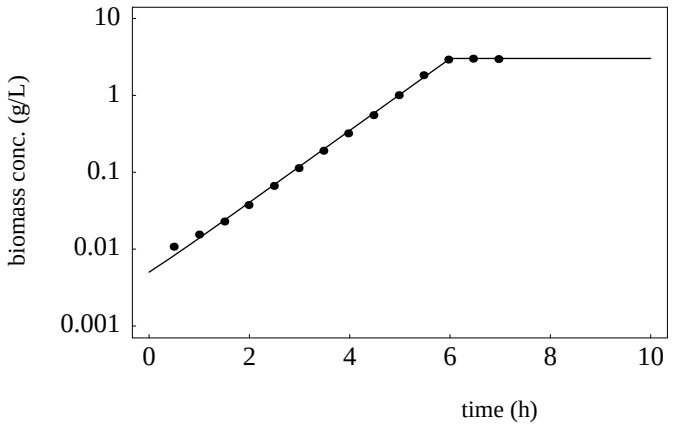

Figure 5.3: Model validation of growth of *K. oxytoca* on glucose after preculturing on glucose. The dots represent experimental data (from [6]), the line represents the model fit.
Adaptation-model parameter: $h = 0.67$ h^{-1}, $p_B/p_A = 0.68$. Monod parameter values from Table 5.1.
Initial conditions: $S_A(0) = 5.8$ g glucose/L, $X(0) = 0.005$ g dry wt/L, $\kappa_A(0) = 0.89$.

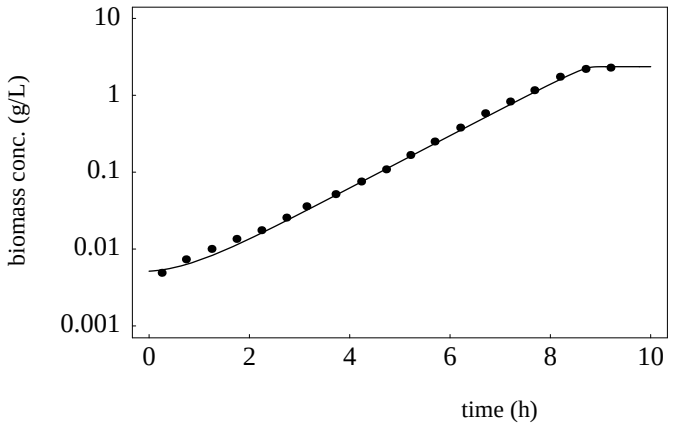

Figure 5.4: Model validation of growth of *K. oxytoca* on xylose after preculturing on glucose. The dots represent experimental data (from [6]), the line represents the model fit.
Adaptation-model parameter: $h = 0.67$ h^{-1}, $p_B/p_A = 0.68$. Monod parameter values from Table 5.1.
Initial conditions: $S_B(0) = 4.7$ g xylose/L, $X(0) = 0.0051$ g dry wt/L, $\kappa_B(0) = 0.11$.

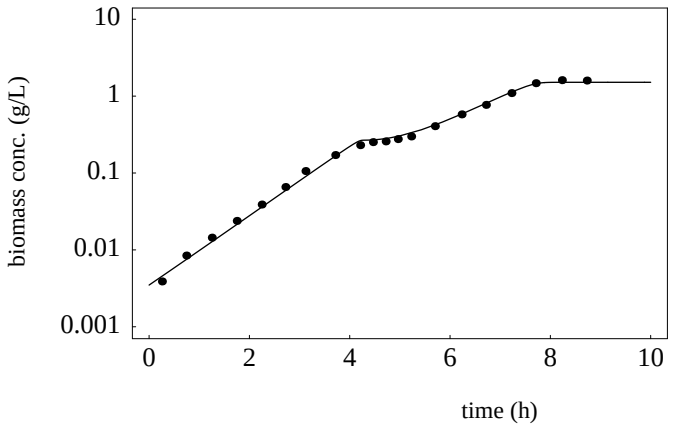

Figure 5.5: Model validation of growth of *K. oxytoca* on glucose and xylose after pre-culturing on glucose. The dots represent experimental data (from [6]), the line represents the model fit.
Adaptation-model parameters: $h = 0.67$ h^{-1}, $p_B/p_A = 0.68$. Monod parameter values from Table 5.1.
Initial conditions: $S_A(0) = 0.5$ g glucose/L, $S_B(0) = 2.5$ g xylose/L, $X(0) = 0.035$ g dry wt/L, $\kappa_A(0) = 0.89$, $\kappa_B(0) = 0.11$.

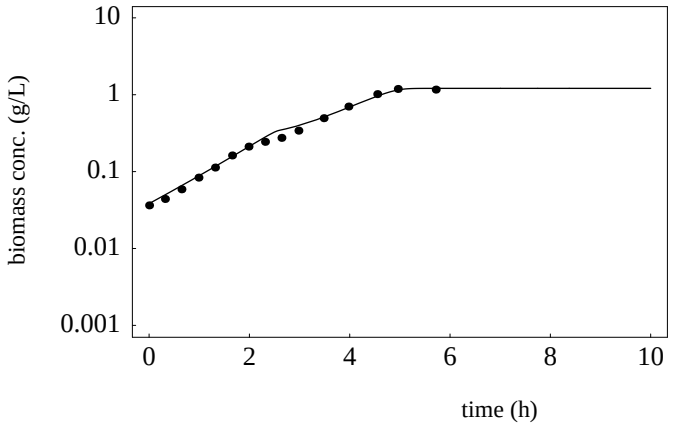

Figure 5.6: Model validation of growth of *K. oxytoca* on glucose and xylose after pre-culturing on xylose. The dots represent experimental data (from [6]), the line represents the model fit.
Adaptation-model parameters: $h = 0.67$ h^{-1}, $p_B/p_A = 0.68$. Monod parameter values from Table 5.1.
Initial conditions: $S_A(0) = 0.33$ g glucose/L, $S_B(0) = 2.0$ g xylose/L, $X(0) = 0.038$ g dry wt/L, $\kappa_A(0) = 0.23$, $\kappa_B(0) = 0.77$.

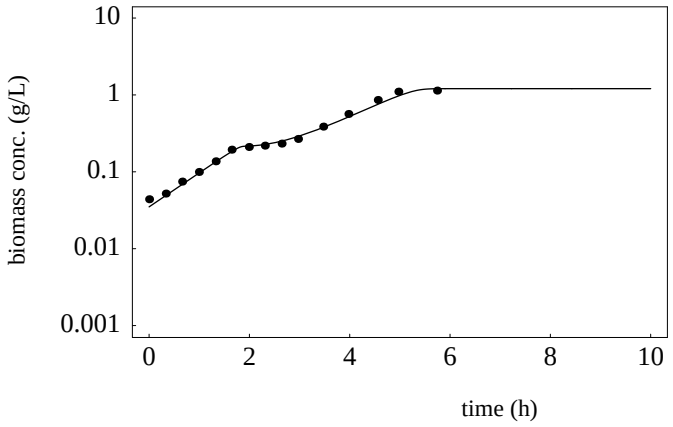

Figure 5.7: Model prediction of growth of *K. oxytoca* on glucose and xylose after pre-culturing on glucose. The dots represent experimental data (from [6]), the line represents the model fit.
Adaptation-model parameters: $h = 0.67$ h^{-1}, $p_B/p_A = 0.68$. Monod parameter values from Table 5.1.
Initial conditions: $S_A(0) = 0.33$ g glucose/L, $S_B(0) = 2.0$ g xylose/L, $X(0) = 0.035$ g dry wt/L.

5.5.2 Diauxic growth on acetate and oxalate

Dijkhuizen et al. [1] have reported the diauxic growth of *Pseudomonas oxalaticus OX1* on acetate and oxalate. To fit our model to this dataset, we set the initial condition of substrate and biomass concentration to the measured values at time zero. Furthermore we fixed the value of the saturation constants on 0.01 mM, because the data do not contain information to estimate these constants well. The estimated values for the other parameters are given in Figure 5.8. The estimated values for the maximum growth rates and yields are within the range values expected under these conditions. The doubling times on acetate and oxalate are usually about 1.8 h and 3.6 h, respectively [1]. Figure 5.8 depicts a fit of the adaptation model to their data. As can be seen from this figure, the model fits the data well.

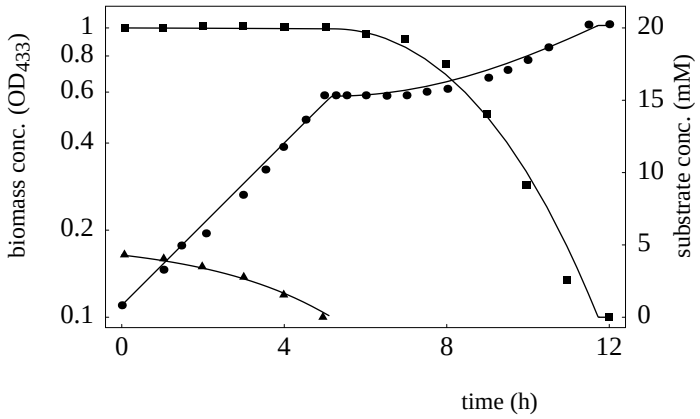

Figure 5.8: Model fit to data on growth of *P. oxalaticus* (●) on acetate (■) and oxalate (▲) after pre-culturing on acetate (data from [1]). Under the experimental conditions, 1 unit optical density (433 nm) is approximately equivalent to 235 mg dry weight per liter.
Parameter values: $r_{A\max} = 0.33\ \mathrm{h}^{-1}$, $r_{B\max} = 0.19\ \mathrm{h}^{-1}$, $Y_A = 0.11$ mM acetate OD^{-1}, $Y_B = 0.022$ mM oxalate OD^{-1}, $K_A = 0.01$ mM (fixed), $K_B = 0.01$ mM (fixed), $h = 0.15\ \mathrm{h}^{-1}$, $p_B/p_A = 0.5$.
Initial conditions: $S_A(0) = 4.3$ mM acetate, $S_B(0) = 20$ mM oxalate, $X(0) = 0.11$ OD, $\kappa_A(0) = 0.99$, $\kappa_B(0) = 0.01$.

5.5.3 Diauxic growth on fructose and succinate

Azospirillum brasilense has shown diauxic growth when incubated with succinate and fructose [14]. To obtain a model fit of the experimental results, we use our adaptation model in combination with the Monod model. The substrates have been radioactively labeled and their consumption as well as their incorporation into biomass have been measured in three experiments. In the model fit shown below, we used a biomass incorporation percentage of 20% for succinate [14] and of 50% for fructose.

Since radioactivity has been measured, a background radioactivity signal exists during the experiment ($^{14}CO_2$, radioactive products). This means that the substrate concentration based on radioactivity is not zero when all (primary) substrate has been consumed. The signal of these radioactive products can be incorporated into the model expression for fructose consumption. The formation of radioactive products equals $\frac{d}{dt}P = -\alpha\frac{d}{dt}S_B - k_d P$. Since we used an incorporation percentage of fructose of 50%, the parameter α has a value of 0.50. Figure 5.9 shows the model fit of fructose disappearance without (solid line) and with (dotted line) the incorporation background radioactivity. The adaptation model fits quite well when we keep in mind that: (*i*) the data comes from three separate experiments and (*ii*) during fructose metabolism, an unknown amount of organic acids is produced causing the disappearance of radioactivity to lag behind the consumption of fructose itself.

We remark that, in the uptake experiment, the total consumption rate of fructose remained constant for one to two generations after the addition of succinate to a culture growing on fructose [14]. This can be explained by an immediate and complete stop of the synthesis of fructose degrading key enzymes. At the moment we have not further investigated this immediate change in enzyme synthesis, since the specific fructose consumption rate in the uptake experiment was about 8 times lower than in the corresponding growth experiment. This means that the cells behaved differently in the growth and uptake experiments, possibly due to the harvesting and washing processes.

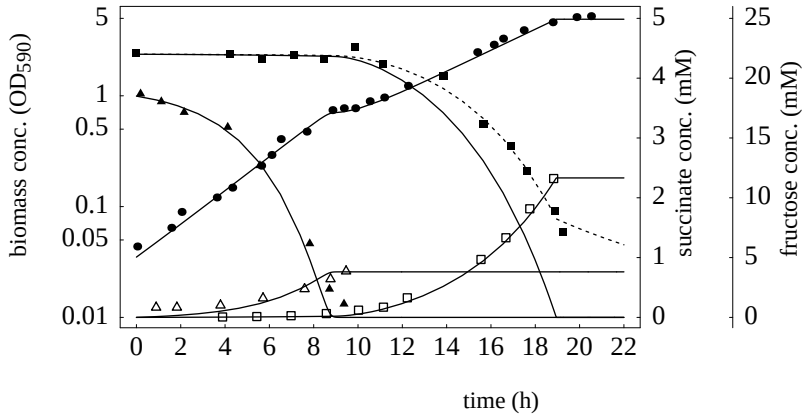

Figure 5.9: Model fit of growth of *A. brasilense* on fructose and succinate after pre-culturing on succinate. The data come from three separate experiments [14]: one measures [1,4-^{14}C] succinate in supernatant (▲) and cells (△), one measures D-[U-^{14}C] fructose in supernatant (■) and cells (□), and another measures growth (●). The dotted line indicates the model fit of fructose consumption when the formation of radioactive products from fructose is included ($\alpha = 0.50$, $k_d = 0.1$). One unit of OD_{590} corresponds to 470 μg dry weight/ml.

Parameter values: Y_A = 80.6 g dry wt/mmol succinate, Y_B = 90.6 g dry wt/mmol fructose, $r_{A\,\max}$ = 0.38 h^{-1} [14], $r_{B\,\max}$ = 0.22 h^{-1} [14], K_A = 0.1 mM (fixed), K_B = 10^{-4} mM (fixed), h = 0.7, p_B/p_A = 0.8.

Initial conditions: $S_A(0)$ = 3.7 mM succinate, $S_B(0)$ = 22 mM fructose, $X(0)$ = 16.5 g dry wt/L, $\kappa_A(0)$ = 0.80, $\kappa_B(0)$ = 0.20.

5.6 Discussion

The adaptation model presented in this chapter fits and predicts data on diauxic growth well. The current approach differs from previous approaches, as cybernetic modeling (e.g. [6, 7]), on some important aspects, which are discussed below.

The description of the adaptation process was obtained by assuming a general regulatory mechanism where the presence of one nutrient can inhibit the utilization of another. This approach has the advantage that it is species independent and parameter sparse. In its simplest version, it describes the adaptation process during diauxic growth with only two parameters: $\kappa_A(0)$ and p_A. A single parameter p_A describes substrate preference during diauxic growth.

In the case of adaptation to a single nutrient, our model predicts a constant maximum key-enzyme level. Thus, the maximum specific consumption rate is always a constant, irrespective of enzyme decay and substrate concentration. Our model differs in this aspect from other adaptation models. Such a constant maximum rate is the basis of most growth models (Monod, Pirt, Droop, DEB [9]). Moreover, it is difficult to know beforehand whether key enzymes for a certain substrate are inducible. Therefore, the application of models for adaptation that do not assume this maximum specific consumption rate to be constant (e.g. [6, 11]) is problematic in the situation where growth on a single substrate is quantified. If a Monod model has successfully been applied to single-substrate situations, but later research reveals that key enzymes are inducible, this implies that earlier work must be redone. Contrary to other adaptation models known to us [6, 7, 11], our adaptation model does not suffer from this problem even when enzyme decay occurs. For a single substrate situation the current adaptation model simplifies exactly to the growth model for cells in steady state. During steady-state growth on a single substrate, the influence of the adaptation process on substrate consumption is absent.

Furthermore, we did not introduce optimal control into the adaptation model *a priori*; bacteria may optimize total biomass, or growth rate [3, 7], or possibly something else. No introduction of optimal control implies that we do not use this method to reduce the number of parameters, as has been done in the cybernetic approach [6, 7]. However, optimal control can be incorporated into the model. The binding probabilities (see page 82), for example, can be a function of an optimal control regime.

We point out that this adaptation model primarily describes slow adaptation taking several cell cycles. It is based on the regulation of the synthesis of key enzymes. When a microorganism adapted to substrate A, is transferred to another substrate, the key enzymes for the use of A can be inhibited. This

inhibition typically occurs in a time frame of seconds, and can be called fast adaptation. It can be included in this model with, for example, an expression for instantaneous inhibition (see Appendix).

We developed a slow adaptation model based on the interaction and inhibition of substrates during enzyme synthesis. The model was applied to data from diauxic growth experiments, but can be applied to growth on more than two substrates as well. Moreover, it can be extended to account for different processes as enzyme inhibition and can even be used with optimal control without altering the structure of the model.

More information about the DEB research program can be found at http://www.bio.vu.nl/thb/deb/. The adaptation model that is discussed in this chapter is coded in the package DEBtool, which can be downloaded from the electronic DEB laboratory.

Nomenclature

The following table lists the parameters used in the Monod and adaptation model. The symbols used for the dimensions are: –, no dimension; l, length; t, time; #, amount (C-mol or mass).

Symbol	Name	Dimension
f_i	$\frac{S_i}{K_i+S_i}$	–
h	enzyme turnover rate	t^{-1}
j_{im}	max. spec. consumption rate of substrate i	$\#\,\#^{-1}\,t^{-1}$
K_i	saturation constant of substrate i	$\#\,l^{-3}$
n_i	number of carriers i per structural mass	$\#\,\#^{-1}$
p_i	preference parameter for adaptation to substrate i	–
r	biomass growth rate	t^{-1}
$r_{\max}$	maximum biomass growth rate	t^{-1}
S_i	concentration of substrate i	$\#\,l^{-3}$
X	biomass concentration	$\#\,l^{-3}$
Y_i	Monod yield factor	$\#\,\#^{-1}$
κ_i	expression fraction of substrate i	–
κ_i°	background expression fraction of substrate i	–
$\kappa_i^{\max}$	max. expression fraction of substrate i	–

Appendix

Adaptation with the DEB model

Our adaptation model can be combined with different biomass growth models. In this chapter we showed how our adaptation model can be applied in combination with the Monod model. Another biomass growth model that can be used is the dynamic energy budget (DEB) model [9], which accounts for reserve dynamics. The main feature of this model is that substrates are assimilated into reserves from which growth costs and maintenance costs are paid. Since in the DEB model, biomass is divided into two compartments, structure and reserves, the biomass composition becomes a function of the growth rate, as has been observed in practice. When the maintenance is negligible and reserve turnover is very fast, the DEB model simplifies to the Monod model. For a thorough introduction to the DEB model we refer the reader to [9, 10]. In batch reactors, the DEB biomass growth model in combination with our adaptation model (equation 5.2 or equation 5.3) results in the following equations:

$$r = \frac{k_E\, m_E - k_M\, y_{EV}}{m_E + y_{EV}} \tag{5.6a}$$

$$\frac{d}{dt} m_E = \sum_i j_{im} \frac{\kappa_i}{\kappa_i^{\max}}\, y_{ES_i}\, \frac{S_i}{K_i + S_i} - k_E\, m_E \tag{5.6b}$$

$$W(t) = w_V X + w_E\, m_E\, X \tag{5.6c}$$

The expression for the substrate consumption (equation 5.4) also applies to the DEB model; j_{im} is the maximum structural-biomass specific consumption rate of substrate i (C-mol C-mol^{-1} h^{-1}). The growth of structural biomass (X) is defined by equations 5.5 and 5.6a. Here, the reserve density of limiting nutrient, m_E (C-mol/C-mol), comes into play. The higher the reserve density, the higher the growth rate. k_E is the reserve turnover rate (h^{-1}) and y_{EV} refers to the amount of reserves needed per amount of structural biomass formed (C-mol/C-mol). For simplicity, we assumed the costs for growth (y_{EV}) remain constant. This means that the costs for key-enzyme synthesis for cells fully adapted to one substrate are the same irrespective of the type of substrate. Maintenance is introduced by the maintenance rate coefficient, k_M (h^{-1}). Reserves are replenished by substrate consumption (equation 5.6b). The efficiency of this process is defined by y_{ES_i} (C-mol/C-mol); the amount of reserves formed per amount of substrate consumed. The total weight (W) of the biomass equals the sum of the weight of reserves and structural biomass (equation 5.6c). Please note that the Monod model is a special case of the DEB model for $k_E \to \infty$ and $k_M = 0$.

Diauxic growth on acetate and oxalate

Dijkhuizen et al. [1] have reported the diauxic growth of *Pseudomonas oxalaticus OX1* on acetate and oxalate. In this example, we use the DEB model for microbial growth (see section 5.3.3). The biomass and substrate concentrations are expressed on a C-mol basis. We assumed that the biomass structure and the reserves have the general composition $CH_{1.8}O_{0.5}N_{0.2}$ (24.6 g/mol). Biomass concentration was reported in optical density units. Under the experimental conditions, 1 unit optical density (433nm) is equivalent to 235 mg dry weight per liter (1 C-mole/L $\times \frac{24.6}{235} = OD_{433}$).

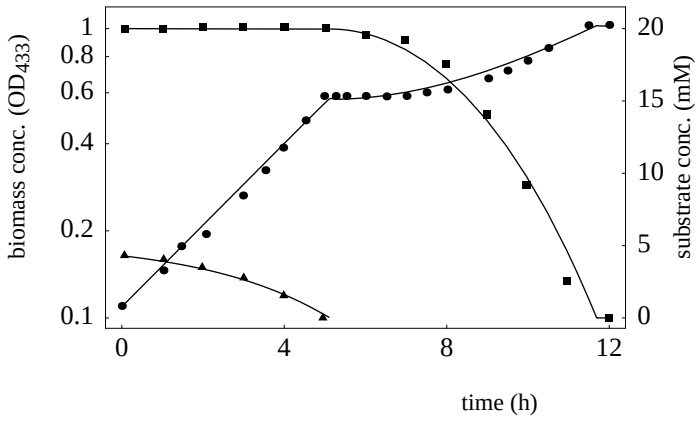

Figure 5.10: Model fit to data on growth of *P. oxalaticus* (●) on acetate (■) and oxalate (▲) after pre-culturing on acetate (data from [1]).
Parameter values: $j_{Am} = 0.66$ C-mol acetate (C-mol biomass)$^{-1}$ h^{-1}, $j_{Bm} = 0.9$ C-mol oxalate (C-mol biomass)$^{-1}$ h^{-1}, $y_{ES_A} = 0.66$, $y_{ES_B} = 0.28$, $y_{EV} = 1.3$, $K_A = 0.01$ mM (fixed), $K_B = 0.01$ mM (fixed), $k_E = 10$ h^{-1}, $k_M = 0$ h^{-1}, $h = 0.16$ h^{-1}, $p_B/p_A = 0.023$.
Initial conditions: $S_A(0) = 4.3$ mM acetate, $S_B(0) = 20$ mM oxalate, $X(0) = 1.0$ C-mol/L, $m_E(0) = 0.044$, $\kappa_A(0) = 0.99$, $\kappa_B(0) = 0.01$.

Fast adaptation

Fast adaptation, or repression of enzyme activity, can also be modeled with bilateral binding inhibition (equation 5.1). In this case, not the synthesis machinery but the enzyme activity is repressed. Substrate consumption with in-

stantaneous inhibition becomes:

$$\frac{dS_A}{dt} = -j_{Am}\frac{j'_A k_B}{j'_A k_B + j'_B k_A + k_A k_B} X$$
$$= -j_{Am}\frac{K_A^{-1} S_A}{K_A^{-1} S_A + K_{BA}^{-1} S_B + 1} X$$

The arrival flux j'_A of substrate A at the carrier (or key enzyme) is proportional to the substrate concentration and equals $\alpha_A \rho_A S_A$, where ρ_A is the binding probability. The saturation constant K_A is $k_A/(\alpha_A \rho_A)$. The influence of substrate B on the consumption of A appears in the denominator as $K_{BA}^{-1} S_B$.

Acknowledgements

The authors thank Paul Doucet, Bob Kooi and three anonymous reviewers for insightful comments.

References

[1] Dijkhuizen L, van der Werf B, Harder W. (1980). Metabolic regulation in *Pseudomonas oxalaticus* OX1. Diauxic growth on mixtures of oxalate and formate or acetate. *Archives of Microbiology* 124:261–268.

[2] Droop MR. (1975). The nutrient status of algal cells in batch culture. *Journal of the Marine Biological Association of the United Kingdom* 55:541–555.

[3] Harder W, Dijkhuizen L. (1982). Strategies of mixed substrate utilization in microorganisms. *Philosophical Transactions of the Royal Society of London B (Biological Sciences)* 297:459–480.

[4] Herbert D. (1958). Some principles of continuous culture. In: Tunevall G, editor. *Recent progress in microbiology*, pp. 381–396. Almquist & Wiksell, Stockholm.

[5] Kimata K, Takahashi H, Inada T, Postma P, Aiba H. (1997). cAMP receptor protein-cAMP plays a crucial role in glucose-lactose diauxie by activating the major glucose transporter gene in *Escherichia coli*. *Proceedings of the National Academy of Sciences of the United States of America* 94:12914–12919.

[6] Kompala DS, Ramkrishna D, Jansen NB, Tsao GT. (1986). Investigation of bacterial growth on mixed substrates: experimental evaluation of cybernetic models. *Biotechnology and Bioengineering* 28:1044–1055.

[7] Kompala DS, Ramkrishna D, Tsao GT. (1984). Cybernetic modeling of microbial growth on multiple substrates. *Biotechnology and Bioengineering* 26:1272–1281.

[8] Kooijman SALM. (1998). The synthesizing unit as model for the stoichiometric fusion and branching of metabolic fluxes. *Biophysical Chemistry* 73:179–188.

[9] Kooijman SALM. (2000). *Dynamic Energy and Mass Budgets in Biological Systems*. Cambridge University Press, Cambridge, second edition.

[10] Kooijman SALM. (2001). Quantitative aspects of metabolic organization; a discussion of concepts. *Philosophical Transactions of the Royal Society of London B (Biological Sciences)* 356:331–349.

[11] Liu PH, Svoronos SA, Koopman B. (1998). Experimental and modeling study of diauxic lag of *Pseudomonas denitrificans* switching from oxic to anoxic conditions. *Biotechnology and Bioengineering* 60:649–655.

[12] Marr AG, Nilson EH, Clark DJ. (1963). The maintenance requirement of *Escherichia coli*. *Annals of the New York Academy of Sciences* 102:536–548.

[13] Monod J. (1958). *Recherches sur la croissance des cultures bactériennes*. Hermann, Paris, second edition. Thèse de 1942.

[14] Mukherjee A, Ghosh S. (1987). Regulation of fructose uptake and catabolism by succinate in *Azospirillum brasilense*. *Journal of Bacteriology* 169:4361–4367.

[15] Pirt SJ. (1965). The maintenance energy of bacteria in growing cultures. *Proceedings of the Royal Society of London B (Biological Sciences)* 163:224–231.

[16] Stryer L. (1995). *Biochemistry*. Freeman, New York, fourth edition.

[17] Stülke J, Hillen W. (1999). Carbon catabolite repression in bacteria. *Current Opinion in Microbiology* 2:195–201.

Samenvatting

Realistische karakteriseringen van biodegradatie

De industrie produceert grote aantallen chemicaliën in soms grote hoeveelheden. Uiteindelijk komen deze stoffen in het milieu en kunnen daar problemen veroorzaken. Pesticides zoals DDT, maar ook synthetische zepen, hebben door hun slechte afbreekbaarheid in het verleden tot vervuilingen geleid. Chemicaliën die op de markt komen moeten tegenwoordig getest worden op een groot aantal eigenschappen, waaronder toxiciteit, carcinogeniciteit, en afbreekbaarheid. Verschillende internationale organisaties (OESO, ISO, EU) hebben richtlijnen opgesteld voor deze tests.

Dit proefschrift gaat over het modelleren van biodegradatie, ofwel het afbreken van stoffen door (micro)organismen. Deze modellen kunnen worden toegepast in de analyse van de resultaten van biodegradatietesten. Binnen dit project zijn een aantal onderwerpen geselecteerd die een rol spelen bij de biodegradatie: stof-transportproblemen, co-metabolisme, en adaptatie.

Hoofdstuk 1 introduceert de biodegradatietests en een aantal modellen. Deze modellen worden in de praktijk gebruikt voor het beschrijven van de resultaten, waarbij de nauwkeurigheid van de beschrijving vaak belangrijker is dan de juistheid van het model. De problemen van deze modellen worden kort besproken.

Voor de oplossing van deze problemen is een raamwerk nodig dat in hoofdstuk 2 wordt besproken en in latere hoofdstukken wordt toegepast bij het formuleren van andere modellen, die een aantal problemen oplossen.

Hoofdstuk 2 introduceert de Dynamische-Energie-Budget (DEB) theorie. Micro-organismen breken stoffen af en zij vermenigvuldigen zich vaak gedurende deze afbraak. De DEB-theorie doet uitspraken over de groei van organismen. Deze algemene theorie, waarbinnen reserves een centrale rol spelen, wordt hier toegepast om de groei van de biomassa te beschrijven. De relatie van het DEB-model tot het Monod, het Pirt en het Droop-model wordt aangegeven. De volgende hoofdstukken (3, 4, 5) behandelen de geselecteerde

onderwerpen (stof-transportproblemen, co-metabolisme, en adaptatie).

Hoofdstuk 3 beschrijft een model voor de afbraak van stoffen door microbiële vlokken. Micro-organismen in actief slib komen meestal voor in vlokken, wat resulteert in een verminderde beschikbaarheid van substraten voor de bacteriën in de vlok. Dit kan de biodegradatiesnelheid een orde van grootte verkleinen. Dit hoofdstuk presenteert een uitbreiding van groeimodellen voor celsuspensies om de verlaging in de afbraaksnelheid te beschrijven. Hiervoor zijn twee extra parameters nodig: de vlokgrootte bij deling, en de 'diffussielengte.' In het begin groeien kleine vlokken exponentieel, net als celsuspensies. Hierna neemt de groeisnelheid geleidelijk af en uiteindelijk is de radius van de vlok een lineair stijgende functie van de tijd. In dit hoofdstuk wordt een expliciete, benaderende expressie afgeleid voor de groei van biomassa in vlokken. Modelsimulaties laten het effect van vlokgrootte op de biodegradatiesnelheid zien.

Hoofdstuk 4 behandelt simultane opname van verschillende stoffen. De beschikbaarheid van meerdere koolstof/energie bronnen kan de afbraak van recalcitrante verbindingen bevorderden. Verschillende manieren van multisubstraatgebruik komen aan bod en worden binnen een algemeen concept van 'Synthesizing Units' geplaatst. Synthesizing Units zijn een soort algemene enzymen. Een substraat kan substitueerbaar of complementair zijn, de manier van opname kan sequentieel of parallel zijn. Dit geeft vier verschillende manieren van substraatinteractie, die alle door een algemeen model omvat worden. Uit het algemene model volgt een expressie voor co-metabolisme van verbindingen die verschillen van moleculaire structuur. Zowel het algemene model als het model voor co-metabolisme hebben als voordeel dat ze met elk microbieel groeimodel gecombineerd kunnen worden. Het model voor co-metabolisme wordt gevalideerd met experimentele data. De verkregen resultaten ondersteunen het idee dat het algemene model een bruikbaar raamwerk is voor het modelleren van multisubstraatgebruik.

Hoofdstuk 5 gaat over de aanpassing van bacteriën aan de verschillende aanwezige substraten. In het milieu komen verschillende substraten voor in variërende concentraties. Bacteriën zullen zich aan de veranderingen in hun milieu aan moeten passen om te overleven. Dit hoofdstuk presenteert een model voor langzame adaptatie als functie van veranderingen in substraatbeschikbaarheid. Het model is gebaseerd op symmetrische inhibitie van de expressie van substraatspecifieke afbraakroutes. De Synthesizing Unit kinetica geeft de inhibitiekinetiek. Indien de bacteriën volledig aangepast zijn aan de opname van een enkel limiterend substraat is de maximale consumptiesnelheid volgens dit model constant. Ofwel, deze maximale snelheid is dan niet meer afhankelijk van de substraatconcentratie (voor groei op één substraat), waardoor bij-

voorbeeld het Monod en het Pirt model nog steeds van toepassing blijven. Andere ons bekende adaptatiemodellen hebben deze eigenschap niet. De meest eenvoudige versie van het hier ontwikkelde adaptatiemodel beschrijft de adaptatie gedurende groei op twee substraten (di-auxie) met slechts één preferentie parameter en één initiële conditie. Om de toepasbaarheid van het model te illustreren, is het gefit aan data van di-auxische groei-experimenten.

De modellen voor groei van microbiële vlokken, co-metabolisme en adaptatie, die in de laatste drie hoofdstukken worden beschreven, kunnen worden toegepast bij de analyse van de resultaten van biodegradatietests.

Dankwoord

Tijdens mijn studies in Wageningen (moleculaire wetenschappen en bioprocestechologie), kreeg ik meer en meer interesse in modelleren en regeltechniek. Gedurende mijn stage kreeg ik (opnieuw) contact met Bas Kooijman, mijn promotor. Hij was bezig met een project over het modelleren van biodegradatie, ik was bezig met de afbraak van bifenyl door bacteriën. Het project van Bas was aantrekkelijk, maar die wiskunde! Dat míj wiskunde moeilijk leek, was toch wel belachelijk. Marco wist dat mij in een decembernacht in Praag, (kennelijk) overtuigend duidelijk te maken. En eigenlijk was de wiskunde die eraan te pas komt, volgens Bas, nauwelijks meer dan die van de middelbare school.

Ik was overtuigd door Marco en Bas, en begon vol goede moed aan het project en aan de partiële differentiaalvergelijkingen. Gelukkig waren er computers, die me een handje konden helpen met rekenen. Kon ik net met Word, Quattro en andere crashende PC programma's overweg, kreeg ik een SUN unix computer met een grote monitor. Dat is leuk. Na jaren ontwikkeling van grafische userinterfaces weer terug naar de commandline; geen Quattro, maar een C compiler en GNUplot; geen Word, maar LaTeX: you don't see what you get, but what you see is what you mean. Dat was dus wel even wennen, vooral als LaTeX mij weer iets gaf wat ik helemaal niet wilde!

Gelukkig had ik ook slimme collega's, die een handje konden helpen. Ik wil hen allen daarvoor hartelijk bedanken. Zonder jullie was het niets geworden. Paul had gelukkig wel wat voorbeeldbestanden, en "ach het komt wel goed." En hij had gelijk. Paul bedankt. Matthijs wist mij goed wegwijs te maken op de unix machine's, en Fleur overtuigde mij om in 'lekker leesbaar' C te programmeren in plaats van in APL. Ik wil ook de computergroep bedanken voor de fantastisch goede service.

Na twee jaar van diffunderen (hoofdstuk 3), werd het even moeilijk om de focus terug te vinden. Ik wil Fleur en Inge bedanken, die mij met al hun enthousiasme hebben overtuigd vooral 'leuke dingen' te gaan doen. Met veel plezier werkte ik vervolgens met Inge, Fleur en Bas aan diverse onderwerpen.

Ook wil ik Inge hartelijk bedanken voor het doornemen van diverse manuscripten.

Het spreekt vanzelf dat vele mensen in verschillende mate en op verschillende manieren hebben bijgedragen aan het tot stand komen van mijn proefschrift. Ik ben Technologiestichting STW en Procter & Gamble zeer erkentelijk voor de financiering van dit project. Een proefschrift schrijven doe je niet alleen. De deur van Bas staat altijd open, en hij vindt altijd wel tijd om wat uit te leggen of om over biodegradatie en DEB te discussiëren. Hugo deed en doet mij steeds weer verbijsterd staan: hoe snel hij iets begrijpt en mij vervolgens kan uitleggen hoe het precies zit. Daarnaast wil ik mijn familie en vrienden bedanken voor hun steun.

Als laatste wil ik de leden van de lees- en promotiecommissie (Harry Painter, Mark van Loosdrecht, Gosse Schraa, Barbara Bakker, Jacques Bedaux, en Pierre Auger) bedanken, die allen het proefschrift wilden beoordelen.

Inmiddels zit ik weer achter een PC, met een kleine monitor. Geen C compiler en GNUplot, maar Excel; geen LaTeX, maar Word. Gelukkig weet ik nu veel meer van computers . . .